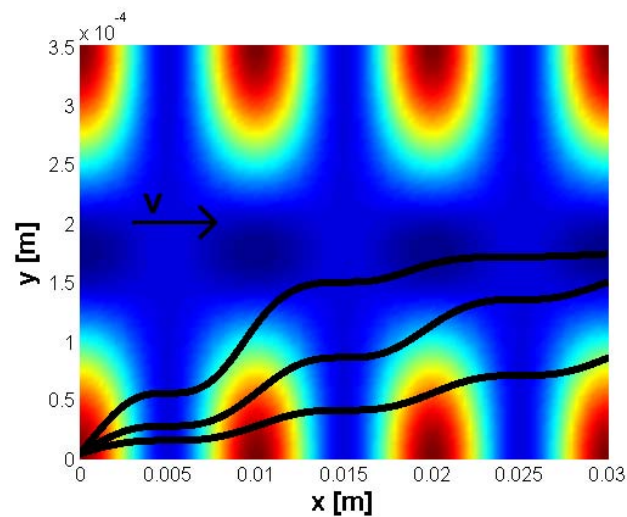


Forces Acting on Microparticles in Acoustofluidic Systems

Bachelor Thesis



Lasse Mejling Andersen, s062087

Anders Nysteen, s062121

Mikkel Settnes, s052944

Abstract

Handling microparticles in lab-on-a-chip systems can be very difficult using traditional mechanical approaches. Acoustofluidics presents a method to manipulate the particles by attaching a piezo-actuator to the chip, where the vibrations cause the particles to move towards the (anti-)nodes of the applied pressure field.

In this thesis we describe the governing equations for acoustofluidics and resonance effects, and with the non-linear Navier–Stokes equation as a starting point we use a second-order perturbation scheme to derive the time-independent acoustic pressure force on spherical, compressible particles in a standing wave. We focus on deriving the acoustic pressure force in details following a classical article by Gor’kov, [14], and look at its applications in three designs proposed by different research groups: Separation of lipid particles from red blood cells, separation of red and white blood cells, and finally how to separate large lipid particles from raw milk. We found that it theoretically was possible to create microchannel systems where these separations were possible using the pressure force. Furthermore we discussed how to optimize the designs to achieve good separation and/or high throughput of the test sample.

An important point in the optimization was to use channels with varying widths to get different patterns of standing waves in the channel, *i.e.* using the first part of the channel to focus the particles in one beam and next leading them into a channel with a different width where the separation is taking place.

Finally we discuss some of the neglected effects in our model. When considering longitudinal modes in standard separation setups, the particle trajectories can be approximated very well by the trajectories in a system neglecting longitudinal modes with half the acoustic energy density. For separation of smaller particles with radii $< 1 \mu\text{m}$, the acoustic streaming is shown to have a greater importance in the description of the particle movement, and for larger particles with radii $> 20 \mu\text{m}$ the interparticle interaction described by the secondary Bjerknes force must be taken into consideration.

Resumé

Håndtering af mikropartikler i lab-on-a-chip-systemer kan være meget besværligt ved hjælp af traditionelle mekaniske fremgangsmåder. Akustofluidik tilbyder en metode til at manipulere partikler på ved at fastgøre en piezo-aktuator på chippen, så vibrationerne får partiklerne til at bevæge sig imod (anti-)knodepunkter for den påtrykte trykbølge.

I denne afhandling beskriver vi de grundlæggende ligninger for akustofluidik og resonanseffekter, og med udgangspunkt i den ikke-lineære Navier–Stokes-ligning benytter vi anden-ordens perturbation til at udlede den tidsuafhængige akustiske trykkraft på sfæriske, kompressible partikler i en stående bølge. Vi vil lægge vægt på at udlede den akustiske trykkraft i detaljer med udgangspunkt i en klassisk artikel af Gor’kov, [14], og kigge på dens anvendelsesmuligheder i tre forskellige designs foreslået af forskellige forskningsgrupper: Separation af fedtpartikler fra røde blodlegemer, separation af røde og hvide blodlegemer og til sidst hvordan store fedtpartikler kan separeres fra råmælk. Vi fandt, at det teoretisk set var muligt at lave mikrokanalsystemer, hvor disse separationer var mulige ved hjælp af trykkraften. Endvidere diskuterede vi, hvorledes designene skulle optimeres for at få god separation og/eller højt gennemløb af prøvematerialet.

En vigtig pointe med hensyn til optimeringen var at benytte kanaler med varierende bredde for at få forskellige stående bølger i kanalen, det vil sige at udnytte den første del af kanalen til at fokusere partiklerne i en stråle og dernæst lede dem ind i en kanal med en anden bredde, hvor selve separationen finder sted.

Til sidst diskuterer vi nogen af de negligerede effekter i vores model. Når vi betragter longitudinale modes i standardkanaler for partikelseparation, kan partikelbanerne tilnærmes meget godt med partikelbanerne i et system, hvor longitudinale modes negliceres, men hvor den akustiske energi er halvt så stor. For separation af mindre partikler med radius $< 1 \mu\text{m}$ er det vist, at den akustiske strømning får større betydning for beskrivelsen af partikelbevægelsen, og for større partikler med radius $> 25 \mu\text{m}$, må der tages hensyn til påvirkningen mellem partiklerne beskrevet ved den sekundære Bjerknes-kraft.

Preface

This bachelor-thesis treats the theoretical background of acoustofluidics as well as looks at its applications. It is written as part of the B.Sc. Eng. education at the Technical University of Denmark.

The thesis corresponds to 15 ECTS points of work for each student, corresponding to a quarter of a year for each, and was prepared at the Theoretical Microfluidics (TMF) group at DTU Nanotech in the spring semester 2009.

We would like to thank the group of Prof. Thomas Laurell at the University of Lund for giving us valuable insights in the practical aspects of acoustofluidics. Furthermore we would also like to thank Jacob Riis Folkenberg at FOSS for giving us ideas on the separation of lipids in milk.

At DTU Nanotech we would especially like to thank M.Sc. student Rune Barnkob for his tireless help and limitless patience when we had questions or problems regarding MATLAB or standing waves in the fluid. We would also like to thank him for sharing his useful experimental results with us, which helped us validate our theoretical model. Last but not least our very deepest gratitude goes to our supervisor Prof. Henrik Bruus for his deep understanding of fluidics and the math involved. He has also been a good guideline on how to improve the writing and presentation of this thesis.

The content of the thesis corresponds to 98 written pages when not counting the blank pages. Due to demands from the Danish Ministry of Education, we are required to write who is responsible for which parts of the thesis. Let $p = \{n \in \mathbb{N} \mid n \leq p_{\text{last}}\}$ where p_{last} is the last page of the thesis. Using this we have made the following division of pages p

$$p_{\text{Anders}} = \{p \mid p \equiv 0 \pmod{3}\}, \quad (1)$$

$$p_{\text{Lasse}} = \{p \mid p \equiv 1 \pmod{3}\}, \quad (2)$$

$$p_{\text{Mikkel}} = \{p \mid p \equiv 2 \pmod{3}\}. \quad (3)$$

It should be understood such that the person responsible for the pages above wrote the initial draft while the two others reviewed it. Chapters 1 and 13 were written together.

Lasse Mejling Andersen, Anders Nysteen, and Mikkel Settnes
DTU Nanotech – Department of Micro and Nanotechnology
Technical University of Denmark
June 18, 2009

Contents

List of Figures	xii
List of Tables	xiii
List of Symbols	xv
1 Introduction	1
1.1 Background for Lab-on-a-chip Systems	1
1.2 Acoustophoresis	2
1.3 Experimental Motivation	2
1.4 Outline of the Thesis	3
I Theory	7
2 Governing Equations and Perturbation Theory	9
2.1 Momentum and Density	9
2.2 Perturbation Theory	10
2.2.1 Zeroth-order Perturbation Equations	11
2.2.2 First-order Perturbation Equations	11
2.2.3 Second-order Perturbation Equations	11
3 Acoustic Waves in Fluids	13
3.1 Inviscid First-order Acoustic Field	13
3.1.1 The Wave Equation for Irrotational First-order Inviscid Velocity Per- turbation	13
3.1.2 Inviscid First-order Harmonic Time-dependent Waves	14
3.2 First-order Viscid Acoustic Field	14
3.2.1 Viscid Harmonic Time-dependent Waves in First-order	15
3.3 Condition for Incompressible Behavior	17
3.4 Inviscid Second-order Acoustic Field	19
3.5 Calculation of Time Average	20

4	Resonance in First-order Theory	21
4.1	Acoustic Resonance in a Single-domain System	21
4.1.1	Considering the Perturbation Parameter and the First-order Velocity	23
4.1.2	Energy in the Resonator	24
5	Forces on Microparticles	27
5.1	The Potential Flow	27
5.2	The Average Force For Second-order Perturbation	28
5.2.1	Calculation of the Velocity Potential	29
5.3	Forces Acting on a Particle in a Plane Running Wave	34
5.4	Forces Acting on a Particle in an Arbitrary Wave	37
5.5	Pressure Force on a Single Particle in a Standing Wave	41
5.6	Visualizing the Pressure Force and the Idea Behind Particle Separation	42
5.7	Considering the Pressure Force in 2D	43
II	Discussion of Applications in the Single-Particle Approach	45
6	Analytic Solution for Single-Particle	47
6.1	Travel Time	47
6.2	Distance Traveled in Longitudinal Direction	49
6.3	Experimental Verification of Theory	51
7	Introduction to Separating Systems	53
7.1	The Channel Setup	53
7.2	The Simulations	55
8	Separation of Red Blood Cells and Lipid Particles	57
8.1	Lipid Size	58
8.2	Finding the Flow Rate	59
8.3	One-inlet Channel	59
8.4	Three-inlet Channel	61
8.5	Five-inlet Channel	61
8.6	A $3/2$ λ -harmonic System	61
8.7	Summary	63
9	Separation of Red and White Blood Cells	65
9.1	Separation by Different Channel Designs	65
9.1.1	Separation in BWB-system, Varying Inner Edge of Blood Inlet	67
9.1.2	Separation in WBWBW-system, With Variable Width of Blood Inlet	69
9.1.3	Separation in WBWBW-system, With Variable Position of Blood Inlet	70
9.2	Concentration of White Blood Cells	71
9.3	Changing the Transport Medium	72
9.4	Summary	74

10 Separation of Lipid Particles in Milk	75
10.1 Design Considerations	75
10.2 Analytical View on the Sorting	78
10.3 An Idea for Milk Separation in Practice	79
10.4 Summary	80
11 Other Possible Applications of the Pressure Force	81
11.1 Size-sorting of Particles with $\Phi > 0$	81
11.2 Creation of Pulses of Particles	81
III Neglected Effects	85
12 Neglected Effects	87
12.1 Longitudinal Modes	87
12.2 The Influence of the Viscosity on the Pouseille-flow	93
12.3 The Fåhræus effect and Fåhræus–Lindqvist effect	95
12.4 Temperature Dependence	96
12.5 Effects of Concentration	97
12.6 Diffusion	98
12.7 Many Particle Forces — Secondary Bjerknes Force	100
12.8 Acoustic Streaming	103
12.9 Summary of Neglected Effects	107
13 Conclusion	109
13.1 Outlook	110
IV Appendices	111
A Bernoulli’s Equation for Incompressible Inviscid Fluids	113
B Multipole Solution to the Spherical Wave Equation	115
C Scattered Wave From Incoming Traveling Plane Wave	121
D RBC/Lipid Separation, Five-inlet	123
D.1 Varying the Position of the Blood Inlets	123
D.2 Varying the Width of the Blood Inlets	124
E Derivation of the Acoustic Streaming Term	127
F Temperature Dependence	131
G Gor’kov’s Article	133

H	MATLAB Source Code	137
H.1	Least-square Fit	137
H.1.1	Source Code for <code>y0Ft.m</code>	137
H.1.2	Source Code for <code>Fit_E_ky.m</code>	138
H.2	Simulation of Single-particle in Rectangular Channel	139
H.2.1	Source Code for <code>constants.m</code>	139
H.2.2	Source Code for <code>Pos_Equation.m</code>	140
H.2.3	Source Code for <code>CalcPosition.m</code>	142
	Bibliography	147

List of Figures

1.1	(a) Principal sketch of the RBC/lipid chip. (b) The front of the microchip. (c) The back of the chip	2
1.2	(a) Sketch of the standing wave in the channel. (b) A picture of the three-outlet system	3
4.1	Sketch of the resonator system	22
5.1	Sketch of the pressure force and channel	43
6.1	Sketch of rectangular channel and coordinate system	48
6.2	(a) 3D-plot of the Pouseille flow. (b) A plot of the Pouseille-flow with more and more terms	50
6.3	Picture from the Tracker program	52
6.4	Fit of experimental and analytical data	52
7.1	Sketch of the inlets and outlets of the channel	54
8.1	Particle trajectories for RCB and lipid-particle.	57
8.2	(a) Distribution of lipid particles. (b) Trajectories of lipid particles with various sizes	58
8.3	(a) Sketch of a one-inlet channel RBC/lipid system. (b) The results for a one-inlet RBC/lipid system	59
8.4	(a) Sketch of a three-inlet channel system for RBC/lipid. (b) Plot of the lengths required for a three-inlet RBC/lipid system	60
8.5	Sketch of the $3\lambda/2$ harmonic system	62
8.6	(a) A comparison of the Pouseille-flow in two RBC/lipid systems. (b) Results for a $3\lambda/2$ RBC/lipid system	63
9.1	(a) The BWB three-inlet system for RBC/WBC separation. (b) Results for a BWB three-inlet system for RBC/WBC separation.	66
9.2	Sketch of blood inlet at the edges of the channel	67
9.3	(a) The width of the inner outlet in a RBC/WBC system. (b) The separation length as a function of the position of the inner edge for a RBC/WBC system	68
9.4	Sketch of five-inlet system with constant width	69
9.5	(a) The separation length as a function of the blood-inlet width in a RBC/WBC system. (b) The required inner outlet width in a RBC/WBC system	70

9.6	(a) Sketch of five-inlet system with varying position. (b) Separation length as a function of the center of the inlet for a RBC/WBC system.	71
9.7	(a) Minimum separation length. (b) The required inner outlet width for a RBC/WBC system	72
9.8	(a) Sketch of a wide center-outlet system for concentration of WBC. (b) Sketch of a narrow center-outlet system for concentration of WBC	73
9.9	(a) Concentration of WBCs as a function of length for wide-outlet. (b) Concentration of WBCs as a function of length for narrow-outlet	74
10.1	(a) Particle trajectories for milk lipids. (b) Channel setup for lipid particle separation in milk	76
10.2	(a) Particle trajectories of lipid particles in milk. (b) Required length for separation of all particles larger than D_0	77
10.3	Comparison of numerical and analytic data	78
10.4	(a) Particle trajectories of lipid particles in milk. (b) Required length for separation of all particles larger than D_0	79
10.5	A sketch of a system for separation of fat in milk	80
11.1	(a) Sketch of a setup for size-sorting of particles with $\Phi > 0$. (b) Sketch of a system for making pulses	82
12.1	(a) The normalized acoustic potential and RBC trajectory for $k_x = 0$. (b) The normalized acoustic potential for $k_y = 0$	88
12.2	(a) The normalized acoustic potential with $n_y = 1$ and $n_x = 1$. (b) $n_y = 1$ and $n_x = 3$	90
12.3	(a) The normalized acoustic potential with $n_y = 1$ and $n_x = 25$. (b) The normalized acoustic potential with $n_y = 1$ and $n_x = 3$ with trajectories for different flow velocities.	91
12.4	(a) Cross-section of Pouseille-flow with various viscosities. (b) Cross-section of Pouseille-flow with constant viscosity	93
12.5	(a) Comparison of the Pouseille-flow in the middle of the channel. (b) Ratio of Pouseille-flows with various viscosities.	94
12.6	(a) Plot of the Fåhræus-effect. (b) Plot of the Fåhræus–Lindqvist effect	95
12.7	(a) Plot of temperature dependence of Φ -factors. (b) Ratio of Φ -factors as a function of temperature	97
12.8	A sketch of the standing wave problem	104
D.1	Sketch of a five-inlet channel system for RBC/lipid varying the center.	123
D.2	(a) Plot of the lengths required for a five-inlet RBC/lipid system varying the center. (b) Zoom of plot (a)	124
D.3	(a) Sketch of a five-inlet channel system for RBC/lipid varying the width. (b) Plot of the lengths required for a five-inlet RBC/lipid system varying the width	125

List of Tables

7.1	Channel dimensions	53
7.2	Properties of the fluids	56
7.3	Properties of the particles	56
7.4	Other parameters	56
12.1	Summary of the neglected effects	108
F.1	Viscosity and speed of sound as a function of temperature	131

List of Symbols

The following table presents the symbols we have used in the thesis. The first part contains the physical variables sorted alphabetically. Greek letters are sorted after their spelling in English. The last part contains the mathematical symbols and functions used in the thesis.

Symbol	Description	Unit
\mathcal{A}	Area	m^2
α	Perturbation parameter	
β	Compressibility	Pa^{-1}
β_{visc}	Related to the second viscosity	
c_a	Speed of sound in fluid	m s^{-1}
D	Diameter	m
E_{ac}	Acoustic energy density	J m^{-3}
\mathbf{e}_r	The radial unit vector	
\mathbf{e}_j	The unit vector in the j -direction	
ε	The spatial averaged-energy density in a resonator	J m^{-3}
η	Dynamical viscosity parameter	Pa s
\mathbf{F}	Force	N
\mathbf{F}_{drag}	The Stokes-drag force	N
$\mathbf{F}_{\text{pressure}}$	The pressure force	N
f	Frequency	s^{-1}
γ	Acoustic damping factor	
H_c	Standard haematocrit	
H_{ct}	Dynamic haematocrit	
h	Channel height	m
\mathbf{J}_E	Energy flux	$\text{J m}^{-2} \text{s}^{-1}$
\mathbf{k}	Wave vector	m^{-1}
k, k_0	Wavenumber	m^{-1}
L	Channel length	m
ℓ	Amplitude of simple resonator	m
λ	Wavelength	m
N	Number of particles	
\mathbf{n}	Surface outward normal vector	

Continued on next page

Continued from previous page

Symbol	Description	Unit
$n, n_{x/y}$	Mode number	
ν	Kinematic viscosity	$\text{m}^2 \text{s}^{-1}$
ω	Angular frequency	rad s^{-1}
p_i	The i th order perturbation of pressure	N m^{-2}
Φ	Φ -factor in pressure force	
ϕ	Velocity potential	$\text{m}^2 \text{s}^{-1}$
ϕ_{in}	Incoming velocity potential	$\text{m}^2 \text{s}^{-1}$
ϕ_{sc}	Scattered velocity potential	$\text{m}^2 \text{s}^{-1}$
Π_{ij}	Momentum flux density tensor	Pa m^{-2}
ψ	Stream function	$\text{m}^2 \text{s}^{-1}$
Q	Volume flow rate	$\text{m}^3 \text{s}^{-1}$
R	Particle radius	m
\mathbf{r}	Position vector	m
Re	Reynold's number	
ρ_i	The i th order perturbation of mass density	kg m^{-3}
$\boldsymbol{\sigma}$	Cauchy stress tensor	N m^{-2}
$T = 1/f$	Period	s
T_x	Spatial period	m
t	Time	s
τ	Temperature	$^{\circ}\text{C}$
U	Scalar force potential	N m
V	Volume	m^3
\mathbf{v}_i	The i th order perturbation term of velocity vector	m s^{-1}
v_j	The j th component of velocity vector	m s^{-1}
$v_x(y)$	Velocity flow profile	m s^{-1}
w	Channel width	m
x	Longitudinal direction of flow velocity	m
y	Transverse direction, width	m
z	Transverse direction, height	m
\ll	Much smaller than	
\gg	Much larger than	
\sim	Of the same order	
\approx	Approximately equal to	
\equiv	Equivalent by definition	
\propto	Proportional to	
$\partial_i = \partial/\partial i$	Partial derivative with respect to i	
$\partial\Omega$	Domain boundary of Ω	
$\Delta \circ$	A change in \circ	
$\delta \circ$	An infinitesimal change in \circ	
$\delta(\circ)$	The 1D delta-function of \circ	
$\delta^3(\circ)$	The 3D delta-function of \circ	

Continued on next page

Continued from previous page

Symbol	Description	Unit
δ_{lm}	Kronecker's delta	
e	Euler's constant, $\ln(e) = 1$	
i	The imaginary unit	
$\text{Im}\{\circ\}$	The imaginary part of \circ	
$\log(\circ)$	The natural logarithm of \circ	
m, n, p	Integer	
\mathbb{N}	Set of positive integers	
\mathbb{N}_0	Set of non-negative integers	
∇	Nabla or gradient operator	
$\nabla \cdot$	Divergence operator	
$\nabla \times$	Rotation operator	
∇^2	Laplace operator	
$\mathcal{O}(x^n)$	Terms of order x^n and higher powers	
$\text{Re}\{\circ\}$	The real part of \circ	
\mathbb{Z}	Set of integers	
$\langle \circ \rangle$	Time average of \circ	
$ \circ $	The absolute value of \circ	
$(\circ)^*$	The complex conjugate of \circ	
$(\dot{\circ})$	Differentiated with respect to the argument of \circ	

Chapter 1

Introduction

1.1 Background for Lab-on-a-chip Systems

A lab-on-a-chip (LOC) is a device that seeks to integrate several laboratory functions on a single (often silicon) chip in the μm -scale. The complex nature of the LOC-systems leads to combination of research areas including microelectronics, fluid mechanics, optics, and biotechnology. The advantage of scaling down is the obvious reduction of required sample size, along with the possibility of analyzing samples considerably faster and simpler than in conventional laboratories. This might make it possible to eliminate the need for specialized human operators. Furthermore the LOC-systems could make way for a mass production of cheap single-use chips which are suitable for field use, thus reducing the need for large and specialized laboratorial facilities.

However, the LOC-systems cannot be made by simple scaling down, as the surface forces for example have a far greater importance due to significantly increased surface area compared to volume size. This means that surface forces like viscosity, surface tension *etc.* dominate body forces like gravity and buoyancy. The LOC-systems therefore call for an understanding of these microscopic effects leading to manipulation of liquids and particles in the μm -scale. This thesis will deal with the manipulation of particles in μm -channels in a LOC-system.

The manipulation can be carried out by many different processes including magnetophoresis, electrophoresis, or dielectrophoresis depending on the specific system. Although these methods are well documented experimentally, they all have some common disadvantages. First of all they often demand integrated micro-structured electrodes or magnetic materials which complicate and add costs to the fabrication of the chips. Secondly they require the samples to have specific electric or magnetic properties to work. As an example, electrophoresis exploits the different charge of the sample particles to accelerate them in an electric field [35], [36]. Dielectrophoresis requires a noticeable difference in the dielectric constant of the particle and the surrounding fluid [40], and magnetophoresis uses coated magnetic beads which bind to the sample particles [13], [19]. These requirements may not always be fulfilled by the sample particles, and furthermore there is a risk that the electric or magnetic field could damage the sample which often is biological material or cells.

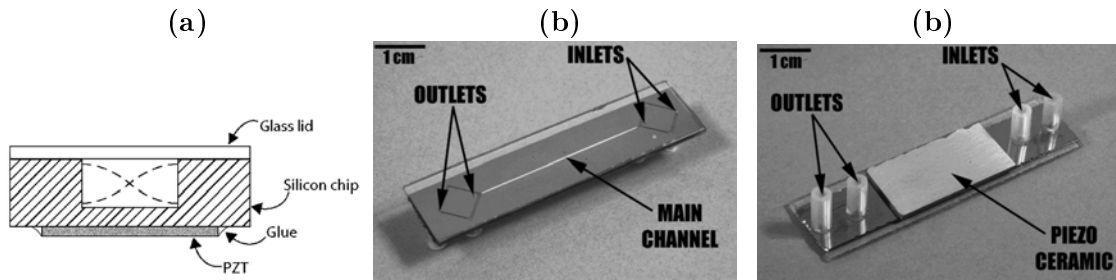


Figure 1.1: (a) A principle sketch of the system used to create the resonant standing wave in a microchannel, taken from [24]. (b) The front of a the silicon based microchip produced in the Laurell group at Lund University, taking from [42]. (c) The back of the microchip shown in Fig. 1.1b, taken from [42].

1.2 Acoustophoresis

The limitations of the other particle separation methods mentioned above is the reason for the increasing interest for finding other ways of separation. Acoustophoresis is a recently considered method allowing separation of all types of particles as long as they differ from the surrounding medium with regard to their acoustic properties.

Acoustophoresis is a unifying term for all effects influencing particles in a fluid due to an acoustic field which in the experimental setup becomes a standing acoustic wave in the channel. Spatial control, manipulation, and separation of particles in fluids by means of ultrasonic standing waves have received re-newed interest in the past decade due to its application in the emerging field of microfluidics. In this thesis we will investigate an example of acoustophoresis — namely the pressure force. The pressure force is a non-linear effect due to particles or other solid objects being present in the sound-field in the fluid leading to a time-independent pressure force acting on the particles.

The pressure force originating from a standing wave produced by a resonator was at first theoretically described for incompressible spheres by King in 1934 [15]. The theory was later extended by Yosioka and Kawasima in 1962 to include compressible spheres [43]. Their work was summarized in a short paper by Gor'kov, [14].

1.3 Experimental Motivation

Several groups have used the theoretical results mentioned in Section 1.2 later on for various particle manipulations and sorting applications [27], [29], [30], [32], [37], and [41]. In this thesis we will focus on systems like the ones proposed by the Thomas Laurell group at Lund University [28], [29]; some of the systems are sketched in Fig. 1.1. They work with a silicon chip with a lid of Pyrex in which a microfluidic channel system is etched as shown in Fig. 1.1b. The sample solution is fed into a separation channel (the main channel) in a laminar flow. In the channel, the solution is exposed to a standing wave excited by a piezo-electrical actuator glued to the back of the silicon chip [24], see Fig. 1.1c. The standing wave created by resonance will in both the transverse and longitudinal direction of the channel give rise to a pressure force. The fundamental transverse mode results in a pressure nodal plane along the center of the channel and an anti-nodal plane along the

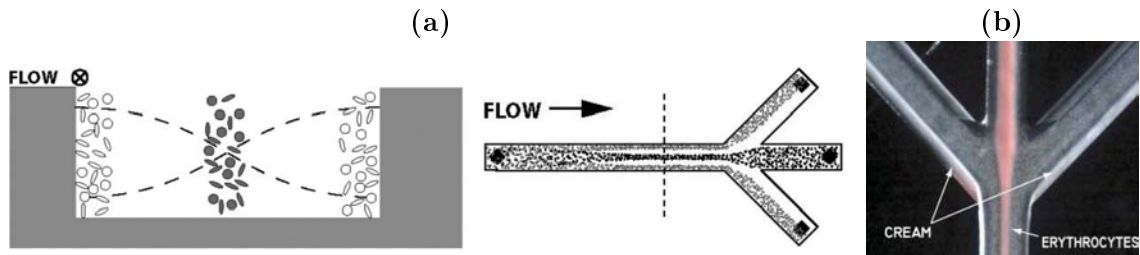


Figure 1.2: (a) A sketch of the standing wave in the channel, and how it is separating the particles in the nodal and anti-nodal planes of the channel, taken from [28] (b) The three-outlet system proposed as a mean to particle separation by the Thomas Laurell group at Lund University, from [28].

edges of the channel when using a channel with a width of half the wavelength of the standing wave as shown in Fig. 1.2a. The particles will move either towards the nodal or anti-nodal plane depending on their density and compressibility compared to those of the fluid. The laminar flow ensures that the particles are moving forward in the channel and the separation is achieved when the particles are leaving the channel in one of the outlets as shown in Fig. 1.2b.

The advantage of this system is first-of-all, that we by resonance are able to build up a considerable acoustic energy density in the channel without a perfect coupling between channel and actuator. Secondly, the acoustic forces have been shown not to be harmful to biological samples and this system is therefore very suitable as a tool in bio-analysis [31].

1.4 Outline of the Thesis

We have divided the thesis into three parts. In Part I we go through the required theory to be able to understand the particle movement described in a simple model. Part II concerns possible applications of the pressure force, and in Part III we discuss the neglected effects which we did not consider in the previous parts.

Part I, Chapter 2: Governing Equations and Perturbation Theory

First of all we will be treating the general theoretical background of microfluidics. We will investigate how the governing equations lead to a formulation suitable for the treatment of the time-independent effects based on a second-order perturbation scheme.

Part I, Chapter 3: Acoustic Waves in Fluids

We will use the governing equations as a starting point for a treatment of acoustic waves in both the inviscid and viscid case. In the first-order inviscid case it leads to the formulation of the velocity potential for irrotational first-order velocity, and the spatial field amplitudes are shown to fulfill the lossless Helmholtz equations. We will discuss how small viscid terms together with harmonic time-dependence give rise to the lossy Helmholtz equation.

In the last part of the general theory we derive expressions for the second-order time-averaged acoustic fields.

Part I, Chapter 4: Resonance in First-order Theory

We will present a classical example of a resonator without or with damping to give a basic understanding of acoustic resonance effects. This becomes helpful in the context of the later chapters where resonance plays an important role in the understanding of the standing acoustic waves.

Part I, Chapter 5: Forces Acting on Microparticles in an Acoustic Field in an Inviscid Fluid

Several groups of experimentalists have quoted the pressure force term from Gor'kov, [14], as the theoretical background for their experimental applications of particle manipulations, see for example [42].

In this chapter we will leap from general microfluidic theory to a re-derivation of the very condensed article from 1962 by Gor'kov [14]. We will work through it thoroughly and derive the expression for the pressure force to get a deeper understanding of the, by Gor'kov often omitted, calculations and limitations leading to this much cited expression.

Part II, Chapter 6: Analytic Solution in Simple Channel

This chapter opens the part of the discussion of applications of the pressure force. We will derive an analytical expression for the trajectory of a single particle affected by a standing wave in a laminar flow and compare it to experimental results.

Part II, Chapter 7: Introduction to Separating Systems in the Single-Particle Approach

This chapter is dedicated to a description of our channel setup and the parameters we use in our simulations.

Part II, Chapter 8: Separation of Red Blood Cells and Lipid Particles

The first separation application we will analyze is inspired by the Laurell group's attempt to separate red blood cells and lipid cells in blood plasma [24], [28], [29]. Red blood cells are affected by the pressure force and move towards the nodal plane, where the lipid particles move towards the anti-nodal plane. We analyze the system by numerically solving the derived coupled differential equations in MATLAB showing the length of channel required in order to obtain separation. Finally we will propose different designs where we consider both the separation length and throughput of the sample solution.

Part II, Chapter 9: Separation of Red and White Blood Cells

In this chapter we will consider separation of red and white blood cells in the light of the ongoing collaboration between DTU Nanotech and The University of Santa Barbara [6]. This separation could be useful in terms of medical research, if we want to make measurements on white blood cells without having red blood cells in the test sample.

The red and white blood cells are affected in the same direction by the pressure force, but the magnitude of the force is different because of the various physical properties of the

particles. We will discuss how the channels should be designed to be able to separate the particles.

Part II, Chapter 10: Separation of Lipid Particles in Milk

This chapter considers separation of lipid particles in milk which is an application under development at the company Foss. In this application the particles only differ in size, and we will discuss a possible design for separating all the particles above a certain diameter from the milk. Furthermore we will examine if we are able to find a simple analytic solution to describe the required channel length to carry out the separation.

Part II, Chapter 11: Other Possible Applications of the Pressure Force

In this chapter we introduce other possible applications of the pressure force, that we have not seen in other papers.

Part III, Chapter 12: Neglected Effects

In the numerical and analytical analyses we neglect numerous effects. This chapter is a brief introduction to the neglected effects and a discussion of how large an impact they presumably would have on the results. The effects include the longitudinal modes which by actuation arise in the channel. The experimentally reported Fåhræus–Lindqvist effect is discussed together with analyses of the temperature dependence of the system parameters. Furthermore we will estimate the forces which arise if we try to go beyond the single-particle picture. These effects include concentration and diffusion effects and interparticle forces expressed by the secondary Bjerknes force. Finally we will give an estimate of the second-order effect called acoustic streaming which is analyzed as a boundary effect caused by the viscosity of the fluid in the boundary area. The chapter will be concluded with a discussion of which of the mentioned effects that have the biggest contribution to the forces acting on a particle in the fluid.

Part I
Theory

Chapter 2

Governing Equations and Perturbation Theory

In this thesis we describe classical fluid dynamics using the continuum hypothesis in which all references to the molecular structure of the liquid are replaced by the basic concept of the fluid „particle”. The fluid particle represents a volume of liquid much smaller than the macroscopic length scales, but large enough $\sim (10 \text{ nm})^3$ to contain a number of molecules big enough to ensure well-defined averages of *e.g.* the density $\rho(\mathbf{r}, t)$ and the momentum density $\rho(\mathbf{r}, t)\mathbf{v}(\mathbf{r}, t)$. In the following we limit ourselves to the equations related to the conservation of momentum and mass, thus disregarding thermal effects.

The central fields in fluid dynamics are the velocity field $\mathbf{v}(\mathbf{r}, t)$, the density field $\rho(\mathbf{r}, t)$, and the pressure field $p(\mathbf{r}, t)$. Often we drop the explicit reference to the time or spatial dependence.

We assume that the systems considered are isothermal. Furthermore in the thesis we will be using the customary *Eulerian* field description *i.e.* that the fields are considered for fixed points \mathbf{r} at all times t , so that \mathbf{r} is independent of t . As an example we emphasize that the Eulerian velocity field $\mathbf{v}(\mathbf{r}, t)$ is the velocity of the fluid at a given point \mathbf{r} and time t . The alternative is the *Lagrangian* description involving changing position vector $\mathbf{r}(t)$ of a fluid particle which means that \mathbf{r} is dependent of t .

2.1 Momentum and Density

The change of momentum density, essentially Newton’s second law adapted to the Eulerian field description, leads to the non-linear Navier–Stokes equation. For a compressible, Newtonian, and viscid fluid we adopt the notation of [5],

$$\rho[\partial_t \mathbf{v} + (\mathbf{v} \cdot \nabla) \mathbf{v}] = -\nabla p + \eta \nabla^2 \mathbf{v} + \beta_{\text{visc}} \eta \nabla(\nabla \cdot \mathbf{v}) + \mathbf{f}_{\text{body}}, \quad (2.1)$$

where η is the dynamical viscosity parameter of the fluid. β_{visc} is related to the second viscosity caused by internal friction during compression. The value $\beta_{\text{visc}} \eta$ is not easily determined, but we will in the following use the approximation $\beta_{\text{visc}} = 5/3$ in accordance with Stoke’s surmise, see [5]. In the following we are ignoring any form of body forces acting on the entire fluid such as gravity or magnetic forces, *i.e.* $\mathbf{f}_{\text{body}} = 0$.

The conservation of mass leads to the continuity equation

$$\partial_t \rho = -\nabla \cdot (\rho \mathbf{v}). \quad (2.2)$$

It is worth noting that in the case of an incompressible fluid we have ρ is constant and thus the continuity equation reduces to $\nabla \cdot \mathbf{v} = 0$.

Besides the governing equations described above we will be using the thermodynamical equation of state expressing the pressure in terms of the density to eliminate one variable from Eqs. (2.1) and (2.2), thus we have

$$p = p(\rho). \quad (2.3)$$

2.2 Perturbation Theory

We consider the thermal equilibrium state described by the three fields: velocity \mathbf{v}_0 , pressure p_0 , and density ρ_0 . We have assumed that the unperturbed state is isentropic, homogeneous, and static *i.e.* $\mathbf{v}_0 \equiv \mathbf{0}$.

In the following we consider small oscillatory movements of a compressible fluid. These movements, interpreted as an acoustic field, are assumed to be a minor perturbation of the thermal equilibrium of the fluid. This implies that the changes in velocity, pressure, and density are small relative to their thermal equilibrium values. Including perturbation terms up to second order, we get

$$\mathbf{v} = \mathbf{v}^{(0)} + \alpha \mathbf{v}^{(1)} + \alpha^2 \mathbf{v}^{(2)} = \mathbf{v}_0 + \mathbf{v}_1 + \mathbf{v}_2 = \mathbf{0} + \mathbf{v}_1 + \mathbf{v}_2, \quad (2.4a)$$

$$\rho = \rho^{(0)} + \alpha \rho^{(1)} + \alpha^2 \rho^{(2)} = \rho_0 + \rho_1 + \rho_2, \quad (2.4b)$$

$$p = p^{(0)} + \alpha p^{(1)} + \alpha^2 p^{(2)} = p_0 + p_1 + p_2, \quad (2.4c)$$

In Eq. (2.4) we have made the perturbation parameter implicit meaning that the first-order velocity \mathbf{v}_1 is understood to contain the perturbation parameter.

We furthermore express the pressure in terms of the density as suggested in Eq. (2.3). This is accomplished with a Taylor expansion around the unperturbed value $p_0 = p(\rho_0)$. Including terms up to second-order we get the following expression,

$$p \simeq p_0 + \partial_\rho p \Big|_{\rho=\rho_0} (\rho - \rho_0) + \frac{1}{2} \partial_\rho^2 p \Big|_{\rho=\rho_0} (\rho - \rho_0)^2 \quad (2.5a)$$

$$\simeq p_0 + \partial_\rho p \Big|_{\rho=\rho_0} \rho_1 + \partial_\rho p \Big|_{\rho=\rho_0} \rho_2 + \frac{1}{2} \partial_\rho^2 p \Big|_{\rho=\rho_0} (\rho_1 + \rho_2)^2 \quad (2.5b)$$

$$\simeq p_0 + c_a^2 \rho_1 + c_a^2 \rho_2 + \frac{1}{2} \partial_\rho (c_a^2) \rho_1^2, \quad (2.5c)$$

where we have neglected terms of third-order or higher in Eq. (2.5b). We have introduced the speed of sound in the fluid, c_a , in terms of the isentropic derivative at $\rho = \rho_0$

$$c_a^2 \equiv \left(\frac{\partial p}{\partial \rho} \right)_s. \quad (2.6)$$

In the first-order approximation c_a is assumed to be constant.

2.2.1 Zeroth-order Perturbation Equations

Inserting the perturbed terms in Eqs. (2.1), (2.2), and (2.3) we get the first-order equations

$$0 = -\nabla p_0, \quad (2.7a)$$

$$\partial_t \rho_0 = 0, \quad (2.7b)$$

$$p = p(\rho_0) = p_0. \quad (2.7c)$$

The only solutions to the equations Eq. (2.7) are evidently constants, and we conclude that the zeroth-order terms corresponding to thermal equilibrium are constants given by ρ_0 and p_0 .

2.2.2 First-order Perturbation Equations

Inserting the perturbations again this time considering only terms of first-order we get the governing equations to first-order

$$\rho_0 \partial_t \mathbf{v}_1 = -c_a^2 \nabla \rho_1 + \eta \nabla^2 \mathbf{v}_1 + \beta_{\text{visc}} \eta \nabla (\nabla \cdot \mathbf{v}_1), \quad (2.8a)$$

$$\partial_t \rho_1 = -\nabla \cdot (\rho_0 \mathbf{v}_1) = -\rho_0 \nabla \cdot \mathbf{v}_1, \quad (2.8b)$$

$$p_1 = c_a^2 \rho_1, \quad (2.8c)$$

where we notice that the constant zeroth-order terms have been pulled outside the differential operators, and p_1 has been expressed by ρ_1 using Eq. (2.5c).

2.2.3 Second-order Perturbation Equations

Using the same approach as above we find the second-order governing equations

$$\rho_1 \partial_t \mathbf{v}_1 + \rho_0 \partial_t \mathbf{v}_2 + \rho_0 (\mathbf{v}_1 \cdot \nabla) \mathbf{v}_1 = -\nabla p_2 + \eta \nabla^2 \mathbf{v}_2 + \beta_{\text{visc}} \eta \nabla (\nabla \cdot \mathbf{v}_2), \quad (2.9a)$$

$$\partial_t \rho_2 = -\rho_0 \nabla \cdot \mathbf{v}_2 - \nabla \cdot (\rho_1 \mathbf{v}_1), \quad (2.9b)$$

$$p_2 = c_a^2 \rho_2 + \frac{1}{2} \partial_\rho (c_a^2) \rho_1^2. \quad (2.9c)$$

Chapter 3

Acoustic Waves in Fluids

3.1 Inviscid First-order Acoustic Field

If we neglect viscid damping in the linear first-order approximation, we get from Eq. (2.8)

$$\rho_0 \partial_t \mathbf{v}_1 = -c_a^2 \nabla \rho_1, \quad (3.1a)$$

$$\partial_t \rho_1 = -\rho_0 \nabla \cdot \mathbf{v}_1, \quad (3.1b)$$

$$p_1 = c_a^2 \rho_1. \quad (3.1c)$$

Our goal is to find wave equations for the first-order quantities ρ_1 , p_1 and \mathbf{v}_1 .

We take the divergence of Eq. (3.1a), exploit that temporal and spatial differential operators commute, and obtain

$$\rho_0 \partial_t (\nabla \cdot \mathbf{v}_1) = -c_a^2 \nabla \cdot (\nabla \rho_1). \quad (3.2)$$

Combining this with Eq. (3.1b) we get $-\partial_t \partial_t \rho_1 = -c_a^2 \nabla \cdot (\nabla \rho_1)$ or

$$\partial_t^2 \rho_1 = c_a^2 \nabla^2 \rho_1. \quad (3.3)$$

From Eq. (3.1c) it is immediately seen that we have a corresponding equation for the first-order pressure perturbation

$$\partial_t^2 p_1 = c_a^2 \nabla^2 p_1. \quad (3.4)$$

3.1.1 The Wave Equation for Irrotational First-order Inviscid Velocity Perturbation

A proper wave equation for the velocity perturbation is not obtainable for arbitrary velocities. We therefore limit ourselves to the case of an irrotational flow, *i.e.* $\nabla \times \mathbf{v} = \mathbf{0}$, which makes us able to determine a velocity potential as

$$\mathbf{v}_1 = \nabla \phi_1. \quad (3.5)$$

With this definition Eq. (3.1a) leads to

$$\rho_0 \partial_t \nabla \phi_1 = -c_a^2 \nabla \rho_1 \quad \Rightarrow \quad \rho_1 = -\frac{\rho_0}{c_a^2} \partial_t \phi_1 + \nabla \times \mathbf{A} \quad \Rightarrow \quad \rho_1 = -\frac{\rho_0}{c_a^2} \partial_t \phi_1, \quad (3.6)$$

where we choose the vector field to be $\mathbf{A} = \mathbf{0}$ without loss of generality. According to Eq. (3.1c) the first-order perturbation in pressure is

$$p_1 = -\rho_0 \partial_t \phi_1. \quad (3.7)$$

We notice that the Eqs. (3.5), (3.6), and (3.7) constitutes the connection between all three desired first-order quantities and the first-order scalar velocity potential ϕ_1 . We have therefore reduced our problem in a given setting, where the first-order velocity field can be assumed irrotational, to finding the appropriate velocity potential.

The velocity potential can be found to fulfill the same type of wave equation as the other first-order perturbation quantities. This can be found by inserting Eqs. (3.5) and (3.6) in Eq. (3.1b),

$$\partial_t^2 \phi_1 = c_a^2 \nabla^2 \phi_1. \quad (3.8)$$

3.1.2 Inviscid First-order Harmonic Time-dependent Waves

We now assume that the velocity perturbation is varying harmonically in time with no time-independent terms, *i.e.* $\mathbf{v}_1 = \mathbf{v}_1(\mathbf{r})e^{-i\omega t}$. When we are looking at harmonic \mathbf{v}_1 , it is readily seen from equation Eq. (3.1a) that \mathbf{v}_1 in this case is a gradient field and thereby irrotational, and we can employ the results derived above.

One simple class of solutions to the wave equation with harmonic time-dependence is the plane traveling wave, of amplitude ϕ_A , propagating in the direction of the wave vector \mathbf{k}_0 and with angular frequency ω . In complex notation this is given as

$$\phi_1(\mathbf{r}, t) = \phi_A e^{i(\mathbf{k}_0 \cdot \mathbf{r} - \omega t)}. \quad (3.9)$$

Inserting this into the wave equation (3.8) gives the linear dispersion relation for sound waves in a fluid, $\omega^2 = c_a^2 |\mathbf{k}_0|^2$, or

$$\omega = c_a k_0. \quad (3.10)$$

Alternatively, we can consider the general class of time harmonic solutions *i.e.* the solutions which have the same harmonic time-dependence. This is expressed as

$$\phi_1(\mathbf{r}, t) = \phi_k(\mathbf{r})e^{-i\omega t}. \quad (3.11)$$

Inserting this into the wave equation for ϕ_1 , Eq. (3.8), using the dispersion relation, leads to the Helmholtz equation

$$\nabla^2 \phi_k(\mathbf{r}) = -k_0^2 \phi_k(\mathbf{r}). \quad (3.12)$$

This eigenvalue problem with k_0^2 as the eigenvalue will only allow certain values of the wave vector \mathbf{k}_0 for a given set of boundary conditions, which results in an eigenmode described by $\phi_k(\mathbf{r})$ and the harmonic time part.

3.2 First-order Viscid Acoustic Field

In the previous section we neglected damping in the linearized model to derive the Helmholtz equation for the first-order harmonic perturbation. Taking into account the attenuation of the waves caused by the atomic interaction, heat transfer, viscosity *etc.*, we can

no longer neglect the viscid terms in the first-order Navier–Stokes equation (2.8a),

$$\rho_0 \partial_t \mathbf{v}_1 = -c_a^2 \nabla \rho_1 + \eta \nabla^2 \mathbf{v}_1 + \beta_{\text{visc}} \eta \nabla (\nabla \cdot \mathbf{v}_1). \quad (3.13)$$

First of all we look for a partial differential equation describing the density (pressure) field. Taking the divergence of this equation, again exploiting that temporal and spatial differential operators commute, gives

$$\rho_0 \partial_t (\nabla \cdot \mathbf{v}_1) = -c_a^2 \nabla^2 \rho_1 + (1 + \beta_{\text{visc}}) \eta \nabla^2 (\nabla \cdot \mathbf{v}_1). \quad (3.14)$$

Using the continuity equation Eq. (2.8b) gives a partial differential equation in ρ_1 ,

$$\partial_t^2 \rho_1 = c_a^2 \nabla^2 \rho_1 + \frac{1}{\rho_0} (1 + \beta_{\text{visc}}) \eta \nabla^2 (\partial_t \rho_1). \quad (3.15)$$

From the connection between density and pressure to first order, Eq. (2.8c), it is clear that p_1 fulfills a similar equation.

3.2.1 Viscid Harmonic Time-dependent Waves in First-order

In the general case of a viscid fluid it is not possible to construct a similar equation for the perturbed velocity \mathbf{v}_1 . This is only possible in the case of an irrotational velocity field. In analogy with the inviscid case we furthermore limit ourselves to the important special case of harmonic time-dependence. Even in this situation the field is strictly speaking not irrotational as we are considering attenuation, but we conclude from Eq. (3.13) that we for a small viscosity η can treat the velocity field as a gradient field. Explicitly we see this by perturbation of the velocity in the viscosity η ,

$$\mathbf{v}_1 = \mathbf{v}_1^{(0)} + \eta \mathbf{v}_1^{(1)} = \nabla \phi_1 + \eta \mathbf{v}_1^{(1)} \quad (3.16)$$

When considering Eq. (3.13) with harmonic time-dependence this perturbation to first-order in η gives

$$-i\omega \rho_0 (\nabla \phi_1 + \eta \mathbf{v}_1^{(1)}) = -c_a^2 \nabla \rho_1 + \eta \nabla^2 (\nabla \phi_1) + \beta_{\text{visc}} \eta \nabla (\nabla^2 \phi_1) + \mathcal{O}(\eta^2), \quad (3.17)$$

$$-i\omega \rho_0 \eta \mathbf{v}_1^{(1)} = \nabla [-c_a^2 \rho_1 + \eta (1 + \beta_{\text{visc}}) \nabla^2 \phi_1 + i\omega \rho_0 \phi_1] + \mathcal{O}(\eta^2). \quad (3.18)$$

where $\mathcal{O}(\eta^2)$ refers to terms containing η^2 or any higher powers of η . Eq. (3.18) shows that to first-order in η the velocity field, ϕ_1 , shown in Eq. (3.16) is a gradient field and hence irrotational.

In analogy to the inviscid case, the assumption of harmonic time-variation leads to a class of solutions in ρ_1 given by

$$\rho_1(\mathbf{r}, t) = \rho_1(\mathbf{r}) e^{-i\omega t}. \quad (3.19)$$

Inserting this in equation Eq. (3.15) we arrive at

$$\omega^2 \rho_1(\mathbf{r}) = -c_a^2 \nabla^2 \rho_1(\mathbf{r}) + \frac{i\omega}{\rho_0} (1 + \beta_{\text{visc}}) \eta \nabla^2 \rho_1(\mathbf{r}), \quad (3.20)$$

or

$$\nabla^2 \rho_1(\mathbf{r}) = -\frac{\omega^2}{c_a^2} \left(1 - \frac{i(1 + \beta_{\text{visc}})\eta\omega}{\rho_0 c_a^2} \right)^{-1} \rho_1(\mathbf{r}) = -\frac{\omega^2}{c_a^2} (1 - 2\gamma i)^{-1} \rho_1(\mathbf{r}), \quad (3.21)$$

where we have defined the acoustic damping factor γ

$$\gamma \equiv \frac{(1 + \beta_{\text{visc}})\eta\omega}{2\rho_0 c_a^2}. \quad (3.22)$$

Equation Eq. (3.21) is the Helmholtz equation with complex wavenumber, if we define the modulus of the complex wavenumber as

$$k = \frac{\omega}{c_a} \frac{1}{\sqrt{1 - i2\gamma}}. \quad (3.23)$$

Insertion of typical parameter values as done in [5] and [22] we find the magnitude of the γ -factor,

$$\gamma \approx \frac{10^{-3} \text{ Pa s} \times 2\pi \times 2 \times 10^6 \text{ s}^{-1}}{2 \times 10^3 \text{ kg m}^{-3} \times (1483 \text{ m s}^{-1})^2} = 5.7 \times 10^{-6}, \quad (3.24)$$

thus justifying the Taylor expansion in the wavenumber to first-order in γ . This results in,

$$k = \frac{\omega}{c_a} \frac{1}{\sqrt{1 - i2\gamma}} \simeq \frac{\omega}{c_a} (1 + i\gamma) = k_0 (1 + i\gamma), \quad (3.25)$$

where $k_0 = \omega/c_a$ is the real-valued wavenumber of the inviscid case Eq. (3.12).

In this way we arrive at the Helmholtz equation for the harmonic varying density perturbation ρ_1 ,

$$\nabla^2 \rho_1(\mathbf{r}) = -\frac{\omega^2}{c_a^2} (1 - i2\gamma)^{-1} \rho_1(\mathbf{r}) \simeq -k_0^2 (1 + i\gamma)^2 \rho_1(\mathbf{r}) = -k^2 \rho_1(\mathbf{r}). \quad (3.26)$$

This is the lossy Helmholtz equation, of which possible solutions are damped traveling plane waves found directly in analogy to the inviscid Helmholtz equation by replacing k_0 with $k = k_0 (1 + i\gamma)$,

$$\rho_1(\mathbf{r}, t) = A e^{i(\mathbf{k}_0 \cdot \mathbf{r} - \omega t)} e^{-\gamma \mathbf{k}_0 \cdot \mathbf{r}}, \quad (3.27)$$

where A is a density amplitude. We notice that the exponential damped term has a damping length of $1/(k_0\gamma)$. Since we are observing attenuation in the system, this system cannot be sustained without an energy supply like a driving force.

We now return to \mathbf{v}_1 to find a similar equation to determine the spatial part of the velocity exploiting that we have already assumed a harmonic time-variation.

The harmonic time-dependence, shown for the density field in Eq. (3.19), changes the first-order continuity equation (2.8b) into

$$\partial_t \bar{\rho}_1 = -\rho_0 \nabla \cdot \mathbf{v}_1 \Leftrightarrow \nabla \cdot \mathbf{v}_1 = -\frac{\partial_t \rho_1}{\rho_0} = i\omega \frac{\rho_1(\mathbf{r})}{\rho_0}. \quad (3.28)$$

When treating only irrotational fields, we have

$$\nabla^2 \mathbf{v}_1 = \nabla(\nabla \cdot \mathbf{v}_1), \quad (3.29)$$

which together with the assumption of harmonic variation transforms the first-order Navier–Stokes equation including the viscid terms, Eq. (3.13), into

$$-i\omega\rho_0\mathbf{v}_1(\mathbf{r}) = -c_a^2\nabla\rho_1 + \eta(1 + \beta_{\text{visc}})\nabla\left(i\omega\frac{\rho_1(\mathbf{r})}{\rho_0}\right) \quad (3.30)$$

$$= -c_a^2(1 - i2\gamma)\nabla\rho_1(\mathbf{r}). \quad (3.31)$$

We notice that \mathbf{v}_1 can be written as a gradient field $\mathbf{v}_1 = \nabla\phi_1$, where we again introduce the first-order velocity potential ϕ_1 . We see from Eq. (3.31) that we can choose the first-order velocity potential as

$$\phi_1(\mathbf{r}, t) = -i\frac{c_a^2(1 - 2\gamma)}{\omega\rho_0}\rho_1(\mathbf{r})e^{-i\omega t}. \quad (3.32)$$

This implies the general formulation of the non-viscid connection between the first-order velocity potential and density, corresponding to Eq. (3.6),

$$\rho_1 = -\frac{\rho_0}{c_a^2(1 - i2\gamma)}\partial_t\phi_1 = -\frac{\rho_0k^2}{\omega^2}\partial_t\phi_1, \quad (3.33)$$

where we in the last equality have used the definition of the complex wavenumber, Eq. (3.23).

Eq. (3.33) turns into a wave equation for the first-order velocity potential with viscosity by remembering the continuity equation Eq. (2.8b),

$$\nabla^2\phi_1 = -\frac{1}{\rho_0}\partial_t\rho_1. \quad (3.34)$$

Inserting into Eq. (3.33) gives us the desired wave equation for the first-order velocity potential including viscosity, assuming an irrotational and harmonic first-order perturbation term

$$\nabla^2\phi_1 = \frac{k^2}{\omega^2}\partial_t^2\phi_1 = -k^2\phi_1. \quad (3.35)$$

We notice that this is the lossy Helmholtz equation as long as the considered viscosity is such that $k = k_0(1 + i\gamma)$ as shown in Eq. (3.25).

3.3 Condition for Incompressible Behavior

An incompressible fluid is much easier to describe, primarily because of the simple form of the continuity equation described in Chapter 2. In this section we want to analyze under which conditions the fluid can be considered as incompressible to first-order.

The first condition is the obvious one that $\Delta\rho/\rho_0 \ll 1$ in time-independent systems. This simply states that the relative change in density is small. To relate this to more tangible quantities, we want to relate $\Delta\rho$ to other quantities involved in the problem. Hence we consider the time-independent inviscid Navier–Stokes equation. From Eq. (2.1) we get

$$(\mathbf{v} \cdot \nabla)\mathbf{v} = -\frac{1}{\rho_0}\nabla p, \quad (3.36)$$

where we have made the assumption that we are considering an incompressible fluid in which the density is ρ_0 everywhere, corresponding to the zeroth-order perturbation in the density where the other perturbations are zero.

If we furthermore consider an irrotational flow, we notice that $2(\mathbf{v} \cdot \nabla)\mathbf{v} = \nabla(|\nabla\phi|^2) = \nabla(|\mathbf{v}|^2) = \nabla(v^2)$. Inserting this in Eq. (3.36), we get

$$\frac{1}{2}\nabla(v^2) + \frac{1}{\rho_0}\nabla p = \nabla\left[\frac{1}{2}v^2 + \frac{p}{\rho_0}\right] = \mathbf{0}, \quad (3.37)$$

where we have used that ρ_0 is independent of the spatial coordinate. From Eq. (3.37) we conclude that

$$\frac{1}{2}|\mathbf{v}|^2 + \frac{p}{\rho_0} = \text{constant}. \quad (3.38)$$

This is called Bernoulli's equation for incompressible steady flows.

From Eq. (3.38) it is now evident that any change in pressure is given by

$$\Delta p = -\rho_0 v \Delta(v^2). \quad (3.39)$$

Thus, we have that $\Delta p \sim \rho_0 v^2$. To first-order we concluded in Eq. (2.8c) that $\Delta p = p_1 = c_a^2 \rho_1$. Hence we observe that to first-order $\rho_1 \sim \rho_0 v_1^2 / c_a^2$. From $\Delta\rho_1 / \rho_0 \ll 1$ we get a necessary condition for incompressibility stated as

$$v_1^2 \ll c_a^2 \Rightarrow v_1 \ll c_a. \quad (3.40)$$

The condition stated in Eq. (3.40) is necessary but not sufficient if we are considering a non-steady flow *i.e.* a time-dependent flow. In this situation we notice from the continuity equation, Eq. (2.2), that the condition for the flow to be considered as incompressible, is

$$|\partial_t \rho| \ll |\nabla \cdot (\rho \mathbf{v})| = |\rho \nabla \cdot \mathbf{v}| \quad (3.41)$$

In the last equality we have used that the condition Eq. (3.40) is assumed to be fulfilled such that we can neglect terms involving the gradient of the density *i.e.* using that $|\rho \nabla \cdot \mathbf{v}| \gg |\mathbf{v} \cdot \nabla \rho|$.

Now considering the time-dependent inviscid Navier–Stokes equation we get to first-order from Eq. (2.8a)

$$\rho_0 \partial_t \mathbf{v}_1 = -c_a^2 \nabla \rho_1. \quad (3.42)$$

If we consider a problem with the characteristic length, L , and the characteristic time, τ , we estimate from Eq. (3.42)

$$\rho_0 \frac{v_1}{\tau} = -c_a^2 \frac{\Delta \rho_1}{L}, \quad (3.43)$$

concluding that the density change to first-order is of the order of magnitude $\Delta \rho_1 \sim L \rho_0 v_1 / \tau c_a^2$. Returning to use this in the condition stated in Eq. (3.41) we see that this is fulfilled to first-order when

$$\frac{\Delta \rho_1}{\tau} \ll \rho_0 \frac{v_1}{L} \Leftrightarrow \frac{L}{\tau^2 c_a^2} \ll \frac{1}{L} \Leftrightarrow \tau \gg \frac{L}{c_a}. \quad (3.44)$$

This condition is interpreted as L/c_a is the time taken for the sound to traverse the characteristic length L . This must then according to Eq. (3.44) be small compared to the time τ it takes the flow to change notably. This way the changes in the fluid may be regarded as instantaneous. The conditions in Eqs. (3.40) and (3.44) are in agreement with [16].

When working with standing waves in the fluid it is more convenient to consider the condition Eq. (3.44) with respect to the wavelength of the standing wave. Noticing that the characteristic time scale of the standing wave is of the order $\tau \sim 1/\omega$ which in turn is related to the wavelength of the standing wave $\omega \sim c_a/\lambda$. This rewrites the condition Eq. (3.44) in terms of the wavelength of the standing wave and the characteristic length of the problem

$$\lambda \gg L, \quad (3.45)$$

indicating that the length scale of the problem should be small compared to the wavelength of the standing wave so that the density change caused by the wave can be neglected.

3.4 Inviscid Second-order Acoustic Field

In the previous discussion we have presented the first-order (or linear) theory. In the linear approximation the harmonic time dependence enters in all terms to first-order, which we saw led to the Helmholtz equation. Consequently taking the time average over a full oscillation period all such terms would average out, leaving no opportunity for a DC drift velocity or DC pressure gradient. However, if we consider the second-order approximation, we introduce products of first-order terms, which will have a non-zero time average. For the harmonic time variation $\cos(\omega t)$, the time average of $\cos^2(\omega t)$ is $1/2$.

The objective is to be able to discuss the pressure force created by the pressure gradient. We therefore consider the second-order pressure perturbation. Since we are operating at high frequencies, we simplify the problem by only considering the time average of the pressure perturbation without loss of practical importance, because for fields oscillating at high frequencies we are only able to observe the time average. The goal of this section is therefore to derive an expression for the time average of the second-order pressure perturbation to be used in later calculations.

We consider the governing second-order Navier–Stokes equation (2.9a) neglecting viscosity

$$\rho_1 \partial_t \mathbf{v}_1 + \rho_0 \partial_t \mathbf{v}_2 + \rho_0 (\mathbf{v}_1 \cdot \nabla) \mathbf{v}_1 = -\nabla p_2. \quad (3.46)$$

We notice the general theorem that the time average of the time-derivative of a T -periodic function, $f(t+T) = f(t)$, is zero because

$$\langle \partial_t f \rangle = \frac{1}{T} \int_t^{t+T} \partial_{t'} f \, dt' = \frac{1}{T} [f(t+T) - f(t)] = 0, \quad (3.47)$$

Assuming that all perturbation terms are periodic, we get the time average of Eq. (3.46)

$$\langle \nabla p_2 \rangle = -\langle \rho_1 \partial_t \mathbf{v}_1 \rangle - \langle \rho_0 (\mathbf{v}_1 \cdot \nabla) \mathbf{v}_1 \rangle. \quad (3.48)$$

Reintroducing the first-order velocity potential as done in Eqs. (3.5) and (3.6), we get

$$\langle \nabla p_2 \rangle = - \left\langle \left(-\frac{\rho_0}{c_a^2} \partial_t \phi_1 \right) \partial_t (\nabla \phi_1) \right\rangle - \left\langle \rho_0 [(\nabla \phi_1) \cdot \nabla] (\nabla \phi_1) \right\rangle, \quad (3.49)$$

or

$$\nabla \langle p_2 \rangle = \frac{\rho_0}{2c_a^2} \nabla \langle \partial_t^2 \phi_1 \rangle - \frac{\rho_0}{2} \nabla \langle |\nabla \phi_1|^2 \rangle, \quad (3.50)$$

exploiting that the spatial differentiation and time-average commute. Spatial integration now yields

$$\langle p_2 \rangle = \frac{\rho_0}{2c_a^2} \langle \partial_t^2 \phi_1 \rangle - \frac{\rho_0}{2} \langle |\nabla \phi_1|^2 \rangle = \frac{\rho_0}{2c_a^2} \langle (\partial_t \phi_1)^2 \rangle - \frac{\rho_0}{2} \langle |\mathbf{v}_1|^2 \rangle. \quad (3.51)$$

Eq. (3.51) expresses the time average of the second-order perturbation in the pressure. We notice that this time average only contains the first-order perturbations in the velocity potential. To calculate the time average of the second-order pressure perturbation we therefore only have to solve the linear problem for the velocity potential.

3.5 Calculation of Time Average

We now want to find out how to calculate these time averages. We are considering two quantities given as the real part of a complex expression,

$$A(t) = \text{Re} \{ A_0 e^{i\omega t} \} \quad \text{and} \quad B(t) = \text{Re} \{ B_0 e^{i\omega t} \}, \quad (3.52)$$

where A_0 and B_0 are complex numbers. The time-average of their product is defined as

$$\langle A(t)B(t) \rangle \equiv \frac{1}{T} \int_0^T A(t)B(t) dt, \quad (3.53)$$

where T is the period. We use the fact that $\text{Re}\{Z\} = \frac{1}{2}[Z + Z^*]$ to get

$$\langle A(t)B(t) \rangle = \frac{1}{4T} \int_0^T \left[A_0 e^{i\omega t} + A_0^* e^{-i\omega t} \right] \left[B_0 e^{i\omega t} + B_0^* e^{-i\omega t} \right] dt. \quad (3.54)$$

Finally we use that the terms containing the exponential cancel out on integration, and we get

$$\langle A(t)B(t) \rangle = \frac{1}{4\tau} \int_0^\tau [A_0 B_0^* + A_0^* B_0] dt = \frac{1}{4} [A_0 B_0^* + A_0^* B_0] = \frac{1}{2} \text{Re} \{ A_0 B_0^* \}. \quad (3.55)$$

Chapter 4

Resonance in First-order Theory

In this chapter we will introduce acoustic resonance in a simple resonator as we will be interested in standing waves in microchannels considered as a resonator. We will concentrate on the one-dimensional single-domain double actuation resonator both without and with viscosity. The multilayer system with transmission is considered to be beyond the scope of this section, because it does not contribute to the simple understanding of the fundamental concept of resonance in an acoustic system, which is the aim of this section. Furthermore we will be discussing the perturbation approach from an estimate of the implicit perturbation parameter.

4.1 Acoustic Resonance in a Single-domain System

We consider a model of a microfluidic system excited by a piezo-electric crystal. We imagine an one-dimensional system as shown in Fig. 4.1. The piezo-actuator gives rise to a harmonic movement of the walls enclosing the fluid. The equilibrium position of the walls is assumed to be at $x = \pm L$, and the walls are assumed to be moving back and forth with opposite phase but both with the maximum amplitude ℓ . The movement of the walls can therefore be described by $\xi(\pm L, t) = \pm \ell e^{-i\omega t}$. We imagine an actuator system with small oscillatory amplitude, $\ell \approx 1$ nm from [5], relatively to the length of the system $\ell \ll L$ so that we can neglect the movement of the walls. The width of the typical system considered in this thesis is approximately 0.3 – 1.1 mm. Even though the displacement is small, the system is driven at a high frequency so that it is not possible to neglect the velocity change. The velocity of the oscillatory motion at the boundary is therefore readily found to be

$$v_{\text{wall}}(\pm L, t) = \pm \omega \ell e^{-i\omega t}. \quad (4.1)$$

We notice that we are considering a situation with harmonic time variation so that the first-order velocity potential is fulfilling the (lossy) Helmholtz equation, $\partial_x^2 \phi_1(x) = -k^2 \phi_1(x)$, like we explained in Sections 3.1.2 and 3.2.1 as long as the viscosity is considered small. Making no distinction here on whether we are including viscosity or not, just writing the possible complex wavenumber as k , the solution for the velocity potential is

$$\phi_1(x, t) = \left[A e^{ikx} + B e^{-ikx} \right] e^{-i\omega t}, \quad (4.2)$$

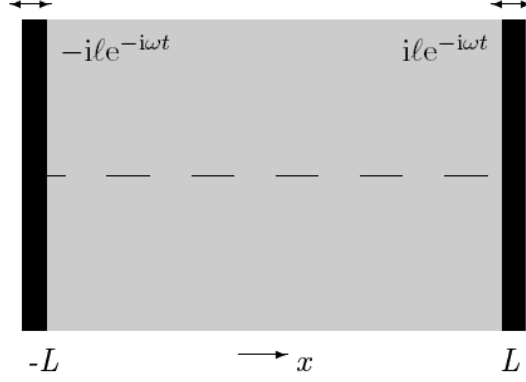


Figure 4.1: A sketch of the single-domain, one-dimensional resonator system. From [22].

where we in the last part have introduced the implicit harmonic time-dependence. A and B are arbitrary integration constants with respect to the spatial coordinate x .

The corresponding first-order velocity is found as

$$v_1(x, t) = \partial_x \phi_1(x, t) = ik \left[Ae^{ikx} - Be^{-ikx} \right] e^{-i\omega t}, \quad (4.3)$$

and the first-order density is found from Eq. (3.33) as the time derivative of the velocity potential,

$$\rho_1(x, t) = -\frac{\rho_0 k^2}{\omega^2} \partial_t \phi_1(x, t) = i \frac{\rho_0 k^2}{\omega} \left[Ae^{ikx} + Be^{-ikx} \right] e^{-i\omega t}. \quad (4.4)$$

We are now using the no-slip boundary conditions formulated via the wall movement Eq. (4.1) to determine the constants. First we notice that the boundary conditions are anti-symmetric *i.e.* $v_1(-L, t) = -v_1(+L, t)$ implying from Eq. (4.3) that $A = B$. Inserting this into Eq. (4.3) together with one of the boundary conditions leads to the magnitude of the coefficients,

$$A = -\frac{\omega \ell}{2k \sin(kL)}, \quad (4.5)$$

where we have used $2i \sin(x) = e^{ix} - e^{-ix}$.

Inserting this into the solutions for the first-order velocity potential Eq. (4.2), velocity Eq. (4.3), and density Eq. (4.4), we obtain

$$\phi_1(x, t) = -\frac{\omega \ell \cos(kx)}{k \sin(kL)} e^{-i\omega t}, \quad (4.6a)$$

$$v_1(x, t) = \omega \ell \frac{\sin(kx)}{\sin(kL)} e^{-i\omega t}, \quad (4.6b)$$

$$\rho_1(x, t) = -i \rho_0 k \ell \frac{\cos(kx)}{\sin(kL)} e^{-i\omega t}. \quad (4.6c)$$

We now have to make a distinction between whether we are considering the viscous or inviscid fluid.

We start by considering the inviscid case where the wavenumber is real, $k = k_0$. From Eq. (4.6) we observe that resonance in this case occurs at wavenumbers k_n and corresponding frequencies ω_n ,

$$\begin{aligned} Lk_{\text{res}} &= n\pi, \quad n \in \mathbb{N}, \\ \omega_{\text{res}} &= c_a k_{\text{res}} = n \frac{\pi c_a}{L}. \end{aligned} \quad (4.7)$$

We observe that in this undamped case the velocity is diverging at resonance. This concludes that a resonator system can be created where it is possible to create significant magnitudes of the field. Taking the real part of Eq. (4.6), we notice a phase shift of $\pi/2$ between the velocity and the density (pressure) in both space and time. From [5] we have the energy flux to second-order is $\mathbf{J}_E = -\rho_0(\nabla\phi_1)(\partial_t\phi_1) = c_a^2\mathbf{v}_1\rho_1$. The phase shift between velocity and density (pressure) then implies that the time-averaged energy flux is zero.

It is also worth noticing that at resonance the first-order velocity will have nodes at the boundary wall, where the velocity potential and density (pressure) will have anti-nodes at the boundary. This is an important observation which will be used extensively in the following chapters as we are considering resonators operating at resonance frequency.

We now turn to the problem of the viscid case. As described in Section 3.2.1, we can approximate the wavenumber for small viscosity as $k = k_0(1 + i\gamma)$, where k_0 is the real wavenumber from the inviscid problem. In the case of a small viscosity such that $\gamma k_0 L \ll 1$, we can make a Taylor expansion of the sine and cosine terms in Eq. (4.6) in k around k_0 . This yields the velocity and density (pressure) in the small damping case

$$v_1(x, t) \approx \omega\ell \frac{\sin(k_0x) + i\gamma k_0x \cos(k_0x)}{\sin(k_0L) + i\gamma k_0L \cos(k_0L)} e^{-i\omega t}, \quad (4.8a)$$

$$\rho_1(x, t) \approx -i\rho_0 k_0\ell \frac{\cos(k_0x) - i\gamma k_0x \sin(k_0x)}{\sin(k_0L) + i\gamma k_0L \cos(k_0L)} e^{-i\omega t}. \quad (4.8b)$$

4.1.1 Considering the Perturbation Parameter and the First-order Velocity

Off-resonance we have $\sin(k_0L) = 1$ in Eq. (4.8) — notice that $\gamma \ll 1$ meaning that the sine term is larger than the cosine term in the denominator — leaving the fields as

$$v_1(x, t) \approx \omega\ell [\sin(k_0x) + i\gamma k_0x \cos(k_0x)] e^{-i\omega t}, \quad (4.9a)$$

$$\rho_1(x, t) \approx -i\rho_0 k_0\ell [\cos(k_0x) - i\gamma k_0x \sin(k_0x)] e^{-i\omega t}. \quad (4.9b)$$

The magnitude of the fields off-resonance are therefore given solely by the prefactor

$$|v_1(x, t)| \approx \omega\ell = \frac{\omega\ell}{c_a} c_a, \quad (4.10a)$$

$$|\rho_1(x, t)| \approx \rho_0 k_0\ell = \frac{\omega\ell}{c_a} \rho_0. \quad (4.10b)$$

where we have used the non-viscid dispersion relation, $c_a k_0 = \omega$.

From Eq. (4.10) it is possible to read off the implicit perturbation factor discussed in Section 2.2. With characteristic parameter values we can estimate this to be

$$\alpha_{\text{off,res}} = \frac{\omega \ell}{c_a} \approx \frac{10^6 \text{ s}^{-1} \times 10^{-9} \text{ m}}{1483 \text{ m s}^{-1}} = 6.7 \times 10^{-7}. \quad (4.11)$$

From this we conclude that off-resonance the perturbation approach is at least self consistent in the sense that it produces a perturbation parameter value $\alpha \ll 1$.

Continuing from Eq. (4.8) at resonance, *i.e.* when the denominator is small, we get $\sin(k_0 L) = 0$ and $\cos(k_0 L) = 1$, indicating the resonance condition stated in Eq. (4.7). At resonance we get the velocity and density (pressure) fields

$$v_1(x, t) \approx \omega \ell \left[-\frac{i}{n\pi\gamma} \sin(k_n x) + \frac{x}{L} \cos(k_n L) \right], \quad (4.12a)$$

$$\rho_1(x, t) \approx i\rho_0 k_n \ell \left[\frac{i}{n\pi\gamma} \cos(k_n x) + \frac{x}{L} \sin(k_n x) \right]. \quad (4.12b)$$

Comparing the fields off-resonance Eq. (4.9) and on-resonance Eq. (4.12) we notice that the resonance fields acquire a resonant component with an amplitude $1/(n\pi\gamma) \approx 3.1 \times 10^4$ (for $n = 1$) times larger than for the off-resonance field. This means a change in the magnitude of the perturbation parameter in the resonant case

$$\alpha_{\text{res}} = \frac{1}{n\pi\gamma} \frac{\omega \ell}{c_a} \approx 3.1 \times 10^4 \times 6.7 \times 10^{-7} = 2 \times 10^{-2}. \quad (4.13)$$

We notice that with strong resonance, which in the limit goes towards the infinite inviscid case treated above, we tend to invalidate the perturbation approach. Hence we conclude the importance of the viscosity of the fluid when regarding resonators. We also conclude that large energy resonances, corresponding to the case of very low viscosity, gives a possible invalidation of the whole perturbation approach, which requires small values of the perturbation parameter, $\alpha \ll 1$, to be valid.

It is also interesting to notice that the first-order velocity in this way is estimated to have the magnitude $|\mathbf{v}_1| \approx 10^{-2} c_a$ at resonance. As pointed out in [22] this is about two magnitudes higher than the experimentally observed values. This is primarily due to the assumption of a perfectly coupled and lossless resonator delivering its energy at resonance, which of course is not the case in the experimental setup. Like [22] we will as an estimate use the experimentally confirmed magnitude $|\mathbf{v}_1| \approx 10^{-4} c_a$, [33].

4.1.2 Energy in the Resonator

It can be shown that the acoustic energy density to second-order of the acoustic fields is given as the sum of the kinetic energy and the potential energy [5],

$$\langle E_{\text{ac}} \rangle = \frac{1}{2} \rho_0 \left[\langle \nabla \phi_1 \rangle^2 + \left\langle \frac{1}{c_a} \partial_t \phi_1 \right\rangle^2 \right] = \frac{1}{2} \rho_0 \left[\langle \mathbf{v}_1^2 \rangle + \left\langle \left(\frac{c_a}{\rho_0} \rho_1 \right)^2 \right\rangle \right], \quad (4.14)$$

where we in the last equality have used the relations between the first-order quantities and the first-order velocity potential, *cf.* Eqs. (3.5) and (3.6).

We will consider the general case including the viscosity. The expressions for the first-order velocity and density is then given in Eq. (4.8). Using the result for the time average of harmonic varying quantities found in Section 3.5, and noticing that the real first-order terms expressed by complex notation in Eq. (4.8) is found by taking the real part of the complex representation, we obtain

$$\langle \mathbf{v}_1^2 \rangle = \frac{1}{2} \omega^2 \ell^2 \frac{\sin^2(k_0 x) + \gamma^2 k_0^2 x^2 \cos^2(k_0 x)}{\sin^2(k_0 L) + \gamma^2 k_0^2 L^2 \cos^2(k_0 L)}, \quad (4.15a)$$

$$\left\langle \left(\frac{c_a}{\rho_0} \rho_1 \right)^2 \right\rangle = \frac{1}{2} \frac{\omega^4 \ell^2 \cos^2(k_0 x) + \gamma^2 k_0^2 x^2 \sin^2(k_0 x)}{c_a^2 k_0^2 \sin^2(k_0 L) + \gamma^2 k_0^2 L^2 \cos^2(k_0 L)}. \quad (4.15b)$$

Inserting Eqs. (4.15a) and (4.15b) in Eq. (4.14) and using the Pythagorean identity for sines and cosines we get

$$\langle E_{ac} \rangle = \frac{\rho_0 \omega^2 \ell^2}{4} \frac{1 + x^2 \gamma^2 k_0^2}{\sin^2(k_0 L) + \gamma^2 k_0^2 L^2 \cos^2(k_0 L)}, \quad (4.16)$$

where we have also used the linear dispersion relation $\omega = c_a k_0$ and that we to first-order in γ have $k^2 = k_0^2$ since $\gamma \ll 1$.

We want to consider the spatial-averaged energy density in the resonator which is located at $x = -L$ to $x = L$. Hence we integrate the energy density over the length of the resonator,

$$\varepsilon = \frac{1}{2L} \int_{-L}^L \langle E_{ac} \rangle dx = \frac{\rho_0 \omega^2 \ell^2}{8L} \frac{L + \frac{1}{3} \gamma^2 k_0^2 L^3}{\sin^2(k_0 L) + \gamma^2 k_0^2 L^2 \cos^2(k_0 L)}. \quad (4.17)$$

We can now expand the sine and cosine terms in the denominator again under the assumption that we are driving the resonator close to the resonance frequency $\omega_{\text{res}} = c_a k_{\text{res}}$. The Taylor expansions of the sine and cosine around the resonance frequency gives

$$\sin(k_0 x) \approx \sin\left(\frac{\omega_{\text{res}}}{c_a} L\right) + \frac{L}{c_a} (\omega - \omega_{\text{res}}) \cos\left(\frac{\omega_{\text{res}}}{c_a} L\right), \quad (4.18a)$$

$$\cos(k_0 x) \approx \cos\left(\frac{\omega_{\text{res}}}{c_a} L\right) - \frac{L}{c_a} (\omega - \omega_{\text{res}}) \sin\left(\frac{\omega_{\text{res}}}{c_a} L\right). \quad (4.18b)$$

Inserting the Taylor expansions Eqs. (4.18a) and (4.18b) into Eq. (4.17) while using the resonance condition Eq. (4.7) means that $k_0 L \approx k_{\text{res}} L = \omega_{\text{res}} L / c_a = n\pi$ leading to $\sin(\omega_{\text{res}} L / c_a) = 0$ and $\cos(\omega_{\text{res}} L / c_a) = (-1)^n$, and gives

$$\varepsilon = \frac{\rho_0 \omega_{\text{res}}^2 \ell^2}{8} \frac{1}{L^2 / c_a^2 (\omega - \omega_{\text{res}})^2 + \gamma^2 L^2 \omega_{\text{res}}^2 / c_a^2} \quad (4.19)$$

$$= \frac{1}{8} \rho_0 c_a^2 \frac{\ell^2}{L^2} \frac{\omega_{\text{res}}}{\gamma} \frac{\gamma \omega_{\text{res}}}{(\omega - \omega_{\text{res}})^2 + \gamma^2 \omega_{\text{res}}^2}, \quad (4.20)$$

where we again use the assumption $\gamma \ll 1$ which is why the last term in the numerator of Eq. (4.17) can be neglected compared to the first one.

We recognize the form of the energy density in the resonator Eq. (4.20) as a Lorentzian, which is the same kind of function we would get when solving for the amplitude of the classical harmonic oscillator. The energy density is centered around the resonance frequency ω_{res} and has a full width at half maximum (FWHM) of $2\gamma\omega_{\text{res}}$. With the typical parameters used in the following chapters FWHM around the resonance frequency is estimated as

$$2\gamma\omega_{\text{res}} \approx 2 \times 10^{-5} \times 2\pi \times 2 \times 10^6 \text{ rad s}^{-1} = 40 \text{ Hz}. \quad (4.21)$$

This example of a resonator is one-dimensional and for a real analysis of the physical system we would of course have to generalize the analysis to three dimensions which is beyond the scope of this thesis where we will not concentrate on the form of the resonance and how it is actually created. An estimate can be given by considering the three-dimensional cavity with homogeneous Neumann boundary because of the assumption of the walls being acoustical hard materials so the pressure gradient is zero normal to the boundary walls, $\mathbf{n}_{\text{normal}} \cdot \nabla p_1 = 0$. This leads to a restrictions on the frequencies determined by the geometry. In a rectangular cavity with the dimensions l_0 , w_0 , and h_0 the solution to the Helmholtz equation with the mentioned boundary conditions gives the resonance frequencies as stated in [22],

$$\omega_{\text{res},3\text{d}} = c_a^2 \sqrt{\left(\frac{2\pi n}{l_0}\right)^2 + \left(\frac{2\pi k}{h_0}\right)^2 + \left(\frac{2\pi m}{w_0}\right)^2}, \quad (n, k, m) \in \mathbb{N}^3. \quad (4.22)$$

Chapter 5

Forces Acting on Microparticles in an Acoustic Field in an Inviscid Fluid

Gor'kov [14] presented in 1962 a paper with derivations on a microparticle in an inviscid fluid under the influence of an acoustic field. This paper is very condensed, so in this chapter we would like to present a detailed derivation of Gor'kov's results.

In the linear approximation described in Section 3.4, there can be no pressure force and hence in average no displacement of the particle, since all first-order terms are harmonic and are time-averaged to zero. Thus we have to go to second order to be able to see these effects. Below we derive an expression for the force acting on a small particle entrained by the fluid in an arbitrary acoustic field. In the following chapter we will only be concerned with inviscid fluids *i.e.* we are neglecting all loss terms and especially viscosity. This assumption is important since we want to describe the system by the velocity potential which in turn demands that the fluid is isentropic. If the rotation is zero at one instant and the flow is not isentropic it will most certainly not be irrotational an instant later, see the discussion in [16].

5.1 The Potential Flow

First we consider the constant flow around a particle in an acoustic field and want to determine if this flow is a potential flow. Using the Stokes theorem the irrotational condition can be written as zero circulation along any closed contour,

$$\oint \mathbf{v} \cdot d\mathbf{l} = \int (\nabla \times \mathbf{v}) \cdot d\mathbf{A} = 0. \quad (5.1)$$

From this it is clear that any constant velocity field is irrotational.

We need to determine if the flow around the particle is a potential flow. The isentropic flow is determined by the non-viscid Navier–Stokes equation, Eq. (2.1),

$$\rho [\partial_t \mathbf{v} + (\mathbf{v} \cdot \nabla) \mathbf{v}] = -\nabla p. \quad (5.2)$$

If we follow the particle immersed in the fluid we have a system where the particle is not moving but the fluid is. Because of the acoustical field the pressure oscillates making the particle surface oscillate at a certain angular frequency ω and amplitude a .

The size of the individual terms of Eq. (5.2) are estimated as follows: The velocity of the fluid close to the particle surface changes by an amount of the same order as the velocity, \mathbf{u} , of the oscillating surface of the particle over the characteristic size of the particle, l . This makes the spatial derivative of \mathbf{v} of the order u/l and the term $(\mathbf{v} \cdot \nabla)\mathbf{v} \sim u^2/l$. Considering the first term in Eq. (5.2) we see that $\partial_t \mathbf{v}$ is of the order ωu . Noticing that the angular frequency is of magnitude $\omega \sim u/a$ we conclude that the first term is of the order $\partial_t \mathbf{v} \sim u^2/a$. Comparing this to the other terms we obtain

$$|\partial_t \mathbf{v}| \gg |(\mathbf{v} \cdot \nabla)\mathbf{v}| \quad \text{if } a \ll l. \quad (5.3)$$

We thus conclude that if the oscillations of the particle surface are small compared to the length of the particle we can neglect the non-linear term of Eq. (5.2). This means that we are limited to only consider sufficiently small variations in the pressure so that the particle surface is not vibrating with too large an amplitude.

Neglecting the second term of Eq. (5.2) and applying the rotation operator on both sides yields $\nabla \times (\rho \partial_t \mathbf{v}) = -\nabla \times (\nabla p) = \mathbf{0}$ because the rotation of a gradient-field is zero. To first order $\rho \partial_t \mathbf{v} = \rho_0 \partial_t \mathbf{v}_1$ which gives that $\nabla \times \mathbf{v}_1$ is a constant with respect to time. Because rotation and time-average commute, $\langle \nabla \times \mathbf{v}_1 \rangle = \nabla \times \langle \mathbf{v}_1 \rangle$ is equal to the same constant. Assuming that v_1 varies harmonically in time, we know that $\langle \mathbf{v}_1 \rangle = \mathbf{0}$ which means that the constant also must be zero, giving $\nabla \times \mathbf{v}_1 = \mathbf{0}$. Therefore to first order the pressure variation is sufficiently small so that the amplitude of the surface oscillations of the particle is small compared to the particle size. The flow around the particle is a potential flow, and we can use the notation of velocity potential described in Chapter 3.

5.2 The Average Force For Second-order Perturbation

In the linear scattering theory we assume that the first-order velocity potential can be written as the sum of the wave incident on the particle, ϕ_{in} , and the scattered wave, ϕ_{sc} ,

$$\phi_1(\mathbf{r}, t) = \phi_{\text{in}}(\mathbf{r}, t) + \phi_{\text{sc}}(\mathbf{r}, t). \quad (5.4)$$

This means that all interference effects are neglected. Furthermore, we are neglecting the scattered waves being reflected back towards the sphere from the wall of the fluid container or other particles.

When neglecting body forces and viscid forces on the particle, the magnitude of the average force is equal to the average flux of momentum through any arbitrary closed surface ∂V of the volume element V in which the particle is enclosed [5],

$$\langle F_i \rangle = - \int_{\partial V} \langle \Pi_{ij} \rangle n_j \, dA, \quad (5.5)$$

where $\langle \Pi_{ij} \rangle = p \delta_{ij} + \rho v_i v_j$ is the time average of the momentum flux density tensor, $n_j = \mathbf{n} \cdot \mathbf{e}_j$ is the component of the outward pointing normal vector \mathbf{n} to the surface in the

direction of \mathbf{e}_j , and ρ is the density of the fluid. Using the perturbation scheme outlined in Section 2.2 we include up to second-order effects for both the velocity and the pressure.

When neglecting viscosity we get the first-order perturbation in pressure from Eq. (3.7)

$$p_1 = -\rho_0 \partial_t \phi_1. \quad (5.6)$$

Restricting ourselves to periodic time varying first-order perturbations, we observe that $\langle p_1 \rangle = 0$ by Eq. (3.47).

The second-order time-average perturbation of the pressure is obtained from Eq. (3.51), and noticing that the second-order expansion of $\rho v_i v_j$ is $\rho_0 v_{1,i} v_{1,j}$, we can rewrite Eq. (5.5) as

$$\langle F_i \cdot \mathbf{e}_i \rangle = - \int_{\partial V} \left\{ \left[-\rho_0 \frac{\langle v_1^2 \rangle}{2} + \frac{\rho_0}{2c_a^2} \langle (\partial_t \phi_1)^2 \rangle \right] \delta_{ij} + \rho_0 \langle v_{1,i} v_{1,j} \rangle \right\} n_j \, dA. \quad (5.7)$$

We see from Eq. (5.7) that we only need to solve the linear scattering problem, *i.e.* determine ϕ_1 , to determine the force. We therefore dedicate the next section to determination of the velocity potential.

5.2.1 Calculation of the Velocity Potential

In Chapter 3 we saw that the velocity potential fulfilled the scalar wave equation Eq. (3.8). Making a multipole expansion of the solution, see Appendix B, taking into account only the terms which are not diverging at infinity, we look for retarded solutions ϕ_{sc} to the velocity potential of the form

$$\phi_{\text{sc}} = \frac{a(t - r/c_a)}{r} + \nabla \cdot \left(\frac{\mathbf{A}(t - r/c_a)}{r} \right) + \dots \quad (5.8)$$

$$= \frac{a(t - r/c_a)}{r} - \frac{\dot{\mathbf{A}}(t - r/c_a) \cdot \mathbf{e}_r}{c_a r} - \frac{\mathbf{A}(t - r/c_a) \cdot \mathbf{e}_r}{r^2} + \dots \quad (5.9)$$

Here and in the following the dot denotes the derivative with respect to the argument. Assuming that $\dot{\mathbf{A}}$ varies periodically in time with angular frequency ω , then $\dot{\mathbf{A}}/c_a \sim \mathbf{A}\omega/c_a \sim \mathbf{A}/\lambda$. This means that in the region close to the particle *i.e.* $r \ll \lambda$, we look for solutions of the form

$$\phi_{\text{sc}} = \frac{a(t)}{r} - \frac{\mathbf{A}(t) \cdot \mathbf{e}_r}{r^2} + \dots, \quad (5.10)$$

where \mathbf{e}_r is a unit vector pointing in the radial direction. This corresponds to only including the largest of the two terms including \mathbf{A} in Eq. (5.9). Notice that Eq. (5.10) is for small r values.

We now look at the situation close to the particle where Eq. (5.9) reduces to Eq. (5.10), to determine the coefficients a and \mathbf{A} . To do this we make a general simplification of the problem. Until now we have been discussing particles of an arbitrary shape. Now we simplify our problem to spherically shaped particles in order to be able to determine the coefficients. In all of the following we will therefore only be concerned with spherically shaped particles.

The strategy for determining the coefficients is to consider different situations where either the first or the second term of Eq. (5.10) vanish, and we therefore can determine the other coefficient.

First Term — Mass Flux

We now consider the first term $a(t)/r$ of Eq. (5.10). This term describes the ejection of the fluid because of the presence of the sphere and the compressibility of the sphere. We therefore consider a stationary sphere in the fluid in an acoustic field which to first-order is carrying the density ρ_{in} at the location of the sphere. This problem has complete rotational symmetry and hence the term including \mathbf{A} vanish because we see that this term includes an angular dependence. It therefore suffices to consider only the first term of Eq. (5.10) for this setup.

First we look at an incompressible sphere of radius R and volume V_s . The volume $V_s \dot{\rho}_{\text{in}}/\rho_0$ would have entered the volume now occupied by the sphere per unit time. This volume would have entered if the sphere was absent and is equivalent to the emission of the same volume from the surface of the sphere by the scattered wave. If the normal vector \mathbf{e}_r is taken as pointing outwards, this means that

$$V_s \frac{\dot{\rho}_{\text{in}}(t)}{\rho_0} = \int_{\partial V_s} \mathbf{v}_{\text{sc}}(t) \cdot \mathbf{e}_r \, dA. \quad (5.11)$$

Because $\mathbf{v}_{\text{sc}} = \nabla \phi_{\text{sc}}$ the integral becomes

$$\frac{4\pi}{3} R^3 \frac{\dot{\rho}_{\text{in}}(t)}{\rho_0} = \int_{\partial V_s} \nabla \phi_{\text{sc}} \cdot \mathbf{e}_r \, dA \quad (5.12)$$

$$= \int_{\partial V_s} \nabla \left(\frac{a(t)}{r} \right) \cdot \mathbf{e}_r \, dA \quad (5.13)$$

$$= - \int_{\partial V_s} \frac{a(t)}{r^2} \mathbf{e}_r \cdot \mathbf{e}_r \, dA \quad (5.14)$$

$$= - \frac{a(t)}{R^2} 4\pi R^2. \quad (5.15)$$

Thus

$$a(t) = - \frac{R^3}{3\rho_0} \dot{\rho}_{\text{in}}(t). \quad (5.16)$$

We can expand this derivation by taking into account the fact that the sphere is compressible. It means that Eq. (5.11) becomes

$$V_s \frac{\dot{\rho}_{\text{in}}(t)}{\rho_0} + \delta \dot{V}_{s,1} = -4\pi a(t), \quad (5.17)$$

where $\delta \dot{V}_{s,1}$ denotes the first-order volume change per unit time due to compression of the sphere.

We now take advantage of the fact that $\delta \dot{V}_{s,1}$ by definition is small, since we only are considering the case where the amplitude of the oscillations of the surface is small compared to the length scale of the particle. This means that we can express it using the chain rule,

$$\delta \dot{V}_{s,1} = \frac{\partial V_s}{\partial \rho_s} \frac{\partial \rho_s}{\partial p_s} \delta \dot{p}_{s,1}, \quad (5.18)$$

where it is understood that the process of changing the volume of the sphere must be isentropic, so we keep considering a lossless system. In analogy with Eq. (2.6) we define the speed of sound in the sphere as the isentropic derivative,

$$c_s^2 = \left(\frac{\partial p_s}{\partial \rho_s} \right)_{\rho=\rho_s}. \quad (5.19)$$

Because the pressure outside the sphere must be the same as inside the sphere at equilibrium we notice from Eq. (2.8c) that the first-order perturbation of the pressure, $\delta p_{s,1}$, is

$$\delta p_{s,1} = p_1 = c_a^2 \rho_1 = c_a^2 \rho_{in} \Rightarrow \delta \dot{p}_{s,1} = c_a^2 \dot{\rho}_{in}. \quad (5.20)$$

Furthermore, using that

$$\frac{\partial V_s}{\partial \rho_s} = \frac{\partial}{\partial \rho_s} \left(\frac{m_s}{\rho_s} \right) = -\frac{m_s}{\rho_s^2} = -\frac{V_s}{\rho_s}, \quad (5.21)$$

with m_s denoting the mass of the sphere, Eq. (5.18) becomes

$$\delta \dot{V}_{s,1} = -V_s \frac{\dot{\rho}_{in} c_a^2}{\rho_s c_s^2}. \quad (5.22)$$

From Eq. (5.17) we finally obtain $a(t)$,

$$a(t) = -\frac{1}{4\pi} \left(V_s \frac{\dot{\rho}_{in}(t)}{\rho_0} - V_s \frac{\dot{\rho}_{in} c_a^2}{\rho_s c_s^2} \right) = -\frac{R^3}{3\rho_0} \rho_{in}(t) \left(1 - \frac{\rho_0 c_a^2}{\rho_s c_s^2} \right). \quad (5.23)$$

This takes into account both the volume that the sphere occupies and thereby the mass which is expelled from the surface and the fact that the sphere changes size when placed in the fluid in an acoustic field.

These effects are present no matter if the sphere is stationary or moving, as long as there is an incoming density perturbation of the size $\dot{\rho}_{in}$, and a following pressure perturbation to make the surface compress.

Second Term — Movement of the Sphere and Fluid in Presence of the Sphere

The second term in Eq. (5.10) can be determined from the fact that in a stationary flow the normal component of the velocity of the fluid and the normal component of the velocity of the surface must be the same for $r = R$. We consider a sphere moving with the constant velocity \mathbf{v}_s in a stationary fluid. This problem clearly involves a direction and hence an angular dependence. The first term of Eq. (5.10) does not exhibit any angular dependence, so for this kind of problem it suffices to only consider the second term. Though the effects described above concerning mass flux is still valid, these effects cannot have any influence on the flow of the fluid around the sphere.

The mentioned continuity condition for the normal component of the velocity of the fluid and the velocity of the surface of the sphere, means that only the radial part of $\mathbf{A}(t)$ enters the equations. Neglecting all other parts we can write $\mathbf{A}(t) = A_r(t) \mathbf{e}_r$, remembering

that the fluid velocity is given as $\nabla\phi_{\text{sc}}$ and only taking the radial part of the gradient, we get

$$\mathbf{v}_s \cdot \mathbf{e}_r = \nabla \left(-\frac{\mathbf{A} \cdot \mathbf{e}_r}{r^2} \right) \cdot \mathbf{e}_r \Big|_{r=R} = A_r \frac{2\mathbf{e}_r}{R^3} \cdot \mathbf{e}_r. \quad (5.24)$$

Thus $\mathbf{A}(t) \cdot \mathbf{e}_r = 1/2\mathbf{v}_s \cdot \mathbf{e}_r R^3$, and the second term of ϕ_{sc} in Eq. (5.10) becomes

$$-\frac{\mathbf{A}(t) \cdot \mathbf{e}_r}{r^2} = -\mathbf{v}_s \cdot \mathbf{e}_r \frac{R^3}{2r^2}. \quad (5.25)$$

In general, the fluid is not stationary, but both the fluid and the sphere is moving, implying that the sphere is entrained by the fluid and moves with a velocity $\mathbf{u}(t)$. We notice that it still suffices only to consider the second term of Eq. (5.10) since this problem still involves directions.

Since the equation for the full potential, Eq. (5.4), is linear and fulfills the scalar wave equation as described in Chapter 3, so must the scattered potential,

$$\nabla^2 \phi_{\text{sc}} = \frac{1}{c_a^2} \partial_t^2 \phi_{\text{sc}}. \quad (5.26)$$

We notice that for a sphere with radius R the velocity potential changes notably over this length scale, hence the spatial derivative in the left-hand side of Eq. (5.26) is of the order $\sim \phi_{\text{sc}}/R^2$. The right-hand side is for harmonic time dependence of the order $\sim \omega^2 \phi_{\text{sc}}/c_a^2 \sim \phi_{\text{sc}}/\lambda^2$. For high frequency acoustic waves, and close enough to the sphere, we have the condition $\lambda \gg R$, and we can neglect the right-hand side of Eq. (5.26) which leads to that close to the sphere, the velocity potential must obey the Laplace equation, $\nabla^2 \phi_{\text{sc}} = 0$.

To determine the coefficient \mathbf{A} we consider the situation close to a sphere entrained by the fluid, when the fluid has a constant velocity and flows in the x -direction. Hence we solve the Laplace equation inside and outside the sphere. Denoting the scattered field outside with subscript O and inside the sphere with subscript I, the Laplace problem is subject to the following boundary conditions:

BC 1 Continuity of the pressure, $p_I = p_O$ at $r = R$. To first order in Eq. (3.7) we get $p_{\text{sc}} = p_0 - \rho_0 \partial_t \phi_{\text{sc}} = \rho_0 + i\rho_0 \omega \phi_{\text{sc}}$, assuming that the time-dependence is on the form $e^{-i\omega t}$. This means that

$$\rho_I \partial_t \phi_I = \rho_O \partial_t \phi_O \Rightarrow \rho_I \phi_I = \rho_O \phi_O, \quad \text{at } r = R, \quad (5.27)$$

BC 2 Continuity of the normal velocity

$$\mathbf{v}_I \cdot \mathbf{e}_r = \mathbf{v}_O \cdot \mathbf{e}_r \Rightarrow \partial_r \phi_I = \partial_r \phi_O, \quad \text{at } r = R. \quad (5.28)$$

BC 3 $\phi_O(r, \theta) \rightarrow v_{\text{in}} r \cos \theta$ for $r \rightarrow \infty$; far from the sphere the scattered velocity field must be like the incoming field.

BC 4 ϕ_I must remain finite.

Using boundary condition 3 we see that the potential only can have a cosine variation (not higher powers of $\cos \theta$). This gives the following linear combination of solutions to $\nabla^2 \{r^p \cos \theta\} = 0$ with p being an integer

$$\phi(r, \theta) = [Ar + Br^{-2}] \cos \theta. \quad (5.29)$$

Inside the sphere the potential cannot diverge according to boundary condition 4, thus $B_I = 0$, and ϕ_I must have the form

$$\phi_I(r, \theta) = A_I r \cos \theta. \quad (5.30)$$

Similarly using boundary condition 3 we conclude that $A_O = v_{\text{in}}$ so that the potential outside the sphere must have the form

$$\phi_O(r, \theta) = [v_{\text{in}} r + B_O r^{-2}] \cos \theta. \quad (5.31)$$

Using boundary conditions 1 and 2, respectively we arrive at the two equations

$$\rho_I A_I R = \rho_O (v_{\text{in}} R + B_O R^{-2}) \quad (5.32a)$$

$$A_I = v_{\text{in}} - 2B_O R^{-3}. \quad (5.32b)$$

By solving Eq. (5.32) with respect to A_I and B_O we find the potential to be given as

$$\phi_I(r, \theta) = v_{\text{in}} r \frac{3\rho_O}{2\rho_I + \rho_O} \cos \theta, \quad (5.33a)$$

$$\phi_O(r, \theta) = v_{\text{in}} \left[r + \frac{\rho_I - \rho_O}{2\rho_I + \rho_O} R^3 r^{-2} \right] \cos \theta. \quad (5.33b)$$

Identifying that $\rho_0 = \rho_O$ and $\rho_s = \rho_I$ as the density of the fluid and the sphere respectively and using that $v_{\text{in}} r \cos \theta = \mathbf{v}_{\text{in}} \cdot \mathbf{r}$, we see that the velocity potential inside the sphere ϕ_I gives the velocity of the sphere itself. Taking the gradient of ϕ_I , we get the velocity $\mathbf{u}(t)$ of the sphere entrained by the fluid with the constant velocity \mathbf{v}_{in} ,

$$\mathbf{u}(t) = \nabla \phi_I = \frac{3\rho_O}{2\rho_s + \rho_0} \mathbf{v}_{\text{in}}(t). \quad (5.34)$$

We see that we have to correct Eq. (5.25) now that the fluid is also moving around the sphere. Placing ourselves in the reference frame of the fluid we again obtain a situation where the fluid is at rest with respect to the chosen coordinate system and the sphere is moving. This situation determines $\mathbf{A}(t)$ as shown in Eq. (5.25) where \mathbf{v}_s is the velocity of the sphere in the chosen system. In the rest-frame of the fluid the sphere will, according to Eq. (5.34), have the velocity $\mathbf{v}_{\text{in}}(t) - \mathbf{u}(t)$ giving the coefficient as

$$\mathbf{A}(t) = -[\mathbf{v}_{\text{in}}(t) - \mathbf{u}(t)] \frac{R^3}{2} = -\frac{R^3(\rho_s - \rho_0)}{2\rho_s + \rho_0} \mathbf{v}_{\text{in}}(t). \quad (5.35)$$

Using the constants a and \mathbf{A} found in Eq. (5.23) and Eq. (5.35) we get the scattered velocity potential by inserting into the general solution Eq. (5.8),

$$\phi_{\text{sc}}(t - r/c_a) = -\frac{R^3}{3\rho_0 r} \dot{\rho}_{\text{in}}(t - r/c_a) f_1 - \frac{R^3}{2} f_2 \nabla \cdot \left(\frac{\mathbf{v}_{\text{in}}(t - r/c_a)}{r} \right), \quad (5.36)$$

where

$$f_1 = 1 - \frac{\rho_0 c_a^2}{\rho_s c_s^2} \quad \text{and} \quad f_2 = \frac{2(\rho_s - \rho_0)}{2\rho_s + \rho_0}. \quad (5.37)$$

5.3 Forces Acting on a Particle in a Plane Running Wave

We want to determine the force on particles in an ideal fluid when the incoming acoustic field is a plane traveling monochromatic wave in the x -direction

$$\phi_{\text{in}}(x, t) = -\frac{u_0}{k} \cos(kx - \omega t). \quad (5.38)$$

Furthermore, we still use the linear approximation for the full first-order perturbation of the velocity potential,

$$\phi_1(\mathbf{r}, t) = \phi_{\text{in}}(\mathbf{r}, t) + \phi_{\text{sc}}(\mathbf{r}, t), \quad (5.39)$$

implying that all quantities with the subscript „in” or „sc” is of first-order.

We see that the projection of the force in the x -direction is given from Eq. (5.7) by an integral over the surface of the sphere ($r = R$)

$$\begin{aligned} \langle F_x \rangle = \langle \mathbf{F} \cdot \mathbf{e}_x \rangle = & - \int_{\partial V} \left\{ \left[-\rho_0 \frac{\langle v_1^2 \rangle}{2} + \frac{\rho_0}{2c_a^2} \left\langle \left(\frac{\partial \phi_1}{\partial t} \right)^2 \right\rangle \right] \mathbf{e}_x \cdot \mathbf{e}_r \right. \\ & \left. + \rho_0 \langle (\mathbf{e}_x \cdot \mathbf{v}_1)(\mathbf{v}_1 \cdot \mathbf{e}_r) \rangle \right\} dA. \end{aligned} \quad (5.40)$$

When inserting the linear splitting of the potential in incoming and scattered quantities indicated in Eq. (5.39), the first term in the curly brackets becomes

$$\zeta = \left[-\rho_0 \frac{\langle v_1^2 \rangle}{2} + \frac{\rho_0}{2c_a^2} \left\langle \left(\frac{\partial \phi_1}{\partial t} \right)^2 \right\rangle \right] \cos \theta, \quad (5.41a)$$

or

$$\begin{aligned} \zeta = & \frac{\rho_0}{2} \left[-\langle v_{\text{in},0}^2 + v_{\text{sc},0}^2 + 2v_{\text{in},0}v_{\text{sc},0} \cos \theta \rangle \right. \\ & \left. + \frac{1}{c_a^2} \langle (\partial_t \phi_{\text{in}})^2 + (\partial_t \phi_{\text{sc}})^2 + 2(\partial_t \phi_{\text{in}})(\partial_t \phi_{\text{sc}}) \rangle \right] \cos \theta. \end{aligned} \quad (5.41b)$$

Here, we have introduced the angle θ between the radial direction, \mathbf{e}_r , and the x direction, \mathbf{e}_x , and used $v_{\text{in},0}$ to denote the amplitude of the incoming velocity *i.e.* $\mathbf{v}_{\text{in}} = v_{\text{in},0}\mathbf{e}_x$, and $v_{\text{sc},0}$ to denote the amplitude of the radial component of the scattered velocity *i.e.* $\mathbf{v}_{\text{sc}} = v_{\text{sc},0}\mathbf{e}_r$.

In Appendix C we have calculated the scattered and incoming velocity field created because of the incoming potential Eq. (5.38). In Eqs. (C.3) and (C.13) we found that $\partial_t \phi_{\text{in}} = -c_a v_{\text{in},0}$ and $\partial_t \phi_{\text{sc}} = -c_a v_{\text{sc},0}$. Using this in Eq. (5.41b) we conclude that

$$\zeta = \frac{\rho_0}{2} \left[-\left\langle v_{\text{in},0}^2 + v_{\text{sc},0}^2 + 2v_{\text{in},0}v_{\text{sc},0} \cos \theta \right\rangle \right. \quad (5.42a)$$

$$\begin{aligned} & \left. + \frac{1}{c_a^2} \left\langle (-c_a v_{\text{sc},0})^2 + (-c_a v_{\text{in},0})^2 + 2(-c_a v_{\text{in},0})(-c_a v_{\text{sc},0}) \right\rangle \right] \cos \theta, \\ & = \rho_0 v_{\text{in},0} v_{\text{sc},0} (\cos \theta - \cos^2 \theta). \end{aligned} \quad (5.42b)$$

The second term in the integrand of Eq. (5.40) is

$$\rho_0 \langle (\mathbf{e}_x \cdot \mathbf{v}_1)(\mathbf{v}_1 \cdot \mathbf{e}_r) \rangle = \rho_0 \langle (\mathbf{e}_x \cdot [\mathbf{v}_{\text{in}} + \mathbf{v}_{\text{sc}}]) ([\mathbf{v}_{\text{in}} + \mathbf{v}_{\text{sc}}] \cdot \mathbf{e}_r) \rangle \quad (5.43)$$

$$= \rho_0 \langle (v_{\text{in},0} + v_{\text{sc},0} \cos \theta)(v_{\text{in},0} \cos \theta + v_{\text{sc},0}) \rangle \quad (5.44)$$

$$= \rho_0 \langle v_{\text{in},0}^2 \cos \theta + v_{\text{sc},0}^2 \cos \theta + v_{\text{in},0} v_{\text{sc},0} (1 + \cos^2 \theta) \rangle. \quad (5.45)$$

Thus the average force on the particle in the direction of the incoming wave (x -direction) is found by inserting Eq. (5.42b) and Eq. (5.45) into Eq. (5.40),

$$\langle F_x \rangle = -\rho_0 \int_{\partial V} \langle v_{\text{in},0}^2 \cos \theta + v_{\text{sc},0}^2 \cos \theta + v_{\text{in},0} v_{\text{sc},0} (1 + \cos \theta) \rangle dA. \quad (5.46)$$

To reduce the expression even further and to realize that the force from a plane traveling wave only depends on the momentum carried away by the scattered wave, we consider the change of energy inside a given volume. Following [5] we find that the change in energy with time inside a given volume V is given by the change in energy flux,

$$\int_V \partial_t E_{\text{ac}} dV = - \int_V \nabla \cdot \mathbf{J}_E dV. \quad (5.47)$$

Taking the time average of Eq. (5.47), remembering that the time average of a time derivative is always zero for periodic functions, see Eq. (3.47), we arrive at

$$0 = \left\langle \int_V \partial_t E_{\text{ac}} dV \right\rangle = \left\langle \int_V \nabla \cdot \mathbf{J}_E dV \right\rangle = \left\langle \int_{\partial V} \mathbf{J}_E \cdot d\mathbf{A} \right\rangle = \int_{\partial V} \langle \mathbf{J}_E \rangle \cdot d\mathbf{A}, \quad (5.48)$$

where we have used Gauss's theorem to convert the volume integral into a surface integral and without loss of generality assumed that the surface does not vary in time. From [5] we have that the energy flux to second order is given as

$$\mathbf{J}_E = \rho_0 (\nabla \phi_1) (\partial_t \phi_1) = \rho_0 \mathbf{v}_1 (\partial_t \phi_1), \quad (5.49)$$

where the subscript 1 as usual denotes the first-order perturbation quantities.

Now we use the linear splitting of the first-order quantities and exploit Eq. (5.48) to get a useful relation between the scattered and incoming velocity components if we let the considered surface be a sphere

$$0 = \int_{\partial V} \left\langle \rho_0 \left(\frac{\partial \phi_{\text{in}}}{\partial t} + \frac{\partial \phi_{\text{sc}}}{\partial t} \right) \mathbf{v}_1 \right\rangle \cdot d\mathbf{A} \quad (5.50a)$$

$$= \rho_0 \int_{\partial V} \left\langle (-c_a v_{\text{in},0} - c_a v_{\text{sc},0})(v_{\text{in},0} \mathbf{e}_x + v_{\text{sc},0} \mathbf{e}_r) \right\rangle \cdot \mathbf{e}_r dA \quad (5.50b)$$

$$= \rho_0 c_a \int_{\partial V} \left\langle [v_{\text{in},0}^2 \cos \theta + v_{\text{sc},0}^2 + v_{\text{in},0} v_{\text{sc},0} (1 + \cos \theta)] \right\rangle dA \quad (5.50c)$$

$$= \left\langle v_{\text{in},0}^2 \cos \theta + v_{\text{sc},0}^2 + v_{\text{in},0} v_{\text{sc},0} (1 + \cos \theta) \right\rangle, \quad (5.50d)$$

where we again have used the relations from Appendix C, $\partial_t \phi_{\text{sc}} = -c_a v_{\text{sc},0}$ and $\partial_t \phi_{\text{in}} = -c_a v_{\text{in},0}$. The last equation follows from the arbitrary choice of integration surface. If the integral is zero for an arbitrary choice of surface, then the integrand must be identical zero. Using Eq. (5.50d) to reduce Eq. (5.46), the average force turns out to be

$$\langle F_x \rangle = \rho_0 \int_{\partial V} \langle v_{\text{sc},0}^2 \rangle (1 - \cos \theta) \, dA. \quad (5.51)$$

The scattered velocity that emerges from the incoming potential Eq. (5.38) through the use of Eq. (5.36) is calculated in Appendix C to lowest order in r

$$\mathbf{v}_{\text{sc}}(t - r/c_a) = \frac{R^3 u_0 \omega^2}{c_a^2 r} \sin[\omega(t - r/c_a)] \left(\frac{1}{3} f_1 - \frac{1}{2} f_2 \cos \theta \right) \mathbf{e}_r + \mathcal{O}(r^{-2}). \quad (5.52)$$

Using that the time average of a sine function squared over a full period is 1/2, we get the desired time average,

$$\langle v_{\text{sc},0}^2 \rangle = \left\langle \left[\frac{R^3 u_0 \omega^2}{c_a^2 r} \sin(\omega(t - r/c_a)) \left(\frac{1}{3} f_1 - \frac{1}{2} f_2 \cos \theta \right) \right]^2 \right\rangle \quad (5.53a)$$

$$= \frac{R^6 u_0^2 \omega^4}{2 c_a^4 r^2} \left(\frac{1}{3} f_1 - \frac{1}{2} f_2 \cos \theta \right)^2. \quad (5.53b)$$

We can now evaluate the integral in Eq. (5.51),

$$\langle F_x \rangle = 2\pi \frac{\rho_0 R^6 u_0^2 k^4}{2} \int_0^\pi \left[\frac{1}{R^2} \left(\frac{f_1^2}{9} - \frac{f_1 f_2}{3} \cos \theta + \frac{f_2^2}{4} \cos^2 \theta \right) \right. \quad (5.54a)$$

$$\left. \times (1 - \cos \theta) R^2 \sin \theta \right] d\theta$$

$$= \frac{\rho_0 R^6 u_0^2 k^4}{2} 2\pi \frac{2}{9} \left(f_1^2 + f_1 f_2 + \frac{3}{4} f_2^2 \right). \quad (5.54b)$$

Letting $I = \rho_0 c_a u_0^2 / 2$ denote the average energy flux density, the average force on a spherical particle with radius R in a fluid in a monochromatic wave is

$$\langle F_x \rangle = \frac{4\pi I}{9c_a} R^2 (kR)^4 \left(f_1^2 + f_1 f_2 + \frac{3}{4} f_2^2 \right). \quad (5.55)$$

We see that the force scales as k^4 . This implies that this force is very small for rapidly oscillating incoming waves. Because we are operating at ultrasound frequencies $f \gtrsim 1.5$ MHz, we conclude that this force is negligible. In the next section we therefore consider the force in an arbitrary wave which is not similar to the plane running wave.

5.4 Forces Acting on a Particle in an Arbitrary Wave

We neglect second-order terms in the scattered and incoming wave thus only taking into account the mixed terms. This reduces Eq. (5.7) to

$$\langle F_i \rangle = - \oint \left(\left[-\frac{\rho_0}{2} \langle \mathbf{v}_1^2 \rangle + \frac{\rho_0}{2c_a^2} \langle (\partial_t \phi_1)^2 \rangle \right] \delta_{ik} + \rho_0 \langle v_{1,j} v_{1,k} \rangle \right) n_k dA \quad (5.56a)$$

$$\begin{aligned} &= -\rho_0 \oint \left(\left[-\frac{1}{2} \langle (\mathbf{v}_{sc} + \mathbf{v}_{in})^2 \rangle + \frac{\rho_0}{2c_a^2} \langle [\partial_t (\phi_{sc} + \phi_{in})]^2 \rangle \right] \delta_{ik} \right. \\ &\quad \left. + \rho_0 \langle (v_{sc,i} + v_{in,i})(v_{sc,k} + v_{in,k}) \rangle \right) n_k dA \end{aligned} \quad (5.56b)$$

$$\begin{aligned} &= -\oint \left(\left[-\frac{\rho_0}{2} \langle 2v_{sc,j} v_{in,j} \rangle + \frac{\rho_0}{2c_a^2} \langle 2(\partial_t \phi_{sc})(\partial_t \phi_{in}) \rangle \right] \delta_{ik} \right. \\ &\quad \left. + \rho_0 \langle v_{sc,i} v_{in,k} + v_{in,i} v_{sc,k} \rangle \right) n_k dA. \end{aligned} \quad (5.56c)$$

Remembering that $\rho_1 = -\rho_0/(c_a^2)\partial_t \phi_1$ from Eq. (3.6) we get for the average force to first order in the scattered and incoming waves

$$\langle F_i \rangle = - \oint \left(\left[-\rho_0 \langle v_{sc,j} v_{in,j} \rangle + \frac{c_a^2}{\rho_0} \langle \rho_{sc} \rho_{in} \rangle \right] \delta_{ik} + \rho_0 \langle v_{sc,i} v_{in,k} \rangle + \rho_0 \langle v_{in,i} v_{sc,k} \rangle \right) n_k dA. \quad (5.57)$$

We convert expression (5.57) to a volume integral using the Gauss's theorem and that summation over all k is implicit,

$$\begin{aligned} \langle F_i \rangle &= - \int_V \partial_k \left(\left[-\rho_0 \langle v_{sc,j} v_{in,j} \rangle + \frac{c_a^2}{\rho_0} \langle \rho_{sc} \rho_{in} \rangle \right] \delta_{ik} \right. \\ &\quad \left. + \rho_0 \langle v_{sc,i} v_{in,k} \rangle + \rho_0 \langle v_{in,i} v_{sc,k} \rangle \right) dV, \end{aligned} \quad (5.58)$$

Noticing that time average and spatial differentiation commute, we get

$$\begin{aligned} \langle F_i \rangle &= - \int_V \left[-\rho_0 \langle (\partial_i v_{sc,j}) v_{in,j} \rangle - \rho_0 \langle v_{sc,j} (\partial_i v_{in,j}) \rangle + \frac{c_a^2}{\rho_0} \langle (\partial_i \rho_{sc}) \rho_{in} \rangle + \langle \rho_{sc} (\partial_i \rho_{in}) \rangle \right. \\ &\quad \left. + \rho_0 \langle (\partial_k v_{sc,i}) v_{in,k} \rangle + \langle v_{sc,i} (\partial_k v_{in,k}) \rangle + \langle (\partial_k v_{in,i}) v_{sc,k} \rangle + \langle v_{in,i} (\partial_k v_{sc,k}) \rangle \right] dV. \end{aligned} \quad (5.59)$$

We note that we are considering a potential flow, and thus

$$\partial_k v_j = \partial_k \partial_j \phi = \partial_j \partial_k \phi = \partial_j v_k. \quad (5.60)$$

Using this interchange of the indices in Eq. (5.59), we get

$$\begin{aligned} \langle F_i \rangle = & - \int_V \left\{ \frac{c_a^2}{\rho_0} \left[\langle (\partial_i \rho_{sc}) \rho_{in} \rangle + \langle \rho_{sc} (\partial_i \rho_{in}) \rangle \right] \right. \\ & \left. + \rho_0 \left[\langle v_{sc,i} (\partial_k v_{in,k}) \rangle + \langle v_{in,i} (\partial_k v_{sc,k}) \rangle \right] \right\} dV. \end{aligned} \quad (5.61)$$

We now consider the inviscid first-order governing equations, Eq. (3.1a) and Eq. (3.1b). Using the linear splitting of the first-order quantities in a scattered and an incoming part, as shown for the potential in Eq. (5.39), we can write the governing first-order equations as

$$\left[\rho_0 \partial_t (\mathbf{v}_{sc} + \mathbf{v}_{in}) \right]_i = \left[-c_a^2 \nabla (\rho_{sc} + \rho_{in}) \right]_i = -c_a^2 \partial_i (\rho_{sc} + \rho_{in}), \quad (5.62a)$$

$$\partial_t (\rho_{sc} + \rho_{in}) = -\rho_0 \nabla \cdot (\mathbf{v}_{sc} + \mathbf{v}_{in}) = -\rho_0 \partial_k (v_{sc,k} + v_{in,k}). \quad (5.62b)$$

From Eq. (5.62a) we conclude that

$$\partial_i \rho_{sc} = -\frac{\rho_0}{c_a^2} \partial_t (v_{sc,i} + v_{in,i}) - \partial_i \rho_{in}, \quad (5.63a)$$

$$\partial_i \rho_{in} = -\frac{\rho_0}{c_a^2} \partial_t (v_{sc,i} + v_{in,i}) - \partial_i \rho_{sc}, \quad (5.63b)$$

and from Eq. (5.62b) we see that we can write

$$\rho_0 \partial_k v_{in,k} = -\partial_t (\rho_{sc} + \rho_{in}) - \rho_0 \partial_k v_{sc,k}. \quad (5.64)$$

Exploiting Eqs. (5.63a), (5.63b), and (5.64) we reduce Eq. (5.61) to

$$\begin{aligned} \langle F_i \rangle = & - \int_V \left\{ \left\langle \left(-\partial_t (v_{sc,i} + v_{in,i}) - \frac{c_a^2}{\rho_0} \partial_i \rho_{in} \right) \rho_{in} \right\rangle + \left\langle \rho_{sc} \left(-\partial_t (v_{sc,i} + v_{in,i}) - \frac{c_a^2}{\rho_0} \partial_i \rho_{sc} \right) \right\rangle \right. \\ & \left. + \left\langle v_{sc,i} (-\partial_t (\rho_{sc} + \rho_{in}) - \rho_0 \partial_k v_{sc,k}) \right\rangle + \rho_0 \left\langle v_{in,i} (\partial_k v_{sc,k}) \right\rangle \right\} dV. \end{aligned} \quad (5.65)$$

We emphasize that we are only considering first-order perturbations in the scattering and incoming fields, *i.e.* we are only considering mixed terms in the scattered and incoming fields. This reduces Eq. (5.65) to

$$\begin{aligned} \langle F_i \rangle = & - \int_V \left\{ -\langle \rho_{in} (\partial_t v_{sc,i}) \rangle - \langle \rho_{sc} (\partial_t v_{in,i}) \rangle - \langle v_{sc,i} (\partial_t \rho_{in}) \rangle \right. \\ & \left. + \rho_0 \langle v_{in,i} (\partial_k v_{sc,k}) \rangle \right\} dV \end{aligned} \quad (5.66a)$$

$$= - \int_V \left\{ -\langle \partial_t (\rho_{in} v_{sc,i}) \rangle - \langle \rho_{sc} (\partial_t v_{in,i}) \rangle + \rho_0 \langle v_{in,i} (\partial_k v_{sc,k}) \rangle \right\} dV. \quad (5.66b)$$

We notice the general case of the time average of a time derivative of an arbitrary periodic function *i.e.*, $\langle \partial_t f \rangle = 0$, see Eq. (3.47). For periodic first-order perturbations we therefore get

$$\langle \partial_t(\rho_{\text{in}} v_{\text{sc},i}) \rangle = \langle \partial_t(\rho_{\text{sc}} v_{\text{in},i}) \rangle = \langle \rho_{\text{sc}}(\partial_t v_{\text{in},i}) + (\partial_t \rho_{\text{sc}}) v_{\text{in},i} \rangle = 0, \quad (5.67)$$

or

$$\langle \rho_{\text{sc}}(\partial_t v_{\text{in},i}) \rangle = -\langle (\partial_t \rho_{\text{sc}}) v_{\text{in},i} \rangle. \quad (5.68)$$

Inserting Eqs. (5.67) and (5.68) into Eq. (5.66b) we get

$$\langle F_i \rangle = - \int_V \left\langle v_{\text{in},i} (\rho_0(\partial_k v_{\text{sc},k}) + \partial_t \rho_{\text{sc}}) \right\rangle dV. \quad (5.69)$$

Reintroducing the velocity potential by the relations $v_{\text{sc},k} = \partial_k \phi_{\text{sc}}$ and $\rho_{\text{sc}} = -\rho_0/(c_a^2) \partial_t \phi_{\text{sc}}$, we get

$$\langle F_i \rangle = -\rho_0 \int_V \left\langle v_{\text{in},i} \left[\partial_k^2 \phi_{\text{sc}} - \frac{1}{c_a^2} \partial_t^2 \phi_{\text{sc}} \right] \right\rangle dV. \quad (5.70)$$

If we consider the integrand of Eq. (5.70) we see that the contents of the squared brackets are similar to the wave equation for the scattered velocity potential, Eq. (5.26). The scattered velocity potential has been determined in Eq. (5.36). We conclude that we are considering the case described in Appendix B with

$$a(t - r/c) = -R^3/(3\rho_0) f_1 \dot{\rho}_{\text{in}}(t - r/c), \quad (5.71)$$

and

$$\mathbf{A}(t - r/c) = -R^3/(2) f_2 \mathbf{v}_{\text{in}}(t - r/c). \quad (5.72)$$

From the analogy with Appendix B we see from Eqs. (B.13) and (B.24) that inserting the velocity potential Eq. (5.36) into the scalar wave equation will give us zero everywhere except at the origin, where the divergence is represented by delta-functions. As usual suppressing the arguments, we see that

$$\left[\nabla^2 - \frac{1}{c_a^2} \partial_t^2 \right] \left[\frac{a}{r} + \nabla \cdot \left(\frac{\mathbf{A}}{r} \right) \right] = -4\pi a \delta^3(\mathbf{r}) - 4\pi \nabla \cdot [\mathbf{A} \delta^3(\mathbf{r})] \quad (5.73)$$

$$= 4\pi \frac{R^3}{3\rho_0} f_1 \dot{\rho}_{\text{in}} \delta^3(\mathbf{r}) + 4\pi \frac{R^3}{2} f_2 \nabla \cdot [\mathbf{v}_{\text{in}} \delta^3(\mathbf{r})]. \quad (5.74)$$

Inserting Eq. (5.74) into Eq. (5.70), we get

$$\langle F_i \rangle = -\rho_0 \int_V \left\langle v_{\text{in},i} \left[\frac{4\pi}{3\rho_0} R^3 f_1 \dot{\rho}_{\text{in}} \delta^3(\mathbf{r}) + 2\pi R^3 f_2 \nabla \cdot (\mathbf{v}_{\text{in}} \delta^3(\mathbf{r})) \right] \right\rangle dV. \quad (5.75)$$

Remembering the general rules for integration by parts,

$$\int_V (\nabla f) \cdot \mathbf{u} dV = \int_{\partial V} f \mathbf{u} \cdot d\mathbf{A} - \int_V f (\nabla \cdot \mathbf{u}) dV, \quad (5.76)$$

where f is an arbitrary scalar function and \mathbf{u} is an arbitrary vector function, we can now carry out the integration¹ in Eq. (5.75) with $f = v_{\text{in},i}$ and $\mathbf{u} = \mathbf{v}_{\text{in}}\delta^3(\mathbf{r})$

$$\begin{aligned} \langle F_i \rangle = & -\rho_0 \left\langle \frac{4\pi}{3\rho_0} R^3 f_1 \dot{\rho}_{\text{in}} v_{\text{in},i} \right\rangle - 2\pi R^3 f_2 \rho_0 \left[\int_{\partial V} \langle v_{\text{in},i} \mathbf{v}_{\text{in}} \delta^3(\mathbf{r}) \rangle \cdot d\mathbf{A} \right. \\ & \left. - \int_V \langle (\nabla v_{\text{in},i}) \cdot \mathbf{v}_{\text{in}} \delta^3(\mathbf{r}) \rangle dV \right]. \end{aligned} \quad (5.77)$$

Here we take the volume to be any volume outside the considered body, because we by definition have placed the origin inside the body.

The first integral in the squared brackets is zero because the integration area does not include the origin, and the three-dimensional delta function therefore is zero everywhere on the integration surface. Hence we get

$$\langle F_i \rangle = -\frac{4}{3}\pi R^3 f_1 \langle \dot{\rho}_{\text{in}} v_{\text{in},i} \rangle + 2\pi R^3 f_2 \rho_0 \langle (\nabla v_{\text{in},i}) \cdot \mathbf{v}_{\text{in}} \rangle \quad (5.78)$$

$$= -\frac{4}{3}\pi R^3 f_1 \langle \dot{\rho}_{\text{in}} v_{\text{in},i} \rangle + 2\pi R^3 f_2 \rho_0 \langle (\partial_k v_{\text{in},i}) v_{\text{in},k} \rangle. \quad (5.79)$$

In Eq. (5.79) it is understood that every variable is taken at the origin, *i.e.* at the position of the particle in consideration.

To make the interpretation of this result more simple we want to express the average force by a force potential. We notice that we have assumed the first-order velocity perturbation to be an irrotational vector field, hence by Eq. (5.79) the average force must also be an irrotational vector field. We can therefore introduce the scalar force potential in analogy to the velocity potential as $\langle \mathbf{F} \rangle \equiv -\nabla U$. Notice that the minus sign is purely conventional to make particles go to places with a small potential.

We notice that we can rewrite the first term of Eq. (5.79) when we only consider periodic perturbations. From Eq. (3.47) we conclude that

$$\langle \partial_t (\rho_{\text{in}} \mathbf{v}_{\text{in}}) \rangle = \mathbf{0} \quad (5.80)$$

or

$$\langle (\partial_t \rho_{\text{in}}) \mathbf{v}_{\text{in}} \rangle = -\langle \rho_{\text{in}} (\partial_t \mathbf{v}_{\text{in}}) \rangle. \quad (5.81)$$

Using the result Eq. (5.80) and the governing equations without viscosity, Eq. (3.1a) and Eq. (2.8c), we can rewrite the first term of Eq. (5.79) to concern only the pressure,

$$-\frac{4}{3}\pi R^3 f_1 \langle (\partial_t \rho_{\text{in}}) v_{\text{in},i} \rangle = \frac{4}{3}\pi R^3 f_1 \langle \rho_{\text{in}} (\partial_t v_{\text{in},i}) \rangle = \frac{4}{3}\pi R^3 f_1 \left\langle \left(\frac{p_{\text{in}}}{c_a^2} \right) \left(-\frac{\partial_i p_{\text{in}}}{\rho_0} \right) \right\rangle \quad (5.82a)$$

$$= -\frac{4}{3c_a^2 \rho_0} \pi R^3 f_1 \langle p_{\text{in}} (\partial_i p_{\text{in}}) \rangle. \quad (5.82b)$$

¹Integration of the three-dimensional δ -function is defined as: $\int_V f(\mathbf{r})\delta^3(\mathbf{r} - \mathbf{r}_0)dV = f(\mathbf{r}_0)$ if the volume V includes the point $\mathbf{r} = \mathbf{r}_0$, otherwise the integral equals zero.

When we want to write the force as the gradient of the scalar force potential, we notice that

$$\partial_i(p_{\text{in}}^2) = 2p_{\text{in}}(\partial_i p_{\text{in}}), \quad (5.83a)$$

$$\partial_i(\mathbf{v}_{\text{in}}^2) = 2v_{\text{in},k}(\partial_i v_{\text{in},k}) = 2v_{\text{in},k}(\partial_k v_{\text{in},i}), \quad (5.83b)$$

where we in the last equality in Eq. (5.83b) have used the assumption that the velocity field is irrotational, and that we therefore can interchange the indices when taking the gradient as shown in Eq. (5.60).

We notice that Eq. (5.83a) and Eq. (5.83b) are the expressions that we have in Eq. (5.79). Using this and the result from Eq. (5.82b), we see that the force can be written as the gradient of a scalar field,

$$\langle F_i \rangle = -\frac{4}{3c_a^2 \rho_0} \pi R^3 f_1 \langle p_{\text{in}} (\partial_i p_{\text{in}}) \rangle + 2\pi R^3 f_2 \rho_0 \langle (\partial_k v_{\text{in},i}) v_{\text{in},k} \rangle \quad (5.84a)$$

$$= -\frac{4}{3c_a^2 \rho_0} \pi R^3 f_1 \left\langle \frac{1}{2} \partial_i (p_{\text{in}}^2) \right\rangle + 2\pi R^3 f_2 \rho_0 \left\langle \frac{1}{2} \partial_i (\mathbf{v}_{\text{in}}^2) \right\rangle. \quad (5.84b)$$

This implies that the scalar field U for which $\langle \mathbf{F} \rangle = -\nabla U$ is given as

$$U = \frac{2}{3c_a^2 \rho_0} \pi R^3 f_1 \langle p_{\text{in}}^2 \rangle - \pi R^3 f_2 \rho_0 \langle \mathbf{v}_{\text{in}}^2 \rangle = 2\pi R^3 \rho_0 \left[\frac{\langle p_{\text{in}}^2 \rangle}{3c_a^2 \rho_0^2} f_1 - \frac{\langle \mathbf{v}_{\text{in}}^2 \rangle}{2} f_2 \right]. \quad (5.85)$$

5.5 Pressure Force on a Single Particle in a Standing Wave

Eq. (5.85) is expressing the force potential on a body given the incoming pressure p_{in} and velocity v_{in} at the position of the particle. Assuming a standing wave in a single direction, the x -direction, we can write the incoming velocity potential as

$$\phi_{\text{in}} = \frac{u_0}{k} \cos(kx) \cos(\omega t), \quad (5.86)$$

where u_0 is the velocity amplitude, k is the wavenumber of the standing wave, and ω is the angular frequency of the wave. From Eqs. (3.5) and (3.7) we get the velocity and the pressure

$$\mathbf{v}_{\text{in}} = \nabla \phi_{\text{in}} = (\partial_x \phi_{\text{in}}) \mathbf{e}_x = -u_0 \sin(kx) \cos(\omega t) \mathbf{e}_x, \quad (5.87a)$$

$$p_{\text{in}} = -\rho_0 \partial_t \phi_{\text{in}} = \frac{u_0 \rho_0 \omega}{k} \cos(kx) \sin(\omega t) = u_0 \rho_0 c_a \cos(kx) \sin(\omega t). \quad (5.87b)$$

Inserting Eqs. (5.87a) and (5.87b) into Eq. (5.85) gives the force potential

$$U = 2\pi R^3 \rho_0 \left[\frac{\langle (u_0 \rho_0 c_a)^2 \cos^2(kx) \sin^2(\omega t) \rangle}{3c_a^2 \rho_0^2} f_1 - \frac{\langle u_0^2 \sin^2(kx) \cos^2(\omega t) \rangle}{2} f_2 \right] \quad (5.88a)$$

$$= 2\pi R^3 \rho_0 u_0^2 \left[\frac{1}{3} f_1 \langle \cos^2(kx) \sin^2(\omega t) \rangle - \frac{1}{2} f_2 \langle \sin^2(kx) \cos^2(\omega t) \rangle \right] \quad (5.88b)$$

$$= 2\pi R^3 \rho_0 u_0^2 \left[\frac{1}{6} f_1 \cos^2(kx) - \frac{1}{4} f_2 \sin^2(kx) \right], \quad (5.88c)$$

where we in the last equality have used that the time-average of cosine or sine functions over a period is $1/2$.

The average force on a particle located at x is then given as $\langle F_x \rangle = -\partial_x U$, from the definition $\langle \mathbf{F} \rangle = -\nabla U$, which leads to

$$\langle F_x \rangle = -2\pi R^3 \rho_0 u_0^2 \left[-\frac{2}{6} f_1 k \cos(kx) \sin(kx) - \frac{2}{4} f_2 k \sin(kx) \cos(kx) \right] \quad (5.89a)$$

$$= -4\pi R^3 \rho_0 u_0^2 k \cos(kx) \sin(kx) \left[-\frac{1}{6} f_1 - \frac{1}{4} f_2 \right] \quad (5.89b)$$

$$= 8\pi k R^3 \langle E_{ac} \rangle \sin(2kx) \left[\frac{1}{6} f_1 + \frac{1}{4} f_2 \right], \quad (5.89c)$$

where we in the last equality have used the trigonometric identity $\sin(2a) = 2 \sin(a) \cos(a)$ and the dispersion relation $\omega = c_a k$. Furthermore we have used that the average acoustic energy in the incoming wave $\langle E_{ac} \rangle$ is given by [5]

$$\langle E_{ac} \rangle = \frac{1}{2} \rho_0 \left[\left\langle (\nabla \phi_{in})^2 \right\rangle + \left\langle \left(\frac{1}{c_a} \partial_t \phi_{in} \right)^2 \right\rangle \right] \quad (5.90a)$$

$$= \frac{1}{2} \rho_0 \left[\left\langle (-u_0 \sin(kx) \cos(\omega t))^2 \right\rangle + \left\langle \left(-\frac{u_0 \omega}{k c_a} \cos(kx) \sin(\omega t) \right)^2 \right\rangle \right] \quad (5.90b)$$

$$= \frac{1}{4} \rho_0 [u_0^2 \sin^2(kx) + u_0^2 \cos^2(kx)] = \frac{1}{4} \rho_0 u_0^2. \quad (5.90c)$$

Returning to Eq. (5.89c) inserting Eq. (5.37) gives the force acting on a small particle in a standing wave in the x -direction:

$$\langle F_x \rangle = 8\pi k R^3 \langle E_{ac} \rangle \sin(2kx) \left[\frac{1}{6} \left(1 - \frac{c_a^2 \rho_0}{c_s^2 \rho_s} \right) + \frac{1}{4} \frac{2(\rho_s - \rho_0)}{2\rho_s + \rho_0} \right] \quad (5.91a)$$

$$= 4\pi k R^3 \langle E_{ac} \rangle \sin(2kx) \left[\frac{\rho_s + \frac{2}{3}(\rho_s - \rho_0)}{2\rho_s + \rho_0} - \frac{1}{3} \frac{c_a^2 \rho_0}{c_s^2 \rho_s} \right] \quad (5.91b)$$

$$= 4\pi k R^3 \langle E_{ac} \rangle \Phi \sin(2kx). \quad (5.91c)$$

We see by comparison with Eq. (5.55) that this force is many times larger because it scales as $(kR)R^2$ and not as $(kR)^4 R^2$ which was the case for the plane traveling wave. For simplicity we define the term in the square brackets in Eq. (5.91b) as Φ .

5.6 Visualizing the Pressure Force and the Idea Behind Particle Separation

When we in the following chapters discuss the acoustophoretic sign, we understand it as the sign of the Φ -factor. We notice that it is the Φ -factor which determines the direction of the pressure force. Hence it is the density and speed of sound of the single particles compared to the fluid that determines the direction of the pressure force.

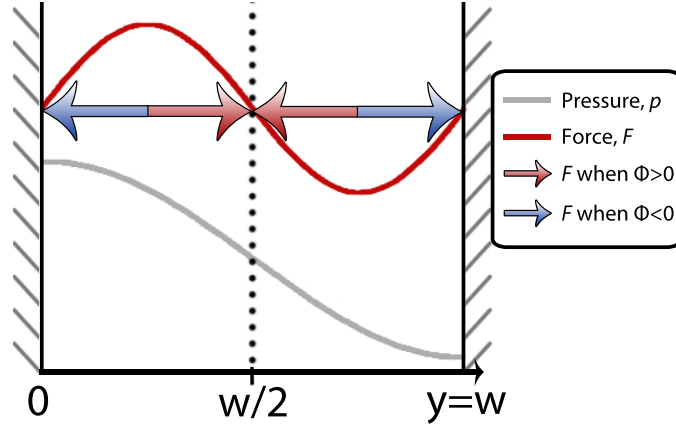


Figure 5.1: A sketch showing the pressure (velocity potential) standing wave in the channel with a wavelength of $\lambda/2 = w$. Furthermore the resulting pressure force as expressed by Eq. (5.91c) is sketched for $\Phi > 0$. If we plotted it for $\Phi < 0$ the sign would change. The arrows indicate the direction of the force on particles with negative or positive Φ -factor respectively.

As an illustration of the principle we consider a resonator of the type discussed in Chapter 4 where the walls are placed at $y = 0$ and $y = w$. At resonance the pressure field (velocity potential) has anti-nodes at the walls as shown in Eq. (4.6). The wavelength is then given as $\lambda/2 = w$ which gives the fundamental mode of the resonance condition derived in Eq. (4.7), $k = n\pi/w$, $n \in \mathbb{N}$. We see from Fig. 5.1 that the wavelength of the force is half the wavelength of the pressure resulting in a positive force in the area $0 < y < w/2$ and a negative force for $w/2 < y < w$ for particles with $\Phi > 0$. The result is that particles with a positive Φ -factor move towards the center of the channel and are thereby collected at the nodes in the pressure. In the same way we observe that particles with $\Phi < 0$ move towards the edges of the channel and end up at the anti-nodes in the pressure. It is this general principle we will be using in order to separate different types of particles in the second part of the thesis.

5.7 Considering the Pressure Force in 2D

The pressure force can also be determined in the two-dimensional case where we use the potential from Eq. (5.85) as a starting point. When considering a standing wave in two dimensions, we can write the velocity potential corresponding to Eq. (5.86) as

$$\phi_{\text{in}}^{2\text{D}} = \frac{u_0}{k} \cos(k_x x) \cos(k_y y) \cos(\omega t), \quad (5.92)$$

where we use the fact that a standing wave can be written as the sum of two counter-propagating waves with wave vectors \mathbf{k} and $-\mathbf{k}$ respectively, such that $k^2 = k_x^2 + k_y^2$. With Eqs. (3.5) and (3.7) we find

$$\mathbf{v}_{\text{in}} = -\frac{u_0 k_x}{k} \sin(k_x x) \cos(k_y y) \cos(\omega t) \mathbf{e}_x - \frac{u_0 k_y}{k} \cos(k_x x) \sin(k_y y) \cos(\omega t) \mathbf{e}_y, \quad (5.93)$$

$$p_{\text{in}} = -\rho_0 \partial_t \phi_{\text{in}}^{2\text{D}} = -\frac{\omega u_0}{k} \cos(k_x x) \cos(k_y y) \sin(\omega t). \quad (5.94)$$

Inserting these equations into Eq. (5.85) we arrive at

$$U^{2D} = U_0 \left[2f_1 \cos^2(k_x x) \cos^2(k_y y) - 3 \left(\frac{k_x^2}{k^2} \sin^2(k_x x) \cos^2(k_y y) + \frac{k_y^2}{k^2} \cos^2(k_x x) \sin^2(k_y y) \right) f_2 \right]. \quad (5.95)$$

with

$$U_0 = \frac{1}{8} \frac{4\pi R^3}{3} u_0^2 \rho_0 = \frac{1}{2} \frac{4\pi R^3}{3} \langle E_{ac} \rangle. \quad (5.96)$$

Because of symmetry in x and y in Eq. (5.95), we will only calculate the pressure force in the x -direction, which becomes

$$\langle F_x \rangle = -\partial_x U^{2D} = 2U_0 k_x \cos(k_x x) \sin(k_x x) \times \left[2f_1 \cos^2(k_y y) + 3f_2 \frac{k_x^2}{k^2} \cos^2(k_y y) - 3f_2 \frac{k_y^2}{k^2} \sin^2(k_y y) \right]. \quad (5.97)$$

Using $k^2 = k_x^2 + k_y^2$ and some trigonometric manipulation, Eq. (5.97) can be reduced to

$$\langle F_x \rangle = U_0 k_x \sin(2k_x x) \left[2f_1 \cos^2(k_y y) + 3f_2 \left(\cos^2(k_y y) - \frac{k_y^2}{k^2} \right) \right]. \quad (5.98)$$

We see that if $k_y = 0$, corresponding to $k = k_x$, we arrive at the 1D equation like we would expect.

Part II

Discussion of Applications in the Single-Particle Approach

Chapter 6

Analytic Solution in Simple Channel

The pressure force gives the possibility of manipulating particles in a laminar flow as experimentally verified in [30], [32], [42]. We would like to point out first that the analyses in this part will be based on the single-particle approach, neglecting all interactions between the particles. Hence the particles will only be affected by the flow of the fluid and by the pressure force originating from the standing wave.

As the simplest case we start with the one-particle approach to particle manipulation by considering the movement of a particle in a channel. We determine the trajectory and travel time of a single particle in the laminar flow given a certain starting position in the channel. Following the experimental results [24], [28], [29], we are considering a channel with width $w = \lambda/2$, where λ is the wavelength of the standing wave (velocity potential or pressure) with anti-nodes at the channel edge as illustrated in Section 5.6.

The particles are placed in a laminar flow in a rectangular channel with width w , height h , and length L as shown in Fig. 6.1. We notice the obvious symmetry of the considered setup around the center of the channel at $y = w/2$. All setups considered in this thesis will feature this symmetry, and we conclude that it suffices only to consider one half of the channel. We will in all the following analyses only consider the left side of the channel as the systems will be mirrored in the right-hand side, such that the x -direction is the direction of the laminar flow. Here a coordinate system is placed with the x -axis parallel to the channel edge with zero at the edge of the channel. The y -axis is placed orthogonally to the channel edge as shown in Fig. 6.1.

6.1 Travel Time

First we want to find an expression for the time a particle uses to travel between two points, $y(t_1)$ to $y(t_2)$, in the transverse direction.

We assume that we have a standing pressure wave in the y -direction and neglect possible standing waves in the x -direction. Furthermore we assume that the flow is laminar, indicating that we have to require a small Reynold's number, *i.e.*, $Re < 10$. The characteristic velocity of the problem is the velocity of the flow in the channel, and the characteristic

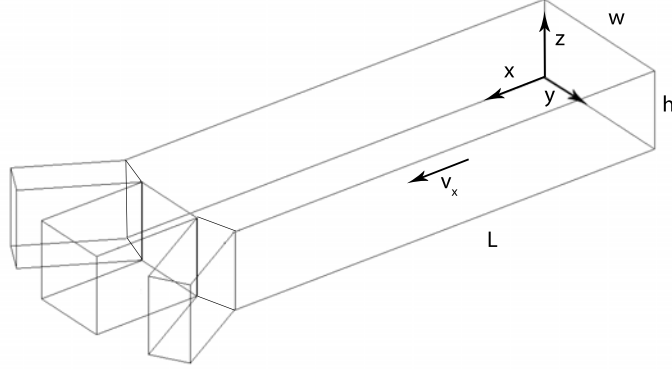


Figure 6.1: A sketch of the rectangular channel with indication of the used coordinate system.

length scale is the radius of the particles, which with the parameters given in Chapter 7 gives

$$Re \equiv \frac{R\rho_0 v_{\text{flow}}}{\eta} \approx \frac{5 \times 10^{-6} \text{ m} \times 10^3 \text{ kg m}^{-3} \times 0.1 \text{ m s}^{-1}}{0.890 \times 10^{-3} \text{ Pa s}} = 0.11 \quad (6.1)$$

We see that the assumption is fulfilled so that the considered flows can be assumed laminar. In laminar flows a spherical particle with a relative velocity of \mathbf{v} compared to the fluid experiences a Stokes-drag given by [5]

$$\mathbf{F}_{\text{drag}} = 6\pi\eta R\mathbf{v}, \quad (6.2)$$

and the force on the particle from the acoustic field in 1D is given as Eq. (5.91c)

$$\mathbf{F}_{\text{pressure}} = 4\pi\langle E_{\text{ac}} \rangle R^2 (k_y R) \Phi \sin(2k_y y) \mathbf{e}_y. \quad (6.3)$$

Assuming that the particle only has a non-zero velocity when a force is acting on it¹ and neglecting the body forces on the particle, the velocity component in the y -direction is determined by balancing the pressure force and the Stokes drag,

$$F_{\text{drag},y} = F_{\text{pressure}} \Leftrightarrow v_y = \frac{2\langle E_{\text{ac}} \rangle R^2 k_y}{3\eta} \Phi \sin(2k_y y) \Leftrightarrow \frac{dy}{dt} = \alpha_y \sin(2k_y y), \quad (6.4)$$

where α_y for simplicity is introduced as the constant in front of the sine in the following analysis. The differential equation Eq. (6.4) can be solved by separation of the variables in an interval

$$p\pi < 2k_y y < (p+1)\pi \Leftrightarrow p\frac{\pi}{2k_y} < y < (p+1)\frac{\pi}{2k_y}, \quad \text{where } p \in \mathbb{Z}. \quad (6.5)$$

Using that

$$\int \frac{1}{\sin(2x)} dx = \log |\tan(x)|, \quad (6.6)$$

¹It can be estimated that the time for acceleration of the particle is on the order of μs , and thus it is reasonable to assume that it is always moving in a local steady-state [5].

gives the travel time

$$t_2 - t_1 = \frac{1}{\alpha_y} \frac{1}{2k_y} \log \left(\frac{\tan[k_y y(t_2)]}{\tan[k_y y(t_1)]} \right), \quad \text{where } \alpha_y = \frac{2\langle E_{ac} \rangle R^2 k_y \Phi}{3\eta}, \quad (6.7)$$

and $\log(a)$ denotes the natural logarithm of a . Notice that if $\Phi < 0$, then the travel time becomes negative, *i.e.* the particle travels from $y(t_2)$ to $y(t_1)$ and not from $y(t_1)$ to $y(t_2)$. It should also be noted that with the resonance condition $k_y = n_y \pi / w$, the solution is valid within the interval from Eq. (6.5)

$$\frac{p}{n_y} \frac{w}{2} < y < \frac{p+1}{n_y} \frac{w}{2}, \quad \text{where } p \in \mathbb{N}_0 \quad \text{and} \quad n_y \in \mathbb{N}. \quad (6.8)$$

$y(t_1)$ and $y(t_2)$ have to be in the same interval, which gives the same sign of the two tangent-terms in Eq. (6.7), and thus we have removed the absolute value from Eq. (6.6). As an example we consider the case with $n_y = 1$, which gives us that Eq. (6.7) is valid in either the left- or the right-hand side of the channel. A particle starting in either of the intervals will theoretically never enter another interval.

6.2 Distance Traveled in Longitudinal Direction

We note from Eq. (6.8) that when $w = \lambda/2 \Leftrightarrow n_y = 1$ and when considering the left-hand side of the channel as explained in the introduction to this chapter, $\tan(k_y y) = \tan(\pi y/w) > 0$, such that we from Eq. (6.7) see that

$$2k_y \alpha_y (t_2 - t_1) = \log \left(\frac{\tan[k_y y(t_2)]}{\tan[k_y y(t_1)]} \right) \quad (6.9)$$

$$\tan[k_y y(t_1)] e^{2k_y \alpha_y (t_2 - t_1)} = \tan[k_y y(t_2)] \quad (6.10)$$

$$y(t_2) = \frac{1}{k_y} \text{Arctan} \left[e^{2k_y \alpha_y (t_2 - t_1)} \tan [k_y y(t_1)] \right]. \quad (6.11)$$

The movement in the x -direction is determined only by the flow profile in the channel, when we neglect all standing waves in the channel except the one in the y -direction. In a rectangular channel with width w and height h the flow profile is given by [5],

$$v_x(y) = \frac{4h^2 \Delta p}{\pi^3 \eta L} \sum_{n, \text{odd}} \frac{1}{n^3} \left[1 - \frac{\cosh \left(n\pi \frac{y-w/2}{h} \right)}{\cosh \left(n\pi \frac{w}{2h} \right)} \right] \sin \left(n\pi \frac{z}{h} \right), \quad (6.12)$$

with our choice of coordinate system, and where $\Delta p/L$ is the applied pressure per length of the channel. We assume throughout the thesis that we are at $z = h/2$, and thus the sine-factor in the equation above becomes $(-1)^{(n-1)/2}$.

We have plotted the Pouseille-flow speed, v_x , in a rectangular channel ($350 \mu\text{m} \times 125 \mu\text{m}$), and the result can be seen in Fig. 6.2a. From the plot we see that the flow-speed has a maximum in the middle of the channel and goes to zero at the boundaries.

To find out how many terms to include in the Pouseille-flow, we have plotted the ratio of the flow-speed with n -terms to the one with $(n-1)$ -terms. The results can be seen in

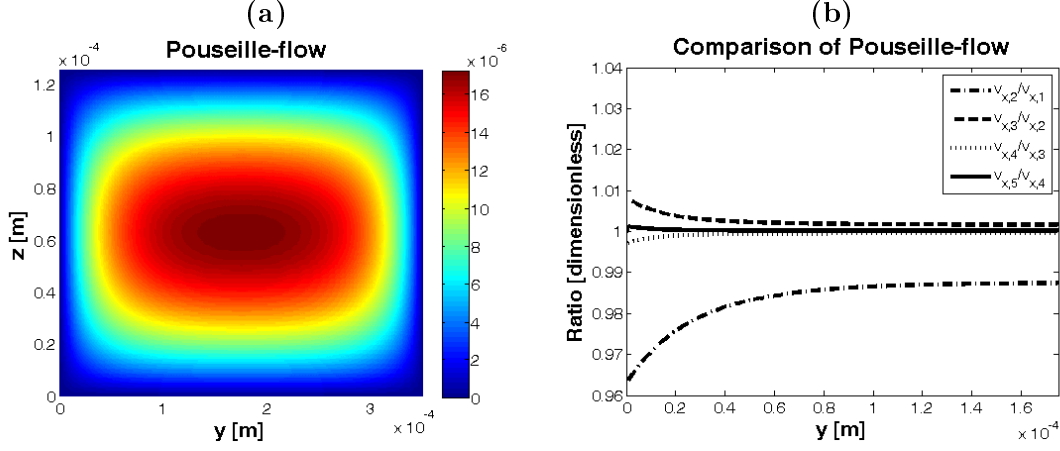


Figure 6.2: (a) The Pouseille-flow in a rectangular channel using the parameters defined in Chapter 7. The colormap shows v_x in units of m s^{-1} . The plot is made using four terms in Eq. (6.12). Notice that the figure in the xy -direction is not to scale. (b) This plot shows a comparison of the terms in the sum included in v_x , Eq. (6.12), where we plot the ratios of the flows with n -terms compared to the one with $(n-1)$ -terms term at $z = h/2$. From this plot we conclude that it is sufficient to include four terms. Notice that we due to the symmetry of the system only have plotted from $0 \leq y \leq w/2$.

Fig. 6.2b. From this plot we conclude that four terms should be enough to get accurate simulations.

Now we can find the total distance traveled in the x -direction from a particle entering the channel at position $y(t_1)$,

$$x(t_1, t_2) = \int_{t_1}^{t_2} v_x[y(t')] dt' = \int_{y(t_1)}^{y(t_2)} v_x(y') \left(\frac{dy'(t)}{dt} \right)^{-1} dy' \quad (6.13)$$

Further on we will use the shorthand notation, y_1 as $y(t_1)$ and y_2 as $y(t_2)$. From Eq. (6.4) we have an expression for dy/dt . Thus we can calculate the traveled distance knowing the entry position and the final position of the particle from Eq. (6.13)

$$\begin{aligned} x(y_1, y_2) &= \int_{y_1}^{y_2} v_x(y') \frac{1}{\alpha_y \sin(2k_y y')} dy' \quad (6.14) \\ &= \frac{4h^2 \Delta p}{\pi^3 \eta L} \frac{1}{\alpha_y} \int_{y_1}^{y_2} \frac{1}{\sin(2k_y y')} \\ &\quad \times \left(\sum_{n, \text{odd}}^{\infty} \frac{1}{n^3} \left[1 - \frac{\cosh\left(n\pi \frac{y' - w/2}{h}\right)}{\cosh\left(n\pi \frac{w}{2h}\right)} \right] (-1)^{(n-1)/2} \right) dy' \quad (6.15) \end{aligned}$$

Note that $1/\alpha_y \propto \eta$ which means that $x(y_1, y_2)$ is independent of the viscosity as long as it is the same everywhere in the channel. The viscosity only affects the individual time profiles $y(t)$ and $x(t)$, but not the trajectory $x(y)$.

Furthermore we would like to point out that $x(y_1, y_2) \propto \langle E_{ac} \rangle^{-1}$. From experiments in [4] we have seen that $\langle E_{ac} \rangle$ scales as the square of the applied voltage over the piezo-

acutator, such that $x(y_1, y_2) \propto V_{\text{PP}}^{-2}$. This means that the travel length can be changed a lot by adjusting V_{PP} .

The integral in Eq. (6.15) cannot be evaluated analytically using simple integral solution techniques. Thus to get an idea of the form of the expression $x(y_1, y_2)$ we will assume a constant flow profile across the channel, *i.e.* $v_x(y) = v_{x,\text{av}}$, which is not the whole truth according to Fig. 6.2, but it seems reasonably at $z = h/2$ for the center part of the channel. Using Eq. (6.14) we find

$$x(y_1, y_2) = \frac{v_{x,\text{av}}}{\alpha_y} \int_{y_1}^{y_2} \frac{1}{\sin(2k_y y')} dy' \quad (6.16)$$

$$= \frac{v_{x,\text{av}}}{\alpha_y} \frac{1}{2k_y} \log \left(\frac{\tan(k_y y_2)}{\tan(k_y y_1)} \right) \quad (6.17)$$

$$= \frac{3\eta v_{x,\text{av}}}{4\langle E_{\text{ac}} \rangle k_y^2 R^2 \Phi} \log \left(\frac{\tan(k_y y_2)}{\tan(k_y y_1)} \right). \quad (6.18)$$

As an example we see that x has a R^{-2} dependence. It is because the larger the particles, the faster they travel from y_1 to y_2 , and thus they travel a shorter distance down the channel in the x -direction. Notice that $v_{x,\text{av}} \propto 1/\eta$ such that $x(y_1, y_2)$ is independent of η even though it explicitly looks like it depends on η .

6.3 Experimental Verification of Theory

To test the simple model that the particle moves according to Eq. (6.11) in the y -direction, we consider a setup with a video camera filming the flow in a channel through a Pyrex-lid placed on the channel. Polystyrene spheres with known radii are let into the channel with a non-zero flow rate. When we are sure that particles have entered the channel, the flow is stopped and the camera starts filming. A piezo-actuator attached to the chip with the channel is activated with a frequency matching $w = \lambda/2$ and the particles (with positive Φ) moves towards the channel center.

The experiments were made by Rune Barnkob [4], and the video was analyzed using the freeware-program **Tracker**², see Fig. 6.3. For simplicity we treat the data of the right-hand side as it was mirrored in the central axis of the channel into the left-hand side. Using MATLAB's `lsqcurvefit` we fit the data with a two parameter fit of k_y and $\langle E_{\text{ac}} \rangle$ to Eq. (6.11) remembering that k_y is also contained in α_y to the first power. For the fitting script see Section H.1.

The fit is shown in Fig. 6.4 and it matches the experimental data very well. Furthermore it gives an estimate of the average acoustical energy and the wavelength. We find $\langle E_{\text{ac}} \rangle = 15.1 \text{ J m}^{-3}$ and $\lambda/2 = 381.5 \text{ }\mu\text{m}$. The value of $\lambda/2$ agrees with the width of the channel, $w = 377 \text{ }\mu\text{m}$. The value of $\langle E_{\text{ac}} \rangle$ gives an estimate of a reasonable value to use in our later simulations. It should be noted that this experiment was made with a peak-to-peak voltage of 1.0 V, but it could also be turned up to at least 10 V as done in [28]. The acoustic energy scales approximately, as noted before, with the square of the peak-to-peak

²<http://www.cabrillo.edu/~dbrown/tracker/>

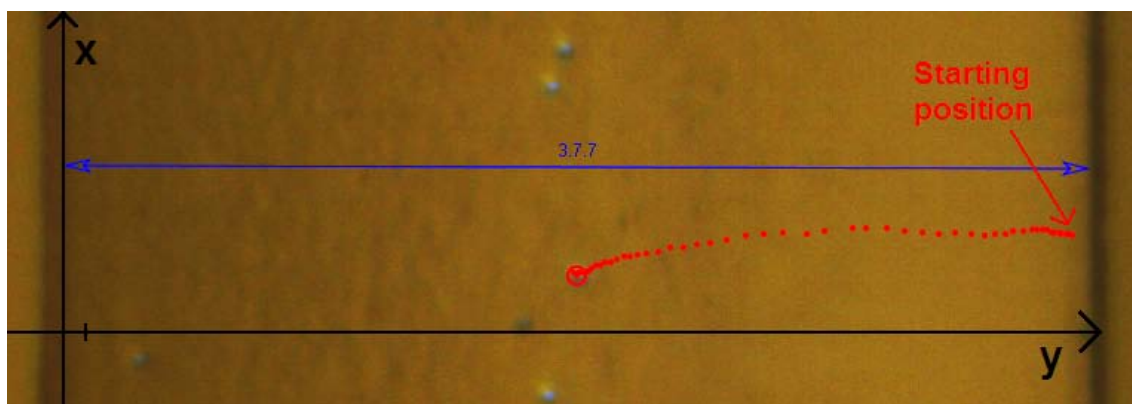


Figure 6.3: Output from the program Tracker. The red dots show the trajectory of a polystyrene particle in a water solution starting from the right side of the channel moving towards the center when the flow in the channel has been turned off for some time, and the piezo-actuator suddenly is turned on. The blue line indicates the channel with width of $377 \mu\text{m}$. The time step between two points is $1/16 \text{ s}$. Even though the flow in the channel is turned off, we see fluctuations in the x -direction. This might be due to longitudinal modes or acoustic streaming, discussed in Part III.

voltage [4], so our value of $\langle E_{ac} \rangle = 1000 \text{ J m}^{-3}$ in the simulations seems like a reasonable estimate.

To be able to interpret these data thoroughly, more particles have to be tracked, but that is beyond the scope of this thesis. The purpose here is to show that our analytical expression for the particle movement in the y -direction actually agrees with the experimental results.

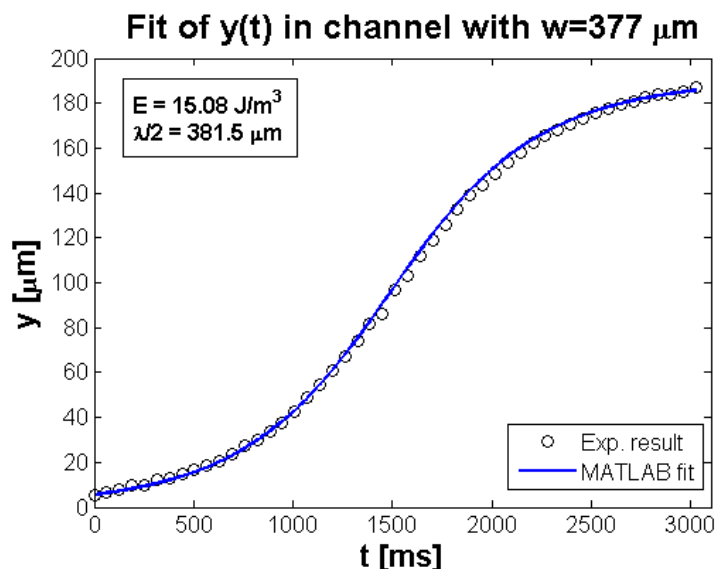


Figure 6.4: Fit of the trajectory shown in figure Fig. 6.3 to Eq. (6.11). The constants for the fitting is given in Chapter 7. It should be noted that the fit depends on the identification of the width of the channel in Fig. 6.3 with the blue ruler, but going into details with that is beyond the scope of this thesis.

Chapter 7

Introduction to Separating Systems in the Single-Particle Approach

This chapter will focus on basic functionality and characteristics of the elements of the system we are to analyze in the following chapters. The considered setup originates from the blood-separation setups proposed by the Thomas Laurell group at University of Lund [24], [28], and from the milk-separation setup proposed by Jacob Riis Folkenberg [1].

7.1 The Channel Setup

The main setup consists of a rectangular channel with the width w , height h and length L as shown in Figs. 6.1 and 7.1. Where nothing else is stated we use the channel measurements given in [29], see Table 7.1. We notice from Chapter 6 that the height of the channel only influences on the flow profile when neglecting transverse modes in the z -direction because $h < w$, and since we only consider the channel in the middle at $z = h/2$, a change in h would not affect our results significantly.

The channel is coupled to a piezo-electric crystal which oscillates at a resonance frequency giving a standing pressure wave in the channel with anti-nodes at the channel edges *i.e.* the wavelength is $n\lambda/2 = w$, where $n \in \mathbb{N}$. The standing pressure wave in the channel causes a pressure force as visualized in Section 5.6. According to our discussion of the one-dimensional resonator in Chapter 4 we get the resonance condition Eq. (4.7), and the fundamental standing wave in the considered channel thus requires a frequency of $f = 2.119$ MHz. This estimate only considers the channel as one-dimensional resonator in

Table 7.1: The dimensions of the channel are the same as used in practice for separation [1], [29].

	Blood separation	Milk separation
Height, h	125 μm	150 μm
Width, w	350 μm	1125 μm

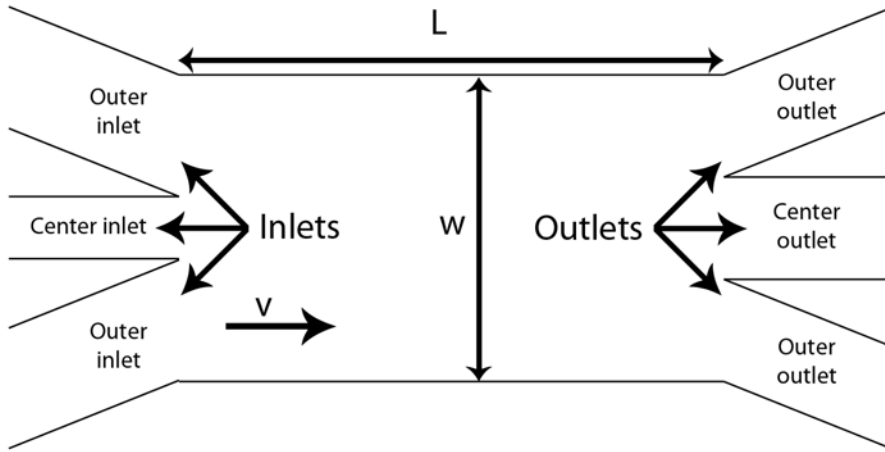


Figure 7.1: A sectional view of the channel setup in Fig. 6.1 with indications of the used terminology.

the y -direction, hence neglecting standing waves in the x - and z -directions.

The sample solution is fed into the channel from the inlet(s) and the separation of the particles then takes place over the length L of the channel after which the flow is separated into the three outlet channels as seen in the sectional view of the setup in Fig. 7.1.

We will through the whole discussion of applications limit ourselves to only consider three outlets, partially because of the practical complications of making more outlet channels and partially to limit the design parameters to be varied through the analyses. The inlet channels on the other hand are varied. In Chapters 8, 9, and 10 we will be discussing systems with both one, three, and five inlets of variable sizes and positions.

In most of Chapters 8 and 9 we are considering the fundamental resonance mode in the channel with $w = \lambda/2$ as this is the standard in experiments [42]. We will however extend the analyses primarily in Chapter 10 to also consider systems actuated to a resonance where the wavelength of the standing pressure wave fulfills $w = 2\lambda/2$ and $w = 3\lambda/2$.

Another important remark about the considered setup is the assumption of steady state. We limit ourselves to only consider steady-state flows as most practical applications will be aiming towards continuous flows through the systems. We merely conclude that after a certain amount of time, we will have a steady flow of particles. The particles which leave the channel may therefore not have entered at the same time, but as long as we keep the steady input and disregard any initializing phase, there will be a steady flow of particles along the single-particle trajectories.

Our simulations are only valid to the point in the channel where the outlets begin because afterwards the channel profile changes, and we are not sure how the pressure waves look like in the region with outlets. Thus we ignore effects that might occur at the entrance to the outlets. Later on when combining different resonance channels in one system we assume that no forces act on the particles and that they only are driven by the laminar flow no matter what form the transition parts have.

7.2 The Simulations

In Chapter 6 we found that the particle movement in the y -direction was described by the equation of motion, Eq. (6.4). The flow in the x -direction is, when neglecting longitudinal modes in the channel (see discussion in Section 12.1), given from the flow profile Eq. (6.12). These constitute a system of coupled first-order differential equations describing the particle trajectory. In the simulations these are solved using MATLAB's `ode45` differential equation solver, which is based on the Runge–Kutta method.

In the simulations we will be utilizing the different transport fluids with properties shown in Table 7.2. Chapters 8 and 9 will be focusing on particles in blood plasma and Chapter 10 will be using milk as transport medium. Through the simulations a simplification is made assuming that the potential buffer-mediums have exactly the same characteristics (compressibility, viscosity, and density) as the transport medium, but that it does not contain the particles which are to be separated.

Furthermore the particles considered in the simulations will have the properties given in Table 7.3. We notice that the red blood cells (RBCs) are actually not spherical in shape, but more cylinder-like with diameter of $6 - 8 \mu\text{m}$ and thickness $2 \mu\text{m}$ according to [6], which gives volumes of approximately $50 - 100 \mu\text{m}^3$. We choose to use $V = 75 \mu\text{m}^3$ as a mean value for our simulations and rewrite this volume to the corresponding radius of a sphere. The white blood cells (WBCs) are approximately spherical in shape with diameter $5 - 20 \mu\text{m}$, and according to [6] a good mean value to use is $D_{\text{WBC}} = 10 \mu\text{m}$. The density of WBCs can vary between $(1060 - 1090) \text{ kg m}^{-3}$, but we choose to use $\rho_{\text{WBC}} = 1060 \text{ kg m}^{-3}$.

When considering the parameters in Table 7.3, we notice that the value of the speed of sound in the particles, as included in the expression of the pressure force Eq. (5.91c), can be replaced with the value for the compressibility of the particle. This property is formally defined as $\beta = -(1/V)\partial_p V$, which by trivial manipulations corresponds to $\beta = 1/(c_a^2 \rho)$, where c_a is the speed of sound and ρ is the density of the particle/fluid. We observe that this is the ratio that enters the expression for the pressure force Eq. (5.91c). We sometimes use the compressibility as the fundamental value instead of the speed of sound depending on what we were able to find as experimentally determined values.

To calculate the pressure force from Eq. (5.91c) it is required to know the time-averaged amplitude of the acoustical energy density. Together with the applied pressure per length the used value of the time-averaged acoustical energy density is shown in Table 7.4, where Q and $\Delta p/L$ are related through Eq. (8.1), and $v_{x,\text{av}} = Q/(hw)$. The biophysicists requires flow rates in the systems above $100 \mu\text{L/hr}$ [3], but we only operate above this limit.

Table 7.2: Fluid properties

	Blood	Water	Milk	Units
Density, ρ	1052 ^a	998 ^{b1}	1029 ^c	kg m ⁻³
Viscosity, η	2.7 ^d	0.890 ^{b2}	2.1 ^c	mPa s
Compr., β	β_{Water}	5.88 ^e	β_{Water}	10 ⁻¹⁰ Pa ⁻¹
Speed of sound, c_a	- -	1483 ^b	- -	m s ⁻¹

^aDepends on the blood owner's type, age, physiological condition *etc.*, but an approximate value can be found in [12].

^bFound in [17]. ^{b1} At 20 °C. ^{b2} At 25 °C.

^cAcquired from [11].

^dValue found in [10], also discussed in Section 12.3.

^eFrom [2] — We consider the fat as Chylomicron, when finding the value of the compressibility.

Table 7.3: Particle properties used in the simulation

	RBCs	Lipid	WBCs	Polystyrene	Milk fat	Units
Density, ρ	1096 ^a	920 ^a	1060 ^b	1050 ^c	890 ^d	kg m ⁻³
Volume, V	75 ^b	14	524	72	- -	(μm) ³
Radius, R	2.62 ^{b1}	1.50 ^e	5.00 ^b	2.58 ^{a2}	- -	μm
Compr., β	3.48 ^{a1}	5.35 ^{a1}	β_{RBC}	- -	β_{Fat}	10 ⁻¹⁰ Pa ⁻¹
Speed of sound, c_a	- -	- -	- -	2350 ^c	- -	m s ⁻¹
Φ -factor	0.150	-0.015	0.139	0.226	0.0077	dim.-less
	<i>in blood</i>	<i>in blood</i>	<i>in blood</i>	<i>in water</i>	<i>in milk</i>	

^aFrom [2] — We consider the fat as Chylomicron. ^{a1} Experimental evaluated at 25 °C. ^{a2} From [4].

^bFrom [6]. ^{b1} For our calculations we assume that the RBCs are not toroidal-like in shape but assume that they are spherical with a radius $R = [3V/(4\pi)]^{1/3}$.

^cFound in [17].

^dData is from [21] at 60 °C.

^eAccording to [2] it is a good approximation to use $R = 1.5 \mu\text{m}$ in blood, which is the average size of the lipid particles in milk.

Table 7.4: Other parameters for separation

	Blood	Milk	Units
Time-averaged acoustical energy density ^a , $\langle E_{ac} \rangle$	1000	1000	J m ⁻³
Pressure gradient, $\Delta p/L$	100	2.77	kPa m ⁻¹
Flow rate, Q ^b	0.295	0.038	mL min ⁻¹
Average flow velocity in channel, $v_{x,av}$	110	3.7	mm s ⁻¹

^aThe validity of this value is discussed in Section 6.3.

^bThe flow rate in the whole $\lambda/2$ -channel, *i.e.* from all inlets.

Chapter 8

Separation of Red Blood Cells and Lipid Particles

Separation of erythrocytes (RBCs) has recently been experimentally reported by Petersson *et al.* [28], [29]. In this chapter we will follow the ideas of these results and focus on the separation of RBCs and lipid cells in blood plasma. This effect has for example medical applications where we would like to remove the lipid particles from the blood collected during open heart surgery. When the blood is collected and returned to the patient, lipid particles originated from adipose tissue are also reintroduced into the circulatory system with the danger of causing massive embolization of various organs.

The parameter values are explained thoroughly in Tables 7.2 and 7.3 and causes the RBCs and lipid particles to have different acoustophoretic sign, *i.e.* different sign of the Φ -factor introduced in Eq. (5.91c). This means that eventually the lipid particles will end up at the pressure (velocity potential) anti-nodes, and the RBC will end up at the pressure

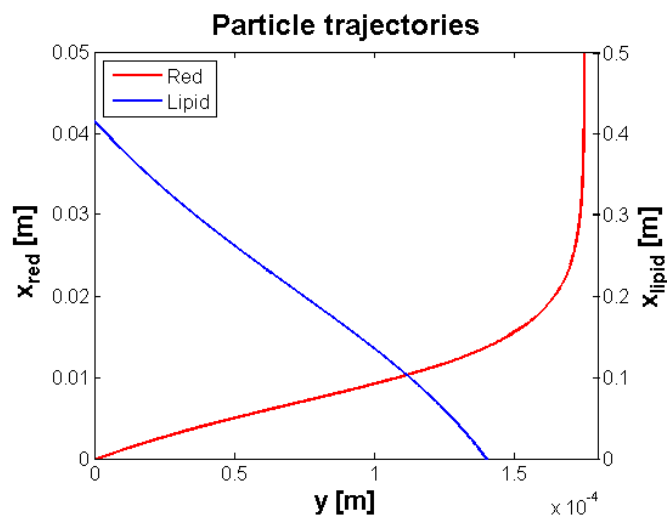


Figure 8.1: Particle trajectories for RBC with radius $R = 2.616 \mu\text{m}$ and lipid-particle with radius $R = 1.5 \mu\text{m}$. We see that the RBC are collecting at the center of the channel and the lipid-particles at the edge of the channel.

(velocity potential) nodes. When following the approach of [28], [29], and [24] we start by considering channels with width of $w = \lambda/2 = 350 \mu\text{m}$, where λ is the wavelength of the standing wave. This would give anti-nodes at the channel edges as explained in the discussion of the one-dimensional resonator covered in Chapter 4. It means that the lipid particles will end up at the channel edge and the RBCs at the center of the channel as shown by the particle trajectories in Fig. 8.1. This system will be investigated in this chapter through several designs with the aim of being able to determine and optimize the length of the channel in order to achieve complete removal of lipid particles from the outlet while still withholding a decent throughput, *i.e.*, the amount of particles flowing through the channel per time.

8.1 Lipid Size

A very important parameter in the pressure force is the size of the particle as we see from Eq. (5.91c) because it scales with the cube of the radius ($\propto R^3$). Results from [26] have shown the distribution in size as seen in Fig. 8.2a where the lipids are those found in raw milk, which we use as an estimate for the lipid particles found in blood. From this figure we have decided to use $R_{\text{lipid}} = 1.5 \mu\text{m}$, since it shows a noticeable peak there. However we have made three simulations to examine the dependence of the lipid-size, and the results can be seen in Fig. 8.2b. We see that the lipid-particle size is very important when we find that the required length of the channel for lipid particles starting at $y = 140 \mu\text{m}$ changes from 0.25 m to 0.95 m. However we find it reasonable to use $R_{\text{lipid}} = 1.5 \mu\text{m}$, since it has the largest peak in the distribution chart.

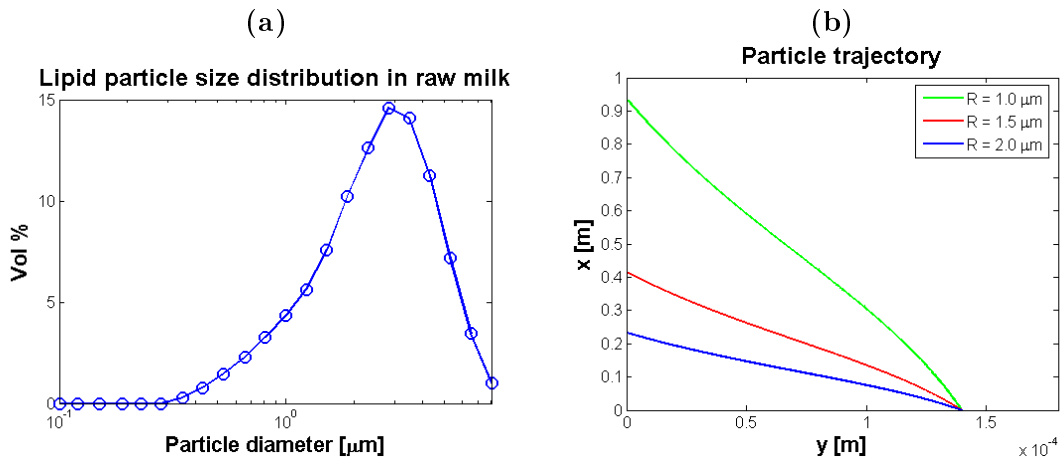


Figure 8.2: (a) The distribution of lipid particle sizes adapted from [26]. Notice that the x -axis depicts the diameter and not the radius. (b) The trajectory of lipid particles starting at $y = 140 \mu\text{m}$. We notice that the particles theoretically is at rest at the outer edge of the channel according to Eq. (6.12), hence we observe the sudden stop in the trajectory.

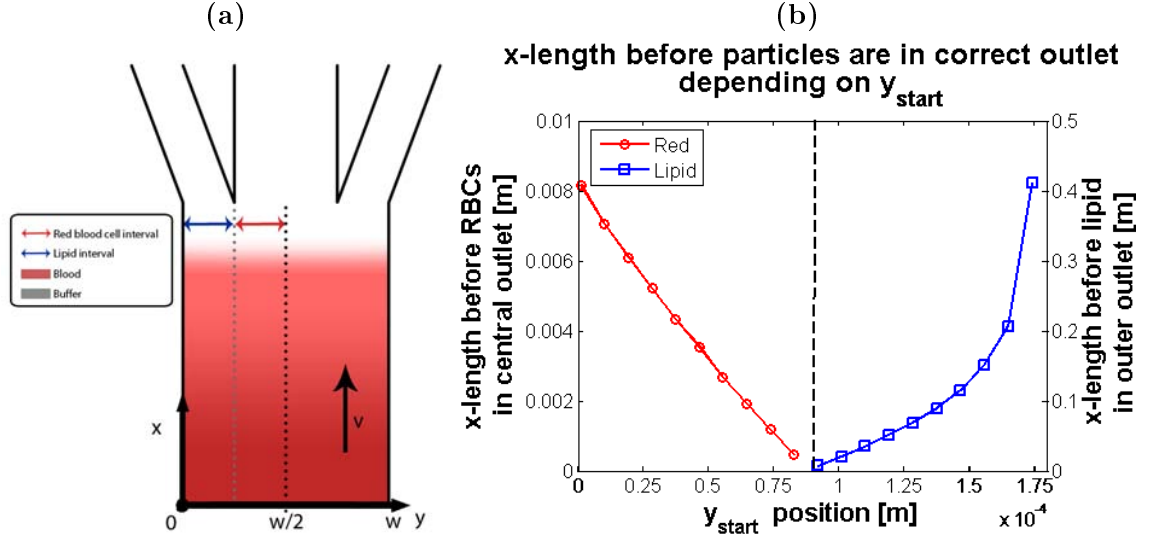


Figure 8.3: (a) The setup for the one-channel system. Here we only want to determine the distance required before the particles are within the outlet interval, *i.e.*, the outer inlets for the lipid particles and the center outlet for the RBCs (b) The simulation results using the one-channel setup. The y -axis depicts the length before the particles have moved into the desired output interval. The vertical, dashed line indicates the splitting point of the two outlets.

8.2 Finding the Flow Rate

An important design parameter for this system is the throughput (flow rate of blood), since we *e.g.* during surgery would like to be able to pump a lot of blood around. The flow rate is simply the flow speed integrated over the inlet area, see [5]. This gives us

$$Q = 2 \int_0^{\frac{1}{2}w} \int_0^h v_x(y, z) dz dy. \quad (8.1)$$

Since we assume that we have blood in the channel in all of the z -direction and using Eq. (6.12), the throughput for a system where the blood inlet is in the interval $y \in [y_{\text{lhs}}; y_{\text{rhs}}]$ becomes

$$Q_{\text{blood}} = 2 \int_{y_{\text{lhs}}}^{y_{\text{rhs}}} \frac{4h^2 \Delta p}{\pi^3 \eta L} \left(\sum_{n, \text{odd}} \frac{1}{n^3} \left[1 - \frac{\cosh\left(n\pi \frac{y-w/2}{h}\right)}{\cosh\left(n\pi \frac{w}{2h}\right)} \right] \right) \frac{2h}{n\pi} dy. \quad (8.2)$$

The throughput can then easily be found using numerical integration taking into account the first four terms of the infinite sum, as we discussed in Section 6.2.

8.3 One-inlet Channel

This setup is similar to what was considered in [28], see Fig. 8.3a and introduced properly in Chapter 7. We will consider the required length of the channel before a lipid-particle or RBC entering the channel at y_0 has reached a position where it will leave through the outer or center outlet respectively.

To reduce the parameter space we consider an outer outlet at $y \in [0; w/4]$ and hence a center outlet at $y \in [w/4; w/2]$. The results can be seen in Fig. 8.3b. It is clear that

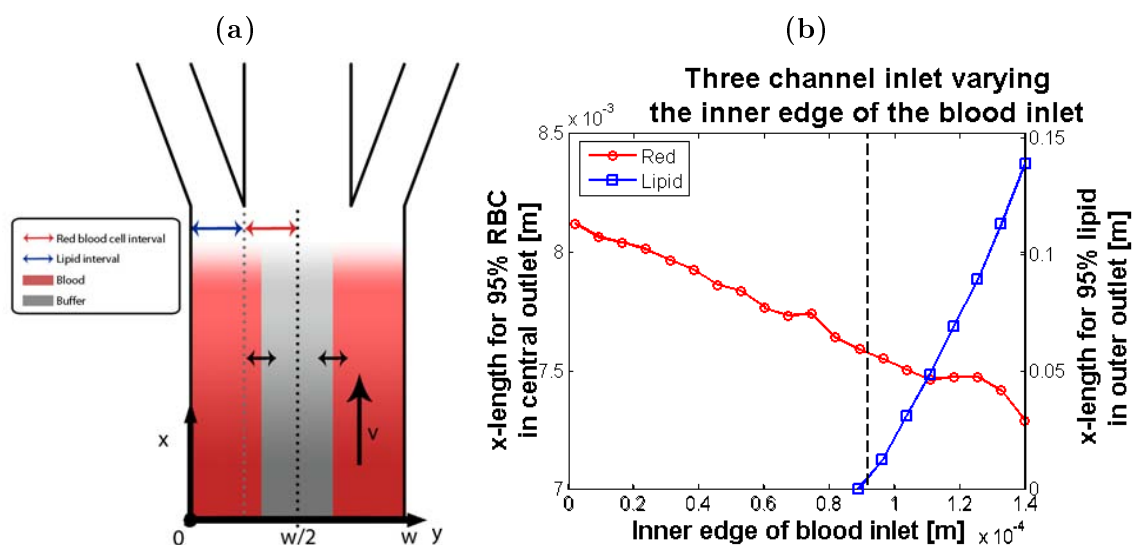


Figure 8.4: (a) The three-inlet system where we vary the width of the center inlet. (b) We vary the width of the center inlet in a three-inlet system. The y -axis shows the required length before 95 % of the particles are within the desired outlet channel. The dashed line indicates the splitting point of the two outlets.

the lipid-particles move slower compared to the RBCs since they are smaller and have a smaller Φ -factor. Therefore we notice that the lipid particles are the limiting factor for the length of this setup. To get a lipid particle starting near the center of the channel to leave through the outer outlet we would have to make the channel approximately 30 cm long with our choice of parameters¹. The reason for this long channel length is that the pressure force is small at the center of the channel, thus the lipid particles starting at the center of the channel are remaining a long time at the center.

This naturally leads to the idea of making a system where a buffer medium is injected in the center of the channel using three inlets, thus ensuring that there are no lipid particles which start at the center, hence making it possible to make a shorter channel. We will discuss this idea in the next section. The advantages of this system however is the high throughput and the simplicity of the design. To get shorter channel lengths without the lipid particles mixing with the RBCs in the center outlet, one could make the center outlet smaller, but this would give problems since the center outlet is too small to let all the RBCs pass through due to the high concentration of RBCs in human blood, *cf.* Section 12.5. This could be fixed by diluting the blood before it enters the system, but this would have a negative impact on the throughput. For this system with one inlet we get from Eq. (8.2) a throughput of blood $Q_{\text{blood}} = 4.82 \times 10^{-9} \text{ m}^3 \text{ s}^{-1} = 0.29 \text{ mL min}^{-1}$.

¹A particle starting exactly at $y = w/2$ would theoretically never be affected by any pressure force according to Eq. (6.3). Thus we have to consider particles near the middle as an estimate.

8.4 Three-inlet Channel

To avoid having lipid particles near the center of the channel we propose another inlet design, namely a blood (B), buffer (W), blood (B), *i.e.* a BWB-system. We vary the width of the center inlet and calculate the required length before 95 % of the particles have entered the desired outlet channel, see figure Fig. 8.4a and Fig. 8.4b. Notice that the required length for the lipid is zero until $y = 87.5 \mu\text{m}$. This is because all of the lipid particles start so that they leave through the outer outlet. The small jumps for the RBC is not a physical phenomena, but due to numerical inaccuracy. We see that the required length for RBCs is way smaller than the lipids. However we see that the required length for the lipids in this case is small, $\sim 10^{-1}$ m, much smaller than for the one-inlet channel.

On the other hand we have lower throughput because we are not having blood in the whole channel. If one wants a channel with a maximum length of 10 cm, we see that the blood inlet should be in the interval $y_{\text{inlet}} \in [0 \mu\text{m}; 125 \mu\text{m}] \cup [225 \mu\text{m}; 350 \mu\text{m}]$ to have less than 5 % of the lipid particles in the blood. For this system the throughput would be, using Eq. (8.2), $Q_{\text{blood}} = 3.15 \times 10^{-9} \text{ m}^3 \text{ s}^{-1} = 0.19 \text{ mL min}^{-1}$. This is only 65 % of the flow rate for the one-channel inlet system, but keep in mind that this channel was three times longer, and thus the BWB-system might be favorable.

8.5 Five-inlet Channel

The RBCs lying closest to the channel edges are near an anti-node in the pressure and are thus affected only by a small pressure force. These will be the last particles to reach the center outlet channel in a separation. To minimize the channel length required to have all the RBCs in the center outlet, we thus consider a WBWBW-system. Since the pressure force has a maximum at $y = w/4$ and $y = 3w/4$, we inject the RBCs in channels around these maxima where we vary the width and position of the channel to find an optimal setup. This is done in Appendix D where we conclude that in this system with lipids these optimizations do not matter compared to the BWB-system; they only give a smaller throughput. The lipids have a separation length of about two orders of magnitude larger than the RBCs. Thus the most important design fact is to make the blood inlet channels to start further out than the center outlet such that we have no lipid particles in the center outlet channel.

8.6 A $3/2 \lambda$ -harmonic System

We will briefly examine if we can optimize the system by considering a system with $w = 3/2\lambda$. For our setup this would mean that $w = 1050 \mu\text{m}$. It would not fundamentally change the way the system behaves, but we would have to introduce the previously mentioned BWB-system in $[350 \mu\text{m}; 700 \mu\text{m}]$. There the lipid-particles would move towards the anti-nodes at $y = 350 \mu\text{m}$ and $y = 700 \mu\text{m}$ while the RBCs would move towards the nodal plane at the center, $y = 525 \mu\text{m}$. In the intervals $[0 \mu\text{m}; 350 \mu\text{m}]$ and $[700 \mu\text{m}; 1050 \mu\text{m}]$ we would have a buffer medium.

The wider channel will not change the pressure force, since $k = \pi n_y/w$ is the same in this channel as in the previous — notice that $n_y = 3$ for $3\lambda/2$ but on the other hand w is also three times the one we considered earlier. If we use the coordinate system shown in

Fig. 8.5, we can use the same y values as for the system we have looked at so far. Basically we are not interested in what happens in the two buffer media on each side of our blood flow. The Poiseuille-flow profile will change with a wider channel we have therefore calculated it for each system. The results can be seen in Fig. 8.6a. Notice that the Poiseuille-flow is almost constant for the wide setup. In the center third of the channel we find the flow profile to be constant to four significant figures. If we were to use this system, this fact could help in the analysis, since a constant speed in the x -direction could be used instead of the Poiseuille-flow. This will also be discussed further when we look into separation of fat in milk, where we will also find an analytically expression, *cf.* Chapter 10.

We are not going to repeat all the previous calculations for the wider channel, but only look at the previously mentioned optimal system. In Fig. 8.6b we have plotted the required length before 95 % of the particles are within the desired outlet where we vary the inner edge of the blood inlet. If we compare this figure with Fig. 8.4b where we plotted the required length for the small channel, we see that the lipid length is almost the same since the slowest lipid particles were the ones near the middle of the channel where the change in v_x is small. However the RBC-length has become larger in this new system because the flow velocity has become greater, thus enabling the particles to move further in the x -direction. However the RBCs are still not the limiting factor of the system.

If we want a system with a channel length of ~ 10 cm and 95 % we see that we should introduce blood in the intervals (now without the aforementioned change in y) [350 μm ; 470 μm] and [580 μm ; 700 μm].

The throughput for this system was found to be $Q_{\text{blood}} = 4.38 \times 10^{-9} \text{ m}^3 \text{ s}^{-1} = 0.26 \text{ mL min}^{-1}$. This is significantly higher than what we have previously found for the same channel length due to the higher flow velocity in the blood inlets. Thus in many respects, although the device is more complicated, this system is better than the smaller system we looked at earlier. However if we were to have multiple parallel systems, the previously mentioned $\lambda/2$ -, BWB-inlet system is superior if we look at the throughput per channel width.

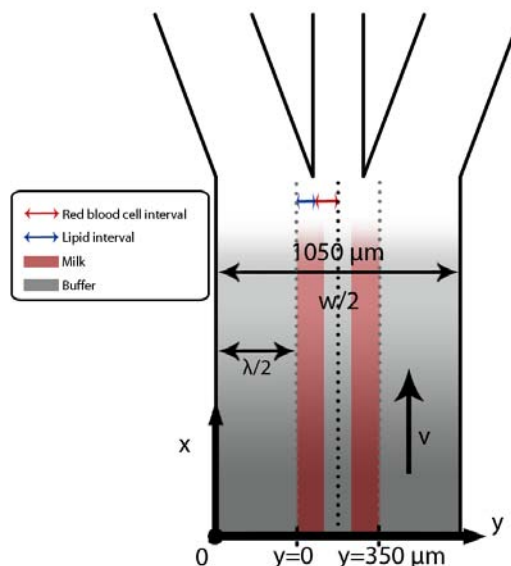


Figure 8.5: A sketch of the $3\lambda/2$ harmonic system. Note that the two dotted lines show the anti-nodes of the pressure field.

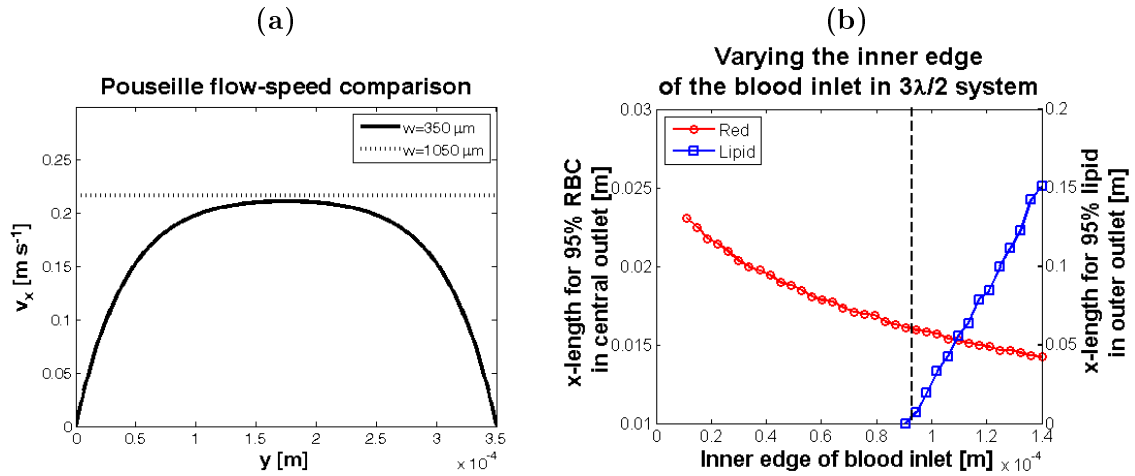


Figure 8.6: (a) A comparison of the Pouseille flow in two different systems. Notice that the y -axis has been moved by $350 \mu\text{m}$ to the left for the wide system. (b) The three channel system where we vary the right hand side. The dashed line indicates the split between the inner and the center outlet.

8.7 Summary

In this chapter we looked at the possibility of using the pressure force to separate RBCs with $\Phi > 0$ from lipid-particles with $\Phi < 0$ in blood plasma. This was done using numerical simulations. We have considered the pros and cons of various designs. When taking into account both channel length as well as the throughput, we found a design utilizing three inlet channels respectively blood, buffer, blood (BWB), to be a good compromise between the two design parameters. The purpose of that design was to get the lipids away from the center part of the channel because they moved much slower in the y -direction than the RBCs, and the lipids thus were the limiting factor of the system. Furthermore we looked at a $w = 3/2\lambda$ system and found that we were able to obtain better throughputs at the cost of a small increase in the channel length.

We also saw that the results were very dependent on the exact size of the particles as well as the Φ -factor. To optimize the design one would have to get more precise values of particle and fluid properties as well as the value for the acoustical energy density.

Chapter 9

Separation of Red and White Blood Cells

In the previous chapter we have concentrated on separating particles with opposite acoustophoretic signs with the example of RBCs and lipid cells. In this chapter we will focus on particles having the same acoustophoretic sign as reported experimentally by Filip Petersson *et al.* [30]. With the same acoustophoretic sign the particles are affected by the pressure force in the same direction. By inspiration from the collaboration between DTU Nanotech and The University of Santa-Barbara we concentrate on separation of RBCs and WBCs. These have nearly the same compressibility and density but differ in size as shown in Table 7.3. Our aim with this chapter is to investigate the possibility of separating RBCs and WBCs. This has major application in biotechnology, where the present, slow separation of these two types in blood is a bottle-neck of many bio-analytic methods where researchers want to investigate the WBCs [6]. Thus they are more interested in having a good separation than having a throughput, which will be our guideline in this chapter too.

9.1 Separation by Different Channel Designs

The RBCs and WBCs are both moving towards the middle of the channel when operating with the usual half wavelength in the velocity potential over the channel. When we are looking to separate these two particles, it is clear that any approach must have an inlet different from the center of the channel to achieve an optimal separation. In this chapter we will furthermore work under the assumption that the WBCs are spherical with a fixed radius of 5 μm . On the other hand we let the RBCs vary from having a volumes of 50 μm^3 to 100 μm^3 (radius of spherical cells varying from 2.285 μm to 2.879 μm) as they do in practice.

First we consider the flow trajectory of the particles when starting from a given point in the channel. As usual by symmetry arguments we are only considering the left-hand side of the channel and everything is mirrored in the other side of the channel. In Fig. 9.1a is shown the channel setup considered in the analysis of the flow trajectories in Fig. 9.1b. We observe that the important trajectories for this separation are the ones from the edges of the inlet. All of a given particle type will be positioned in between these two trajectories.

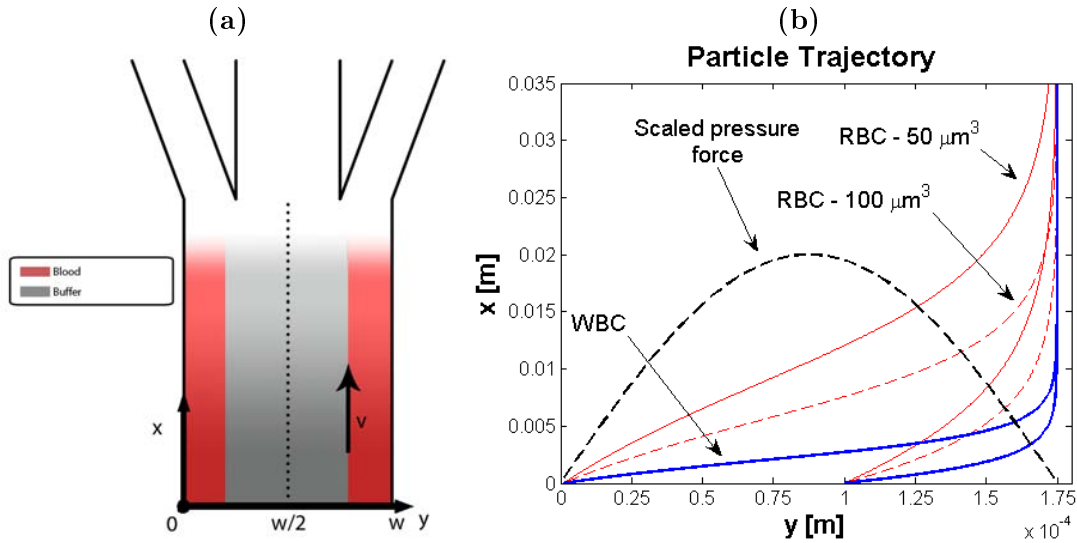


Figure 9.1: (a) The BWB-channel setup considered in Fig. 9.1b. (b) We are considering an inlet channel from $y \in [0; 100 \mu\text{m}]$ as sketched in Fig. 9.1a. The graph shows the trajectories of WBCs and the two extrema sizes of the RBCs when these are started at the outer or inner edge of the inlet.

When we want to determine whether or not it is possible to separate the WBCs from the RBCs we therefore consider the trajectory of a WBC starting at the outer edge of the inlet and the trajectory of the particular RBC starting at the inner edge of the outlet. Fig. 9.1b clearly shows this fact because the WBCs are influenced by a larger pressure force and hence are moving faster towards the center of the channel. When the RBC from the inner edge crosses the WBC trajectory from the outer edge, the particles are separated in two non-mixing beams. At this point we can choose to end the channel and let the two separate beams exit the channel through different outlets. This gives a theoretical total separation of the particles.

Even when total separation is not possible in cases where the beams always are mixed, it is in general possible to calculate how much of the outer inlet's RBCs that have been removed in the outlet channel. Afterwards one could repeat the process to obtain a higher concentration of WBCs compared to RBCs. We could consider the case where the RBCs and WBCs are not totally separated and try to calculate how good separation we achieve. But since it turns out that we actually are able to have total separation, we will only consider this case.

To ensure that it is possible in practice to let separate beams leave the channel in different outlets, we are in general not considering the intersection between the two trajectories. Instead in the following we are considering the channel length (referred to as the separation length) at which the „white beam” and the „red beam” are separated by more than $7.5 \mu\text{m}$ (corresponding to one-half particle size of the WBCs). From Fig. 9.1b it is also worth noticing that with this definition of the separation length, there exist an interval where the separation is possible; the interval where the two considered beams are separated by more than $7.5 \mu\text{m}$.

9.1.1 Separation in BWB-system, Varying Inner Edge of Blood Inlet

We have argued that the inlet cannot be placed at the center of the channel. Therefore we start the analysis of the separation of RBC and WBC with the BWB-system sketched in Fig. 9.2: A blood inlet at the edge of the channel where the outer edge of the inlet is fixed at the channel edge, and where we vary the position of the inner edge of the blood inlet. The separation length interval is shown as a function of the position of the inner edge of the inlet in Fig. 9.3a. In Fig. 9.3a we have furthermore shown the channel length at which the „red beam” has become narrow enough for the concentration to exceed 91 % (as explained in Section 12.5 this is the maximum concentration to be obtained by optimal stacking of the RBCs, assuming they are non-compressible and cylindrical). Above this length we can no longer rely on the calculated beam widths because we cannot expect to be able to compress the particles that closely in the beam. Notice that the WBCs start out at a very low concentration in standard blood ($\sim 1\%$ Vol¹) so they will never obtain a critically high concentration before the RBCs have done so.

We see that the minimum separation length grows approximately linearly with the position of the inner edge of the blood inlet. The shorter separation length at narrow inlet channels is caused by the fact that the slower inner RBC trajectory and the faster outer WBC trajectory are starting closer to each other, and hence the WBC catches up with the RBC faster (at shorter channel lengths). Narrower inlets give less throughput, but this is not our concern in this chapter.

By comparison of the slopes of the linear parts of the minimum of the separation lengths, we conclude that the channel length must be longer for larger RBCs because they move faster and are harder to be passed by the WBCs.

It is important to notice that it is no longer possible to separate the two beams when the inlet becomes too wide, indicated when the intervals are no longer present at a given inlet width. This is the result of the slower RBCs starting to close to the center of the channel while the faster WBCs pass them by enough space to make a non-mixing separation possible. This point occurs at narrower inlet channels for larger RBCs, because they move faster to the center. This is also the effect that causes the large RBCs to require a longer minimum channel length in order to separate them from the WBCs.

Another interesting point is that the size of the separation length intervals decreases as we increase the width of the blood inlet regardless of the size of the RBCs. We conclude that the small inlet is the most optimal because it is the most stable with respect to the

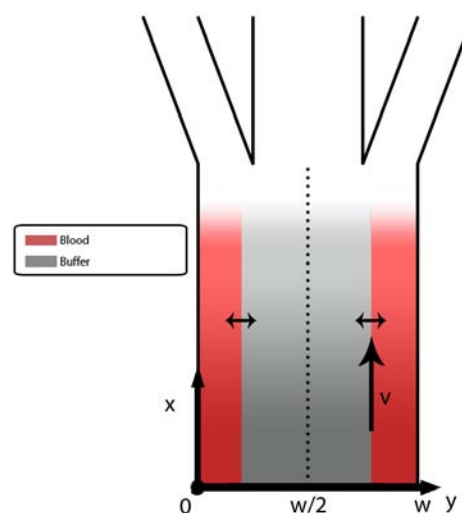


Figure 9.2: Shows the setup of a channel with blood inlet at the edges of the channel. The outer edge of the inlet is fixed at the channel edge and we are varying the inner edge of the inlet. This is the setup which is used in Fig. 9.3.

¹http://en.wikipedia.org/w/index.php?title=White_blood_cell&oldid=295545544

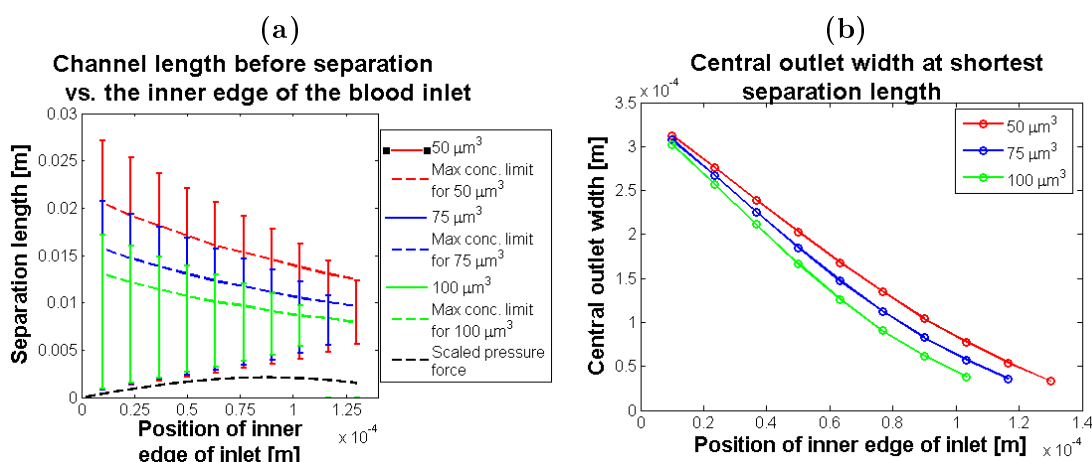


Figure 9.3: (a) The outer edge of the blood inlet is kept fixed at the channel edge as shown in Fig. 9.2. The graph shows the separation length as a function of the position of the inner edge of the blood inlet, *i. e.*, in the shown intervals full separation would be possible for a given position of the inner edge of the blood inlet. The dashed lines indicates the channel length above which the „red beam” has a concentration which exceeds 91 %. Finally the size of the pressure force at the position of the inner edge of the inlet is also indicated as a scaled quantity. (b) The graph shows the width of the inner outlet at the minimum separation length shown in Fig. 9.3a in order to get full separation.

chosen channel length in order to obtain separation. In Fig. 9.3a it is also clear that we obtain the longest possible channel lengths before the concentration rises too high, if we choose a narrow inlet channel. For a narrow channel we therefore observe both larger separation intervals and a longer possible channel length. Most important is that it is possible to separate the different types of RBCs from the WBCs with the same device (same separation length).

Considering the width of the inner outlet required to catch all the WBCs we look at Fig. 9.3b. In the figure is shown the width of the outlet required to catch the whole WBC beam in the inner outlet. This width is defined as the midpoint between the „red beam” and the „white beam” at the minimum possible separation length, and we notice that a more narrow outlet still gets the RBCs and WBCs separated but will not catch all the WBCs present in the inlet. We notice that the wide blood inlet channels require a small inner outlet in order to catch the whole beam of WBCs in the outlet because RBCs are injected closer to the center of the channel. Furthermore we observe that the relationship between the blood inlet width and the required inner outlet width is approximately linear making it easy to scale the device design.

9.1.2 Separation in WBWBW-system, With Variable Width of Blood Inlet

Next we consider a fixed blood inlet center in a WBWBW-system and examine how the separation length changes as we change the width of the blood inlet symmetrically around this fixed center. The system is sketched in Fig. 9.4. From Fig. 9.5a we observe that the minimum separation length grows approximately linearly with the width of the beam until the limit where it is no longer possible to separate the particles.

By comparing the slopes we again find that the largest RBCs give rise to the biggest change in minimum channel length per inlet width. Notice that these changes are comparable with what we found when only varying the inner edge of the blood inlet in the BWB-system.

By comparison between Figs. 9.3a and 9.5a we also notice that the separation length intervals are smaller for the narrow inlet channels in the setup where the center of the inlet is $50\ \mu\text{m}$ from the channel edge (Fig. 9.5a). This is due to two effects. First of all we have removed the WBCs from the region near the edge where the pressure force is small. Secondly the RBCs at the inner inlet edge are starting closer to the center of the channel for a given width than for the BWB-setup used in Fig. 9.3a. But we also notice that this difference is decreasing as the width of the inlet in Fig. 9.5a is increasing. This is because the WBCs are coming closer to the edge and the RBCs starting points are more similar to the setup in Fig. 9.3a, corresponding to what we would expect from our previous analyses.

The maximum separation length possible before the concentration in the „red beam” is too high, is decreasing with the inlet width in the BWB-system (Fig. 9.3a) whereas in the WBWBW-system (Fig. 9.5a) they are increasing with the inlet width.

In the BWB-system (Fig. 9.3a) the outer edge of the blood inlet is invariant — fixed at the channel edge. The decrease is here caused by the inner edge of the blood inlet getting closer to the center and hence reaching the center faster to make a narrow beam with high concentration.

In the WBWBW-system (Fig. 9.5a) we also observe this effect, but in this setup the outer edge of the blood inlet is not fixed. As the inner RBCs are reaching the center faster when we increase the width of the blood inlet, the outer RBCs are reaching the center slower. Because a narrow beam (high concentration) requires both beam edges to get close to the center, we notice that the maximum separation length is increasing with the width of the blood inlet.

Again considering the required width of the inner outlet in order to catch all the WBCs in the outlet, we look at Fig. 9.5b. We notice that the blood inlet and the inner outlet width is linearly related making design scaling easier. Furthermore we notice that at

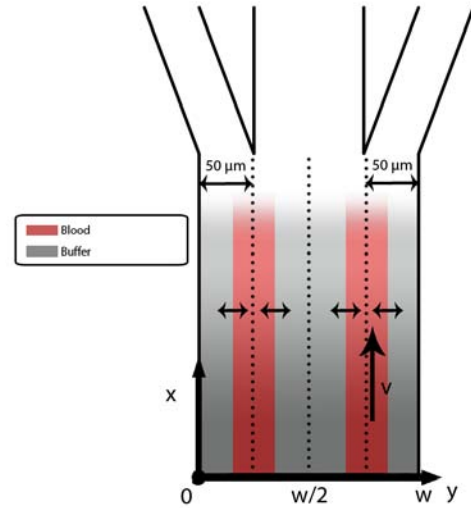


Figure 9.4: Shows a WBWBW-system with a blood inlet with center of $50\ \mu\text{m}$ from the edge of the channel. We vary the width by symmetrically expanding the inlet keeping the center fixed to obtain the system that is used in Fig. 9.5.

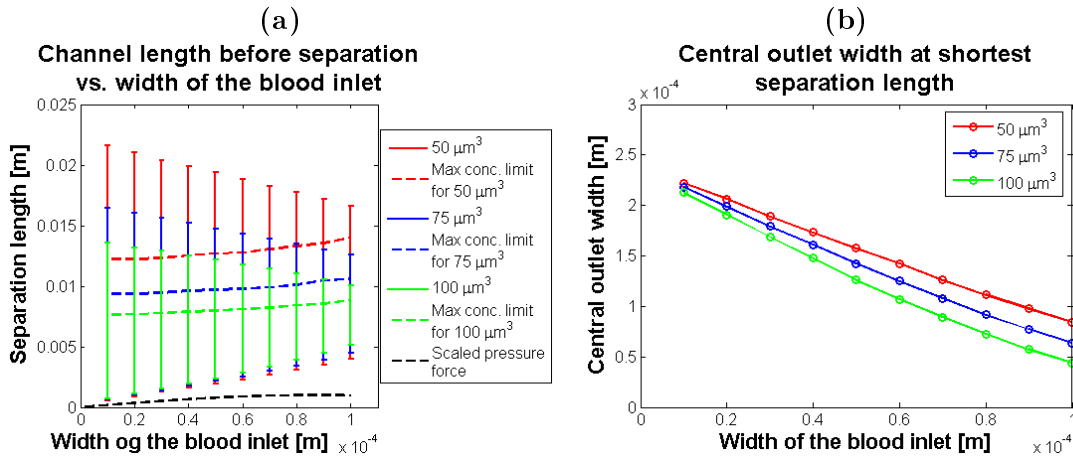


Figure 9.5: (a) The separation length interval is shown as a function of the width of the blood inlet channel, when the center of the inlet beam is placed 50 μm from the outer edge of the channel as shown in Fig. 9.4. Furthermore the dashed line indicate the length above which the concentration of RBCs exceeds 91 %. (b) Shows the required inner outlet width at the minimum separation length shown in Fig. 9.5a in order to get all the WBCs captured in the inner outlet channel.

narrow blood inlets we observe a more narrow inner outlet when we have positioned the blood inlet away from the channel edge as done in Fig. 9.5b (compared to Fig. 9.3b). This indicates that the separation takes place closer to the center of the channel, thus giving smaller outlets, when the blood inlet is placed closer to the center of the channel. This motivates the next analysis of the influence of the position of an inlet of fixed width.

9.1.3 Separation in WBWBW-system, With Variable Position of Blood Inlet

Finally we consider a fixed blood inlet width to study how the separation length vary with position of the inlet channel. We choose a narrow inlet of 30 μm because this beam width is used frequently in experimental setups. The setup is sketched in Fig. 9.6a and the resulting separation length intervals is shown in Fig. 9.6b.

We first notice that the minimum separation length has a minimum and hence that we get an optimal positioning of the inlet as shown in the section view of Fig. 9.6b shown in Fig. 9.7a. We see that this position is where the 30 μm wide inlet lies on the outer side of the maximum of the pressure force. For the chosen parameters the maximum of the pressure force is at $y = 87.5 \mu\text{m}$ and the optimal position of the center of the 30 μm wide channel is about $y = 60 \mu\text{m}$ from the channel edge. This position ensures that all the particles in the inlet channel benefit from passage of the maximum in pressure force.

Furthermore we observe that the position near the edge of the whole channel gives rise to the largest separation length intervals for all sizes of the RBCs. This is the result of the smaller pressure force at the edge of the channel like we saw and discussed in Section 9.1.1.

It is the same effect that causes the decrease in the maximum separation length before we reach a problematic concentration in the „red beam“. The closer to the channel edge the blood inlet is, the longer channel is needed in order for the RBCs to get concentrated because they start out by experiencing a very small pressure force. The big decline in the

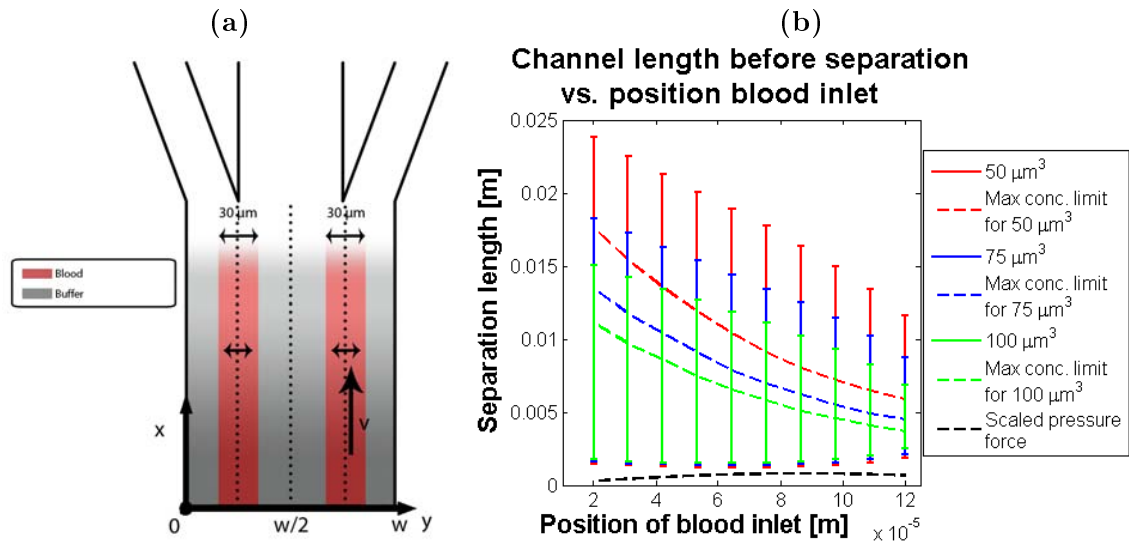


Figure 9.6: (a) Shows the setup at which the position of a $30 \mu\text{m}$ wide inlet is varied. This setup is used in Fig. 9.6b. (b) The separation length interval for varying positions of the center of a blood inlet with a fixed width of $30 \mu\text{m}$ as sketched in Fig. 9.6a. The length at which the concentration in the „red beam” exceeds 91 % is also shown as dashed lines. Furthermore the size of the pressure force at the center of the inlet is indicated as a scaled value.

maximum possible length at positions closer to the channel center is then caused by the inlet beam getting into the region with a higher pressure force right away, thus getting concentrated at shorter channel length.

The effect mentioned at the end of Section 9.1.2 is now easily seen in Fig. 9.7b, where the required inner outlet width in order to catch all the WBCs in the inner outlet channel at the minimum separation length is shown. We observe that the closer the inlet with fixed width gets to the center, the smaller outlet is needed because the separation occurs closer to the center of the channel. Furthermore we notice that there is a linear relationship between the position of the outer inlet and the size of the required outlet, and that the largest RBCs require the most narrow inner outlets indicating that the separation occurs closest to the center.

9.2 Concentration of White Blood Cells

After we have separated the RBCs and WBCs we are interested in concentrating the WBCs and thus making them easier to find/analyze afterwards. Below we are focusing on the most simple system for concentrating the cells. As shown in Fig. 9.8 we use only one inlet filling the whole channel. The WBCs will be moving towards the center of the channel as discussed earlier. The longer we make the channel the more WBCs will therefore be collected in the center outlet as we found with RBCs in Section 8.3. It is clear that, when we have chosen only to focus on the one inlet design for concentration, the size of the inner outlet plays an important role.

In Fig. 9.9a the concentration is shown as a function of channel length for the two

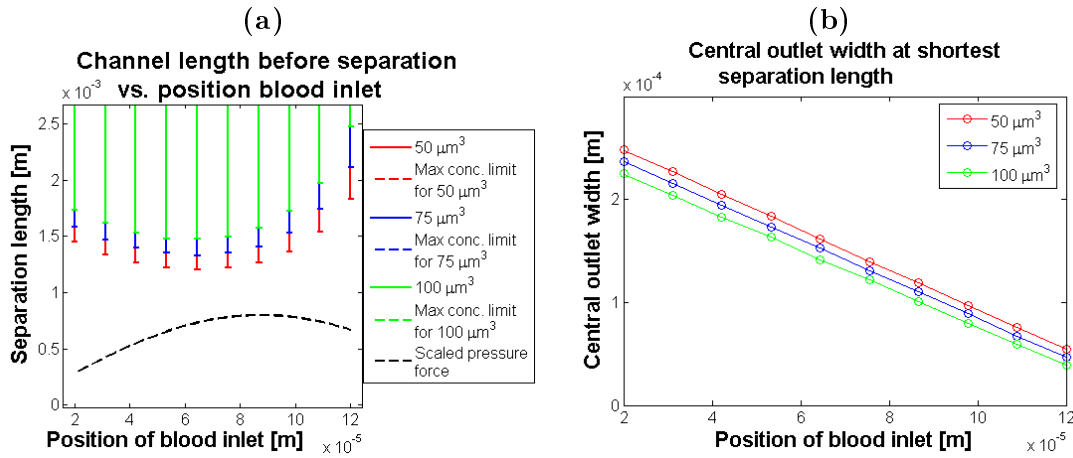


Figure 9.7: (a) A zoom of the minimum of the separation lengths shown in Fig. 9.6b. (b) The required inner outlet width for the minimum possible separation length found in Fig. 9.6b to have full separation.

setups sketched in Fig. 9.8. We have chosen to concentrate from an initial concentration of 1 % Vol., corresponding to the approximately ratio of WBCs in an adult persons blood as mentioned earlier. It is clear that if we have separated the RBCs and WBCs earlier, we have already concentrated the WBCs. Hence this section does not claim generality with respect to the initial concentration but is included to show how much it is possible to concentrate the cells, and how long a channel will be needed in order to do this.

From Fig. 9.9a we find that we are not able to concentrate to more than approximately 5 % Vol. if we choose the narrow outlet and to approximately 2 % if we use the wide outlet, no matter how long we make the channel. Hence we conclude that the size of the outlet is a very important parameter when we want to concentrate particles. The narrower the outlet is made the better concentration can be obtained, provided we make the channel sufficiently long. Consequently it is the ratio between the blood inlet and the central outlet that determines the concentration which can be achieved by a given design. Hence it is possible to get a higher concentration than the considered 5 % by reducing the width of the central outlet, but we notice that the central outlet should be wide enough to contain a flow of WBCs, and that there is a lower boundary on how narrow an outlet can be before the concentration rises to high, *cf.* Section 12.5.

9.3 Changing the Transport Medium

In the above sections we have sought to separate the RBCs and WBCs by appropriate channel designs. Inspired by talks with Jacob Riis Folkenberg at FOSS we could also seek to separate the RBCs and WBCs by a change of transport-medium. The change of transport-medium from blood plasma to some other fluid is experimentally reported by Per Augustsson *et al.* [38]. The characteristics of the transport medium enter in the Φ -factor introduced in Eq. (5.91b) and thus affect the acoustophoretic sign. Hence we want to examine if it is possible to find a fluid where the RBCs and WBCs have different acoustophoretic sign like RBCs and lipid cells as discussed in Chapter 8. The fundamental

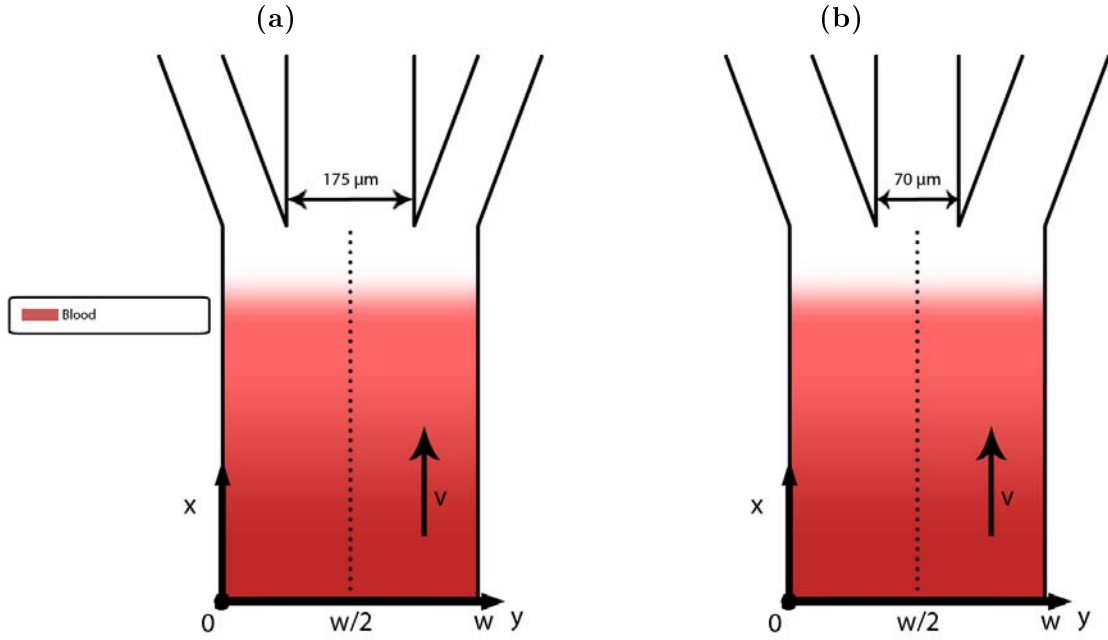


Figure 9.8: (a) Shows the one-inlet setup with center outlet of half the full channel width, $w = 350 \mu\text{m}$. (b) Shows a sketch of the one-inlet setup with a center outlet of width $w/5 = 70 \mu\text{m}$.

idea is previously used by F. Petersson *et al.* [30] to separate normally acoustical inseparable particles by changing the density of the transport medium, and hence altering the pressure force.

We start by considering the expression for the Φ -factor from Eq. (5.91b),

$$\Phi = \frac{\rho_s + \frac{2}{3}(\rho_s - \rho_0)}{2\rho_s + \rho_0} - \frac{1}{3} \frac{c_a^2 \rho_0}{c_s^2 \rho_s}. \quad (9.1)$$

We see that it only depends on the fluid in ρ_0 and c_a . We are interested in the case where they have different signs, which means that $\text{sgn}[\Phi_{\text{red}} \cdot \Phi_{\text{white}}] = -1$. We have indicated the values of ρ_0 and c_a , where this is the case in Fig. 9.9b. Notice that it is a very small band of possible pairs of values. Furthermore the required speed of sound decreases with growing density, which is a problem because the speed of sound usually increases with growing density. However we were able to find one fluid that satisfied our requirements, namely nitrobenzene ($\text{C}_6\text{H}_5\text{NO}_2$). The density of nitrobenzene is $\rho_0 = 1199 \text{ kg m}^{-3}$, and the speed of sound is $c_a = 1463 \text{ m s}^{-1}$ [17]. With these values we find

$$\Phi_{\text{red}} = 0.0053 \quad \text{and} \quad \Phi_{\text{white}} = -0.0062. \quad (9.2)$$

This shows that nitrobenzene has the exact property of making the WBCs moving to the edges of the channel and the RBCs moving towards the center. *But* the drawback is that it is highly toxic and possibly a carcinogen, which would make it dangerous to use in practice. Furthermore these calculations require accurate values for the compressibility and speed of sound of both the RBCs and WBCs.

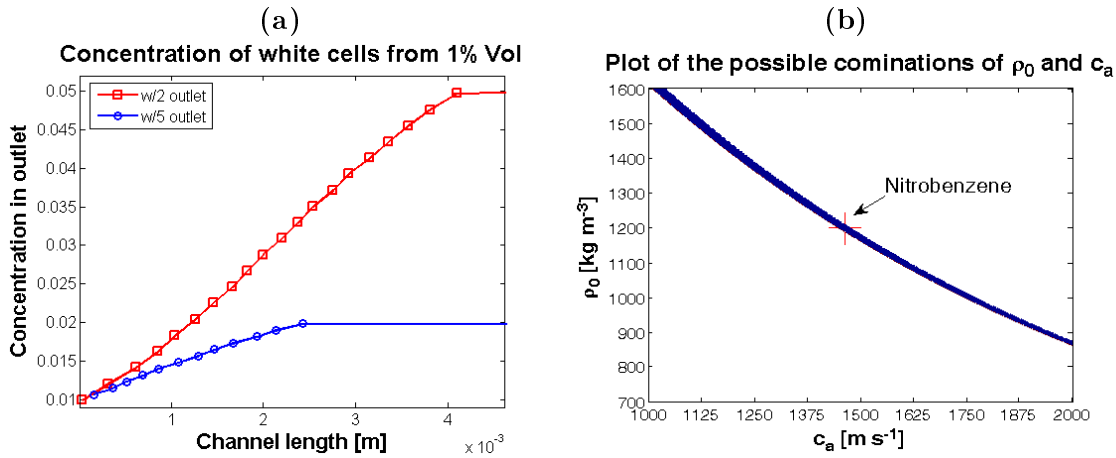


Figure 9.9: (a) Shows the concentration as a function of the channel length for the two setups shown in Fig. 9.8. (b) The allowed values for ρ_0 and c_a where the acoustophoretic sign is different for RBCs and WBCs.

9.4 Summary

We have by numerical simulations analyzed different channel designs for separation of particles with $\Phi > 0$, here with the example of RBCs and WBCs in blood plasma. We find that the WBCs are affected by a larger pressure force and that separation from RBCs of different sizes is obtainable in intervals of channel lengths. The larger the considered RBCs, the larger is the effect of the pressure force, making it more difficult to separate the RBCs from the WBCs. By varying the position of the blood inlet we have shown that the minimum separation length is obtained when the inlet is placed asymmetrically in the channel a little towards the edge of the channel and not exactly where the pressure force is largest. In this way all particles pass through the maximum of the pressure force.

Furthermore we have discussed concentration of the WBCs and shown that after channel lengths of about 2 – 5 cm, maximum concentration is obtained with the chosen outlet sizes. In this context we have observed that the width of the outlet channel is a very important design parameter when considering concentration the way it influences both the maximum achievable concentration and the length at which this occurs.

Finally we have discussed separation by varying the Φ -factors of the particles by using another transport medium. It is shown that it theoretically is possible to achieve different acoustophoretic sign of RBCs and WBCs but in practice it would be difficult to find a suitable transport medium.

Chapter 10

Separation of Lipid Particles in Milk

Until now we have sought to separate particles with different compressibility, density, and size. Inspired by Jacob Riis Folkenberg at the company FOSS who works on separation of lipid particles in milk this chapter will focus on this separation.

FOSS produces measurement equipment for the food industry. In this respect the fat particles are mixed with cells present in the milk, thus hindering the analysis of these cells by other means (often optical). Therefore it is interesting to be able to remove the fat from the milk, in such a way that the milk is not containing fat particles larger than a certain size. This ensures that the analyses sensitive to particle size (for instance scattering effects) are not influenced by the fat particles [1].

10.1 Design Considerations

We use the parameters for milk and fat particles found in Tables 7.2 and 7.3 resulting in the fact that the fat particles are moving towards pressure anti-nodes (anti-nodes in the velocity potential).

In practice when dealing with lipid particles in microchannels there is a tendency that the particles in the milk will stick to the sidewalls, according to [1]. This would be the case when using the above described channels with a width of $\lambda/2$. A way to avoid this is to use channels of width $w = 3\lambda/2$, where the lipid particles are injected in the middle part of the channel in an inlet not wider than $w/3$ centered around the middle of the channel. This means that the particles would move towards the two anti-nodes at $w/3$ and $2w/3$.

Particles injected exactly at $y = w/2$ would according to the analytic solution, Eq. (6.3), never begin to move in the y -direction because the pressure force is exactly zero at that point. However this would never be seen in practice since there would be some fluctuations (or other not yet understood processes) pushing the particle a little away from $y = w/2$ leading to a non-zero pressure force on the particle. In our analysis we have to estimate the effects of these fluctuations, and we do this by assuming that particles are injected at least a particle radius away from the middle of the channel.

Due to the symmetry of the problem we run our simulations in the region $y = w/3$

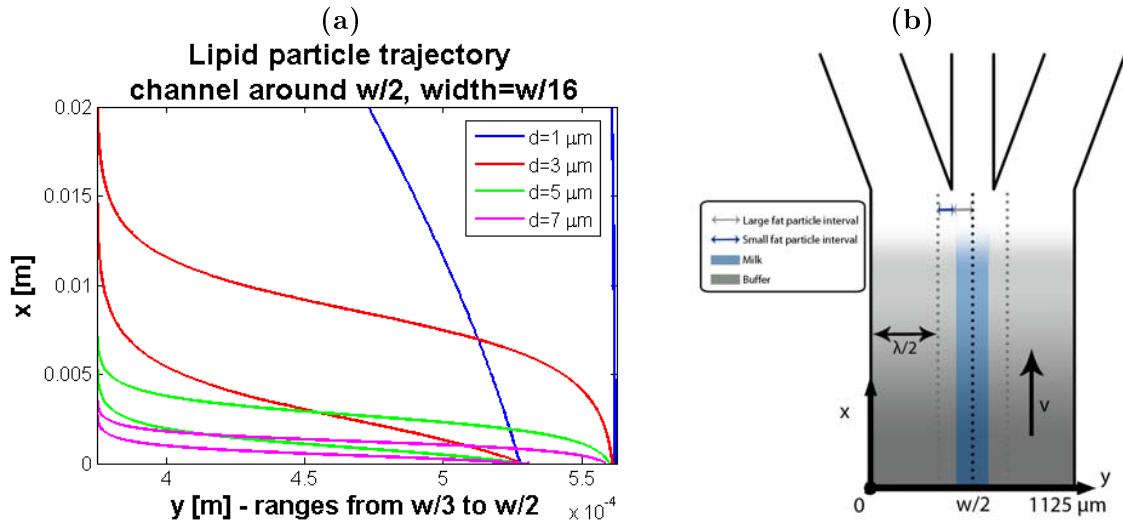


Figure 10.1: (a) Particle trajectories of particles injected in a inlet of width $w/16$ around the center of the channel (such that we only see half of the inlet channel in the plot). For each particle size the trajectory of the inner- and outermost particle in the inlet channel is plotted. (b) Channel setup for lipid particle separation. The idea is that at the inner outlet all particles above a diameter D_0 should be near the dotted lines and flow through the outer outlet channels. These particles will move faster towards the anti-nodes at $w/3$ and $2w/3$ (green lines), which are values of y lying in the outer outlet channels.

to $y = w/2$, where the results can be mirrored onto the other side of the channel. As in Chapters 8 and 9 we are considering steady-state situations where it can be assumed that there are particles along all the single-particle trajectories.

A plot of the particle trajectories is seen in Fig. 10.1a where we use the dimensions from Table 7.1. At first we focus on the problem of sorting all particles above a certain diameter away from the milk. A setup for this sorting is shown in Fig. 10.1b. The purpose of the setup is to use that the velocity of a particle in the y -direction is proportional to the square of the particle radius, and thus the distance before a particle reaches an anti-node depends strongly on R , see Eq. (6.4).

To be sure that all particles with a diameter greater than D_0 have moved away from the center outlet (where the milk exits) we must look at the trajectory of the innermost particle which is the last particle of a given size to reach an anti-node. As an example we consider three different channels where the center outlet width is set to $335 \mu\text{m}$, $295 \mu\text{m}$, and $255 \mu\text{m}$, see Fig. 10.2. For each particle diameter we find the required length of the channel before the particle exits in the outer outlet channel (which corresponds to the intersection between the trajectory and the black dashed line in Fig. 10.2a). These lengths are given as a function of the particle diameter D_0 in Fig. 10.2b. At a given length all particles of a diameter larger than D_0 must be in the outer outlet channels. We see that the required length does not depend very much on the center outlet width. This is because the velocity of the particles in the y -direction is large compared to the velocity in the x -direction. This leads to a range of y -values for which the trajectory curves are „flat” as seen in Fig. 10.2a. Thus the particles will move very quickly over a large part of the channel

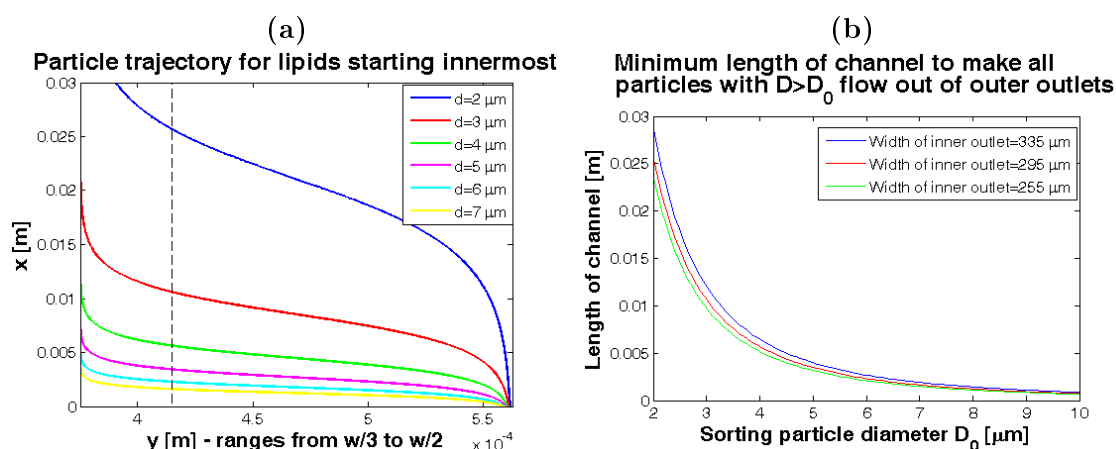


Figure 10.2: (a) Particle trajectories of the innermost particles in the considered channel. The black dashed line must be understood as when the particles are to the left of this, they exit in an outer outlet channel. (b) Length of channel required for all particles of diameter D_0 to be only in outer outlet channels.

making it less important where in the „flat” part of the trajectory the outlet change is. From Fig. 10.2b we conclude that it is possible to choose a length of the channel for sorting large particles away from the milk. If we for example want to remove all particles larger than $3 \mu\text{m}$ from an inner outlet $295 \mu\text{m}$ wide we must use a channel with a length of ~ 1 cm.

Comments on the flat trajectory

Due to the flat trajectory, the particle can almost all the time be considered as lying either near the center of the channel or near the anti-node, where the anti-node in the $\lambda/2$ -case would be at the channel edge. This is because the shift from the center to the anti-node happens over a very short channel length, and thus making the device very sensible to variations in channel lengths. In Section 6.2 we found that the travelled distance in the x -direction scales with $\langle E_{ac} \rangle^{-1}$. Because the acoustical energy density is difficult to determine exactly in a given channel in practice, there is an uncertainty in the theoretical predictions of the required channel length to promote a certain separation. If we try to design and make calculations on a setup where some of the particles are taken out somewhere in between the center and the anti-node, it would be difficult to determine the exact size of the particles that would flow out of that channel.

In an experimental setup we would be able to see separation in multiple outlet channels where the particles are sorted according to their size in the different channels with the largest in the outermost channels as reported in [30]. The situation where the separation takes place is found by tuning the applied voltage or by adjusting the flow velocity until the desired particle flows out of the various outlets. In our opinion it would be difficult to make good theory for this multiple separation system because of the uncertainty in the acoustical energy density, which experimentally is taken care of by tuning the parameters. But we find that it would be possible to make a reasonable estimate if a particle of a given size is near the center or the edge of a channel for a given channel length. This we will consider in the following.

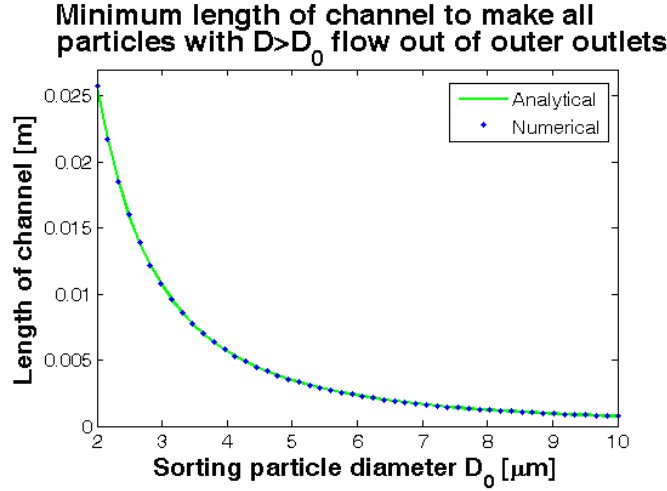


Figure 10.3: Comparison of numerical results with Eq. (10.1) with $y_s = w/3 + 40 \mu\text{m}$ corresponding to a center outlet width of $295 \mu\text{m}$. It is seen that the analytical solution matches almost perfectly.

10.2 Analytical View on the Sorting

We see from Eq. (6.15) that the required length of the channel scales linearly with $\Delta p/L$ (as the velocity in the x -direction scales linearly with $\Delta p/L$), so if we want to sort for other D_0 than the channel was designed for, we just have to adjust the flow velocity.

Because of the flatness of the flow velocity profile in the x -direction, $v_x(y)$, around the middle of the channel, see Fig. 8.6a, we are tempted to assume, that we can consider the flow velocity of the milk as constant here. In Section 8.6 we saw that the velocity was constant to four significant figures in the center third of the channel, so this is a reasonable assumption. According to Eq. (6.18), the required length of the channel when the particle travels from a position y to the position of the splitting point between the middle and outer outlet channel, y_s , is:

$$x(y, y_s) = \frac{3\eta v_{x,av}}{4\langle E_{ac} \rangle k_y^2 R^2 \Phi} \log \left(\frac{\tan(k_y y_s)}{\tan(k_y y)} \right), \quad (10.1)$$

where $k_y = 2\pi/\lambda = 3\pi/w$ and where y must be the position of the innermost particle where it enters the channel. This gives the minimum length of the channel to be sure that, according to our assumptions, all particles with radius $R = D_0/2$ are not exiting through the center channel. That this analytic expression can be used instead of numerical simulations is apparent from the plot of Eq. (10.1) together with the numerical solution given in Fig. 10.3.

Knowing the geometry of the channel, we can easily regulate the average flow velocity according to Eq. (10.1) thus avoiding the need for numerical calculations in order to be able to sort particles of a given size from a sample.

As another interesting example of particle sorting, though not very viable for the application of removing all large fat particles from the milk, we will also discuss another sorting opportunity this setup can provide. Consider the case where we only want to have particles

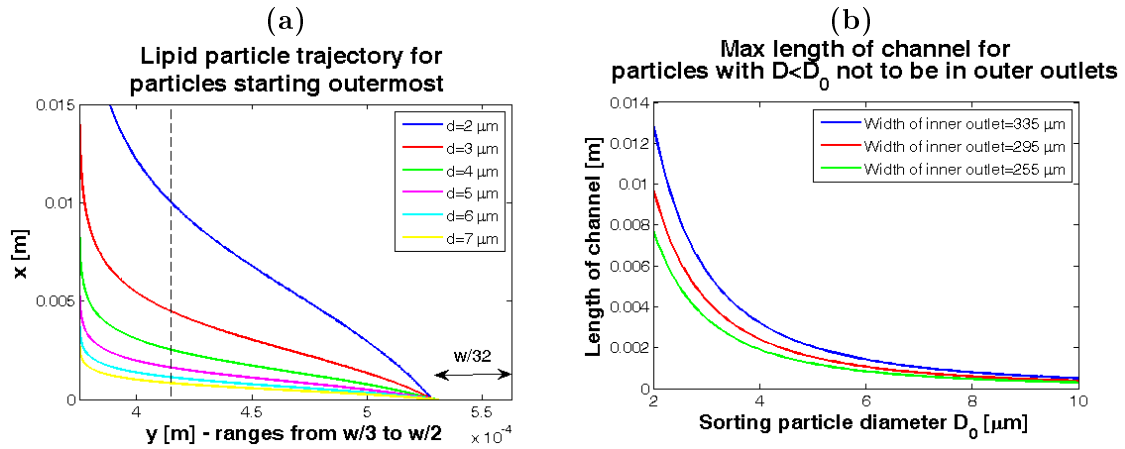


Figure 10.4: (a) Particle trajectories of the outermost particles in the considered channel. The black dashed line must be understood as when the particles are left of this, they exit in an outer outlet channel. To the right of the dashed line they exit through a central outlet of the width 295 μm . (b) Length of channel required for no particles of diameter below D_0 to leave the outer outlet channels.

above a certain radius in the outer outlets. Since this is not directly linked to removing all particles above a certain threshold, we will only consider this case from an analytical point of view, where Eq. (10.1) also is applicable. To be sure that no particles with a diameter smaller than D_0 enters the outlet channels, we have to consider the outermost particles in the inlet channel. The trajectories of these particles are given in Fig. 10.4a and the corresponding plot for the diameters is given in Fig. 10.4b. We see that it is possible to design a channel where the particles in the outer outlets are only above a certain diameter. For example if we want to make sure that no particles with a diameter below $D_0 < 4 \mu\text{m}$ is entering through the outer outlets, when the central outlet is 295 μm , we can have a maximum channel length of 2.5 mm.

10.3 An Idea for Milk Separation in Practice

In this section we want to describe a way that lipid separation in milk could be done in practice. The channel setup is shown in Fig. 10.5, and the basic idea is to use the $3\lambda/2$ -channel as described above for the separation remembering that lipid particles have a negative acoustical sign. We require that the particles enter the $3\lambda/2$ -channel in a small interval around the middle of the channel to optimize the separation. A way to make this focusing is to let the particles enter in the middle of a channel of width $2\lambda/2$, long enough for the pressure force to be able to focus a particle beam in the middle of the channel. The lipid particles will be focused in the middle due to the anti-node at the center.

An experimental procedure for separation would be first to determine the acoustic energy in the channel, then calculate the required length of the channel to separate certain particles from Eq. (10.1) with a given flow rate, and at last do the separation of the desired particles in the channel.

A way to estimate the acoustical energy could be to use a test-fluid with known viscosity

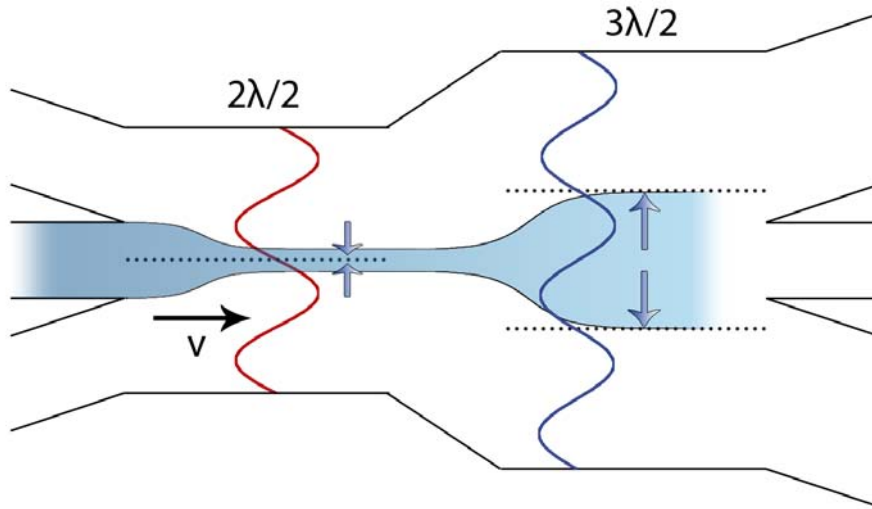


Figure 10.5: System for separation of particles with $\Phi < 0$. The particles are focused in a beam in an area of width $w = 2\lambda/2$ and are afterwards separated in a channel of width $w = 3\lambda/2$.

and test particles with known Φ -factor and radius. One has to inject the test-fluid into the channel and then have to adjust the flow velocity to find the flow velocity where the particles change from exiting through the inner outlet to exiting from the outer outlet or *vice versa*. This value together with the channel length can be inserted in Eq. (10.1) to find an expression for $\langle E_{ac} \rangle$. In the equation y would be the outermost point of the focused particle beam entering the $3\lambda/2$ -area, and y_s would be the y -coordinate of the splitting point between the center and outer outlet channels.

There are uncertainties related to this process of determining the acoustic energies. For example we are not certain how the particles are affected at the interface between transport-medium and buffer-medium which would require further investigations beyond the scope of this thesis. By choosing a buffer-medium with viscosities close to the one of milk, we might be able to minimize these effects. Similar viscosities in buffer and milk would also strengthen the assumption of a constant flow profile in the middle region of the channel (according to Section 12.2). If the same flow velocity in the fluid inlets is used we will avoid any questions about how laminar flows with different velocities affect each other.

10.4 Summary

We have by numerical analyses suggested a design and procedure for separation of $\Phi < 0$ particles with the example of lipid particles in milk, where we were able to sort large particles away from the milk. We have seen that by only operating in the 1/3-central part of a $3\lambda/2$ -channel with the same viscosity in the whole channel, we can approximate the flow velocity profile with a constant average velocity. This leads to a simple analytical solution which describes the separation length from which we with well-known particles are able to determine the average acoustical energy density in the channel. One could try theoretically to estimate how precisely we are able to split the particles in size, but a lot of experimental factors influence on this.

Chapter 11

Other Possible Applications of the Pressure Force

In this chapter we will present other possible applications of the pressure force, besides what we have learned that other research groups have worked with.

11.1 Size-sorting of Particles with $\Phi > 0$

The principle of sorting similar particles with $\Phi > 0$ is like the situation with $\Phi < 0$ illustrated by the separation of fat-particles in milk, *cf.* Chapter 10, but we have to design the channel in another way because the particles now move towards nodes and not anti-nodes of the pressure field, see Section 5.6. A setup with this functionality is shown in Fig. 11.1a where the particles first are focused in two beams in a $2\lambda/2$ -channel. These two beams function as inlets for a succeeding $\lambda/2$ -channel. In this way the situation in the $\lambda/2$ -channel is similar to the WBWBW-system for blood we have discussed in Section 8.6 for the purpose of separation of RBCs and lipid particles. In the setup sketched in Fig. 11.1a we would just have a higher concentration of RBCs in the inlet channels than we would have if we had inlets of „regular” blood which had not been concentrated. Therefore this system would be good for optimizing the blood separation setup where we both have high throughput and short channel lengths. Furthermore it is convenient to have the same viscosity in the channel, as we would have using this system, according to the discussion on velocity flow profile in Section 12.2.

The experimental procedure is the same as for milk, as we described in Section 10.3, where a known test-particle is used to determine the acoustical energy density for calculating the required flow velocity by Eq. (10.1).

11.2 Creation of Pulses of Particles

For practical microfluidic applications it could be useful to be able to have particles arriving in a pulses. We illustrate a channel for particles with $\Phi < 0$, and a similar system could be made for particles with $\Phi > 0$.

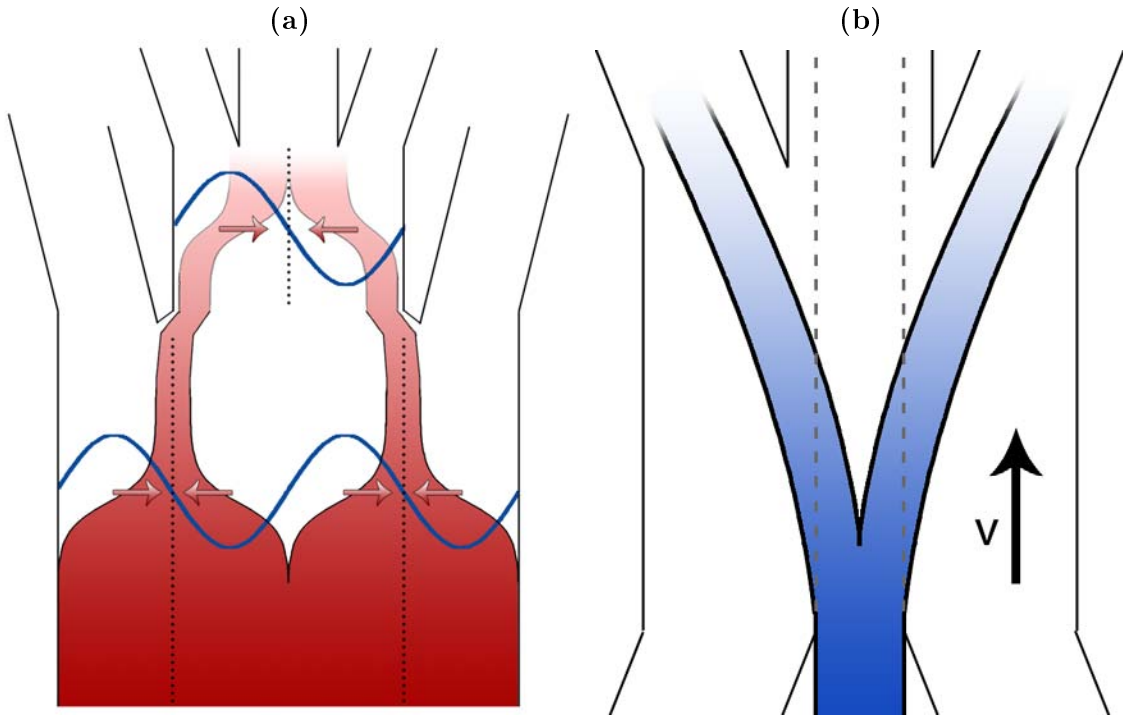


Figure 11.1: (a) Setup for size-sorting of particles with $\Phi > 0$. First a channel of width $2\lambda/2$ focuses the particles into two beams at the pressure nodes. These beams are by a laminar flow led into a channel of width $\lambda/2$ in such a way that the two beams lie near the edge of this channel. This is done by leading some of the fluid out from the $2\lambda/2$ -part in some outer outlet channels as illustrated. In the $\lambda/2$ -part the particles are focused into the center of the channel. (b) Setup to create pulses for particles with $\Phi < 0$. The piezo-actuator is periodically turned on an off causing the particles to be periodically sent either into the inner or the outer outlet(s). Note that the pressure force is assumed large compared to the flow velocity such that when the actuator is on, the particles move very fast to the edge. The dashed lines outline the flow profile when the actuator is turned off.

The pressure force could be used to create pulses by turning on and off the piezo-actuator (or at least varying the frequency between the resonance frequency and off-resonance frequency), for the channel setup in Fig. 11.1b. The particles are injected in the center inlet of a WBW-system in a $\lambda/2$ -channel of length L (this situation could also be achieved by focusing of the beam in a $2\lambda/2$ -channel as described in Fig. 10.5). We assume that the pressure force on the particles, when the actuator is turned on, is so large, that the traversed length in the x -direction before the particle is at a y -position, where it would exit through the outer outlet channel, $x(y_1, y_2)$, is very small compared to L . This means that when the actuator is switched on, almost all particles in the channel at that time will flow out of the outer outlets.

We assume that the velocity in the center of the channel is v_x , and that the actuator is switched on in a time interval t_{on} . It gives a total length of a pulse of, $\ell \approx L + v_x t_{\text{on}}$ — including the contribution both from the particles in the channel when the actuator is turned on and the particles entering the channel while the actuator is turned on also

contribute to the length of the pulse. From these assumptions we also see that the time between the piezo is turned off until it can be turned back on again must be $t_{\text{off}} > L/v_x$. Because the pulse length with this simple model is $\ell > L$, a period of switching the actuator on and off is $T = t_{\text{on}} + t_{\text{off}}$, which must be equivalent to $T = \ell/v_x + \Delta t$, where Δt is the time between the pulses.

To get an estimate of the pulse frequency we can obtain, we assume that the time between pulses is the same as the time we experience a pulse, *i.e.* $\Delta t = \ell/v_x$. This gives a period of $T = 2\ell/v_x$ corresponding to a frequency of $f = v_x/(2\ell) < v_x/(2L)$, limited by the length of the channel and the flow velocity. Using standard parameters $v_x = 0.1$ m/s and $L = 5$ mm, we find $f < 10$ Hz.

The frequency can be made larger and the pulses smaller by looking at exactly how long time a particle entering in the middle of the channel uses to get to a point where it would flow out of an outer outlet channel. For optimization, analysis like in Chapter 8 could be made, but it is beyond the scope of this thesis.

Part III

Neglected Effects

Chapter 12

Neglected Effects

In the previous chapters we ignored many effects in our simulations. In this chapter we are going to look closer into what was reasonable to ignore, and what should be included in an extended model. We will examine each effect one at a time and at last summarize the effects and compare their contributions to the models.

12.1 Longitudinal Modes

When we examined the pressure force, we ignored all acoustic modes but the ones in the y -direction. However, it is also possible that longitudinal modes in the channel affects the flow of the particle down the channel. It would give a total flow in the x -direction $v_x(x, y)$ of

$$v_x(x, y) = v_{x,\text{flow}}(y) + v_{x,\text{long}}(x), \quad (12.1)$$

where the flow profile in the channel, $v_{x,\text{flow}}(y)$, is given by Eq. (6.12), and $v_{x,\text{long}}(x)$ is the contribution from the longitudinal modes.

To analyze the longitudinal modes, we have to consider the force in the two-dimensional scheme as done in Section 5.7. We neglect the presence of the inlets and outlets of the channel, assuming that the channel is rectangular with boundaries consisting of acoustical hard material such that the pressure gradient normal to the surface vanish, $\mathbf{n}_{\text{normal}} \cdot \nabla p_1 = 0$. This translates into corresponding homogeneous Neumann boundary conditions for the first-order velocity potential via the relationship $p_1 = -\rho_0 \partial_t \phi_1$, Eq. (3.7). For harmonic varying first-order perturbation terms, a solution to the inviscid Helmholtz equation, Eq. (3.12), for the velocity potential with the mentioned boundary conditions is

$$\phi_{\text{in}}^{2\text{D}} = \frac{u_0}{k} \cos(k_x x) \cos(k_y y), \quad (12.2)$$

where the resonance frequencies (eigenvalues of the Helmholtz equation) is determined from

$$k^2 = k_x^2 + k_y^2 = \left(\frac{\pi n_x}{L}\right)^2 + \left(\frac{\pi n_y}{w}\right)^2, \quad n_x, n_y \in \mathbb{N}_0. \quad (12.3)$$

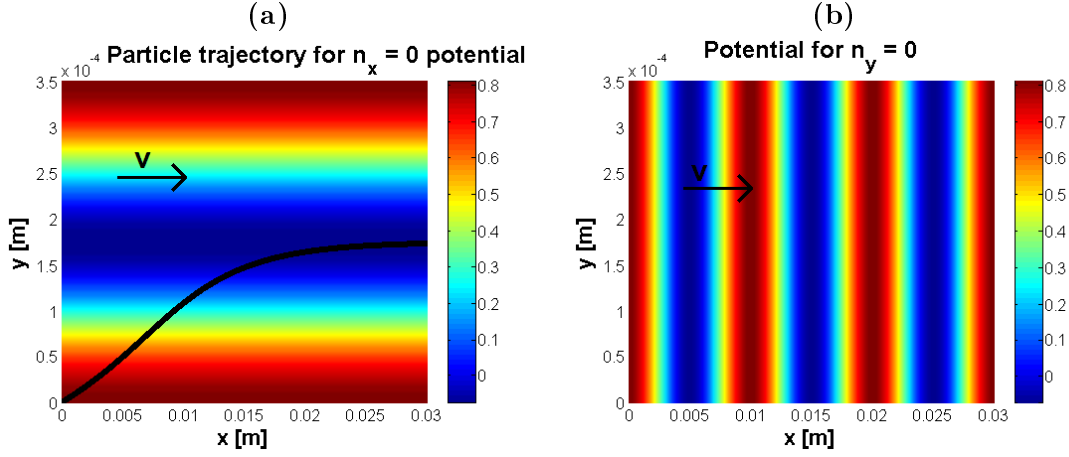


Figure 12.1: (a) Contour plot of the normalized acoustic potential U_{2D}/U_0 in the case of no longitudinal modes, $k_x = 0$ and $\lambda/2 = w$, in a channel with $w = 350 \mu\text{m}$ and $L = 3 \text{ cm}$. Furthermore a RBC trajectory in blood starting near the channel edge is indicated. (b) Contour of the normalized acoustic potential U_{2D}/U_0 in the case of $k_y = 0$ and $n_x = 3$. Parameter values for (a) and (b) are given in Chapter 7. Note that the axis are not equal.

In Section 5.7 we found that the harmonic velocity potential Eq. (12.2) leads to an acoustic potential, Eq. (5.95), given by

$$U^{2D} = U_0 \left[2f_1 \cos^2(k_x x) \cos^2(k_y y) - 3 \left(\frac{k_x^2}{k^2} \sin^2(k_x x) \cos^2(k_y y) + \frac{k_y^2}{k^2} \cos^2(k_x x) \sin^2(k_y y) \right) f_2 \right], \quad (12.4)$$

where $U_0 = (1/2)(4\pi R^3/3)\langle E_{ac} \rangle$ has been introduced as a natural energy scale for the acoustic potential.

Below we choose to make analyses of a system as the one indicated for blood separation in Chapter 7 with $w = 350 \mu\text{m}$, and with a channel length $L = 3 \text{ cm}$ as used as a typical length for separation of particles in practice [30].

In Part II we have only been considering the special case where $k_x = 0$. In Fig. 12.1a a plot of the potential together with a particle trajectory for a RBC in blood is seen where $f = 2.119 \text{ MHz}$ and $n_y = 1$, corresponding to only having one node in the y -direction. We see that the acoustic potential is invariant in the x -direction, which also can be seen from Eq. (12.4) with $k_x = 0$.

Considering the $k_y = 0$ mode

The opposite situation with no modes in the y -direction, $k_y = 0$, is shown in Fig. 12.1b and has $f = 0.742 \text{ MHz}$. We notice that the pressure force in this situation is only affecting the particles in the x -direction. In the x -direction the particles already have the velocity $v_{x,\text{flow}}$ due to the flow profile in the channel. Hence the pressure force will either counteract or amplify the flow velocity depending on the x -position of the particle. We see that the

magnitude of the pressure force in this setup in analogy of the case with $k_x = 0$ where $\langle F_x \rangle = 4\pi k_x R^3 \langle E_{ac} \rangle \Phi \sin(2k_x x)$. In equilibrium this force is balanced by the Stokes drag, $F_{x,\text{drag}} = 6\pi\eta Rv$, giving a maximum contribution from the longitudinal modes of

$$|v_{x,\text{long}}| = \frac{2}{3\eta} k_x R^2 \langle E_{ac} \rangle \Phi = \frac{2\pi n_x}{3L\eta} R^2 \langle E_{ac} \rangle \Phi, \quad n_x \in \mathbb{N}_0. \quad (12.5)$$

This must according to Eq. (12.1) be compared with the magnitude of the velocity flow profile to determine which of the velocities that gives the major contribution to $v_x(x, y)$.

Using typical values as given in Chapter 7 for the blood simulations, we estimate the drag velocity in the channel with $L = 3$ cm to have the magnitude $|v_{x,\text{long}}| \approx 0.27$ mm s⁻¹ for the mode $n_x = 10$. This must be compared with the average magnitude of the flow profile of $v_{x,\text{flow}} = 0.11$ m s⁻¹, and thus the longitudinal modes on the whole do not change the flow in the x -direction in this considered case.

If the flow velocity in the flow profile is comparable but still larger than the velocity contribution from the longitudinal mode, the particles will move in the x -direction periodically slowing down and speeding up according to the sine variation of the longitudinal modes from the pressure force. On the other hand if the velocity in the x -direction from the flow profile is smaller than the magnitude of the longitudinal contribution, the particles will collect at the nodes (for $\Phi > 0$) in the acoustic potential. At a threshold flow velocity $v_{x,\text{flow}}^*$, the flow velocity exactly balances the velocity from the pressure force in a given mode,

$$v_{x,\text{flow}}^* = |v_{x,\text{long}}| = \frac{2\pi n_x}{3L\eta} R^2 \langle E_{ac} \rangle \Phi, \quad n_x = \mathbb{N}_0. \quad (12.6)$$

From this we can experimentally determine an estimate of $\langle E_{ac} \rangle$ in a given channel using the threshold flow velocity as suggested in [6].

The Maximum Magnitude of the Longitudinal Velocity Contribution

When looking at the maximal velocity contribution from the longitudinal modes, we consider the the pressure force in the x -direction for arbitrary wavenumbers, Eq. (5.98),

$$\langle F_x \rangle = U_0 k_x \sin(2k_x x) \left[2f_1 \cos^2(k_y y) + 3f_2 \left(\cos^2(k_y y) - \frac{k_y^2}{k^2} \right) \right], \quad (12.7)$$

$$\langle F_x \rangle \leq U_0 k_x [2|f_1| + 3|f_2|], \quad (12.8)$$

which is equal to the magnitude of the one-dimensional force, where $k_y = 0$, as seen by comparison with Eq. (5.89c). Hence we conclude that the estimate of the magnitude of the longitudinal velocity contribution made above in the case of $k_y = 0$ is in fact also an estimate of the maximum magnitude of the longitudinal velocity contribution in 2D. It should be noted that the maximum magnitude is proportional to the mode number, so for very high order of modes or small velocity profiles the velocity originating from the modes can have influence.

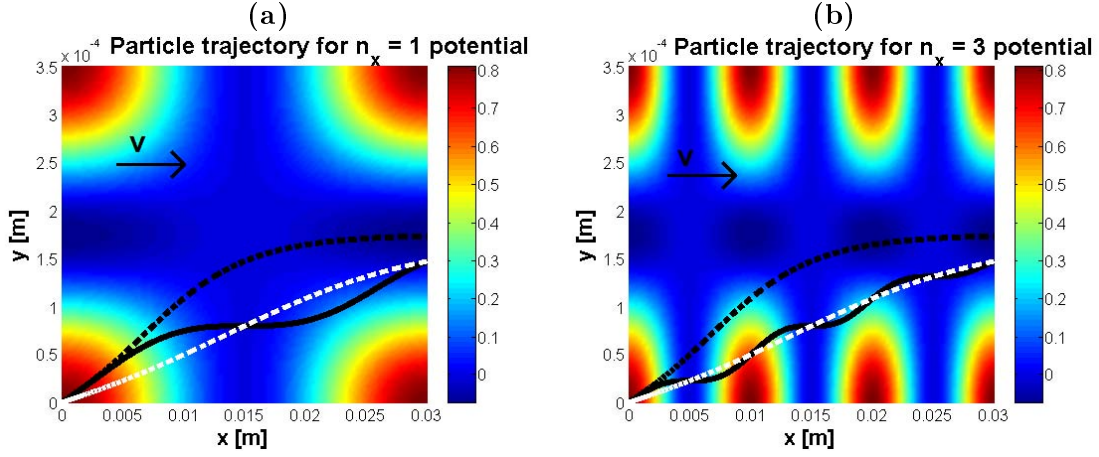


Figure 12.2: (a) Contour plot of the normalized acoustic potential U_{2D}/U_0 with $n_y = 1$ and $n_x = 1$. (b) Contour plot of the normalized acoustic potential U_{2D}/U_0 with $n_y = 1$ and $n_x = 3$. In both (a) and (b) we see the trajectories of RBCs experiencing the shown potential (solid black line), a potential corresponding to $k_x = 0$ (dashed black line) and a potential corresponding to half the force from a $k_x = 0$ field (dashed white line) are plotted.

Considering Longitudinal Modes with one Transverse Mode

Even though the pressure force in the x -direction is very small compared to the flow velocity profile, the longitudinal modes introduce changes overall in the potential field. Hence the potential in the y -direction is changed and it thus alters the trajectory of a particle. We will in the following investigate this effect in our standard configuration for blood with one node in the y -direction, corresponding to $n_y = 1$ or as previously denoted $w = \lambda/2$, and look at multiple nodes in the x -direction.

First of all we consider a situation with only a few nodes in the x -direction. The acoustic potential for $n_x = 1$ and $n_x = 3$ is seen in Fig. 12.2 together with trajectories for a RBC in blood. The modes have frequencies of $f_{n_x=1} = 2.119$ MHz and $f_{n_x=3} = 2.120$ MHz from Eq. (12.3). As the second thing we consider the case of $n_x = 25$, corresponding to a frequency of $f = 2.207$ MHz shown in Fig. 12.3a. We see that the longitudinal modes introduce periodic plateaus in the y -direction, corresponding to the minima in the potential, where particles are not affected by the pressure force in the y -direction. Due to the flow velocity profile the particles move forward in the x -direction even in areas without pressure force. Hence this mode setup cannot prevent the particles with $\Phi > 0$ from following the flow in the x -direction as we could for $k_y = 0$, because the potential has a minimum in the center of the channel. Eventually the $\Phi > 0$ particles will collect at the center and experience no pressure force and just follow the flow in the x -direction.

When considering a case with $n_x = 25$, see Fig. 12.3a, the potential qualitatively looks a lot like that with $k_x = 0$, but it is seen that that the trajectories in these two cases differ a lot. We thus search for an explanation of this behaviour in the following.

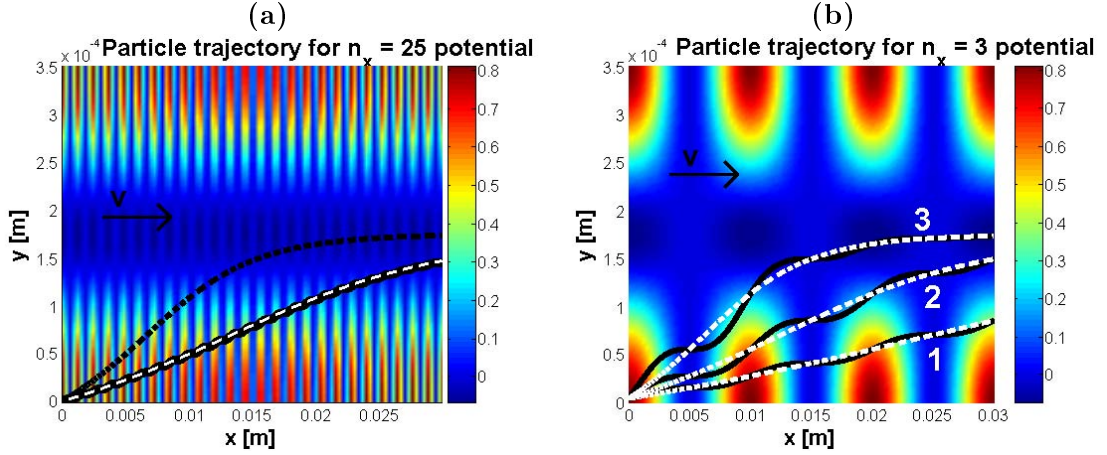


Figure 12.3: (a) Contour plot of the normalized acoustic potential U_{2D}/U_0 with $n_y = 1$ and $n_x = 25$. The trajectories of RBCs experiencing the shown potential (solid black line), a potential corresponding to $k_x = 0$ (dashed black line) and a potential corresponding to half the force from a $k_x = 0$ field (dashed white line) are plotted. (b) Contour plot of the normalized acoustic potential U_{2D}/U_0 with $n_y = 1$ and $n_x = 3$. The trajectories of RBCs experiencing the shown potential (solid black line) and a potential corresponding to half the force from a $k_x = 0$ field (dashed white line) are plotted. The trajectory marked 1 is for an average flow velocity of $2v_{x,\text{flow}}$, 2 is for $v_{x,\text{flow}} = 0.11 \text{ m s}^{-1}$, and 3 is for $1/2v_{x,\text{flow}}$.

The Average Force Exerted

When considering the introduced periodicity in the x -direction, it is natural to average the pressure force experienced by the particle over the period in the acoustic potential, T_x , in the x -direction, $T_x = 2\pi/k_x$. It is reasonable to consider the particle trajectory by the average over the spatial coordinate x , if the change in the potential/force which a particle experiences varies on a much shorter length scale in the x -direction than in the y -direction. The characteristic time scale of the potential change is the time it takes for a particle to move one period in the given direction, Δt . If the characteristic velocity in the x -direction is denoted v_x , and one period in the x -direction has a length of the order L/n_x , the time it takes for the potential to change notably is of the order $\Delta t_x \sim L/(n_x v_x)$. Similarly the change in y -direction is of the order $\Delta t_y \sim w/(n_y v_y)$. Hence we must require for the average to be in good agreement with the actual particle trajectory that

$$\Delta t_x \ll \Delta t_y \Leftrightarrow \frac{n_y v_y}{w} \ll \frac{n_x v_x}{L}. \quad (12.9)$$

This should be understood such that the nodes passed per time by the particle must be larger in the x -direction than in the y -direction. It ensures that it is possible to consider the y -coordinate as constant while we experience a notable change in the x -coordinate. Hence the larger number of modes per length or the bigger the characteristic velocity in the x -direction, the better we can expect an average to describe the particle trajectory.

The characteristic velocity in the x -direction is the velocity from the flow profile. In the systems discussed in part II we are considering flow velocities of the order $v_{x,\text{flow}} \approx 0.11 \text{ m/s}$. The characteristic velocity in the y -direction is the velocity originating from the

pressure force in the y -direction. This can be estimated in the same way as done in the x -direction for the case $k_y = 0$ in Eq. (12.5). Using typical values for RBCs we estimate $v_{y,\text{long}} = 2.3 \text{ mm s}^{-1}$. Therefore we fulfill the condition for the average to be close to the particle trajectory in the considered setup.

Thus it is valid to use the spatial average of $\langle E_{ac} \rangle$ in the x -direction, and from Eq. (5.98) we find

$$\langle F_x \rangle = U_0 k_x \sin(2k_x x) \left[2f_1 \cos^2(k_y y) + 3f_2 \left(\cos^2(k_y y) - \frac{k_y^2}{k^2} \right) \right], \quad (12.10a)$$

$$\langle F_y \rangle = U_0 k_y \sin(2k_y y) \left[2f_1 \cos^2(k_x x) + 3f_2 \left(\cos^2(k_x x) - \frac{k_x^2}{k^2} \right) \right], \quad (12.10b)$$

leading to

$$\langle F_{x,\text{average}} \rangle = 0. \quad (12.10c)$$

$$\langle F_{y,\text{average}} \rangle = \frac{1}{2} U_0 k_y \sin(2k_y y) \left[2f_1 + 3f_2 \left(1 - 2 \frac{k_x^2}{k^2} \right) \right] \quad (12.10d)$$

$$= \frac{1}{2} \langle F_{y,k_x=0} \rangle - 3f_2 U_0 k_y \sin(2k_y y) \frac{k_x^2}{k^2}. \quad (12.10e)$$

The last equality follows from comparison with the expression for the one-dimensional force Eq. (5.91a). This shows that the average force exerted on the particles is half the force from a potential field with $k_x = 0$ but including an extra term with the same sine-variation as the pressure force in the y -direction. Thus the deviation from the $(1/2)\langle F_{y,k_x=0} \rangle$ effect is biggest when the pressure force in the y -direction is largest, hence when the velocity in the y -direction is largest.

Comparison with the Potential Without Longitudinal Modes

When considering the average force in Eq. (12.10c) we notice that it corresponds to half the force exerted from a potential than in the situation with $k_x = 0$ when the term $2k_x^2/k^2 \approx 0$. This is the case when

$$\frac{k_x^2}{k_x^2 + k_y^2} \ll 1 \Leftrightarrow \frac{1}{1 + \left(\frac{n_y L}{w n_x}\right)^2} \ll 1 \Leftrightarrow \frac{n_y}{w} \gg \frac{n_x}{L}. \quad (12.11)$$

This means that when the nodes per length is greater in the y -direction than in the x -direction, the average force exerted from a mode with $n_x \neq 0$ corresponds to $(1/2)\langle F_{y,k_x=0} \rangle$. For the considered channel setup we have $n_y/w = 1/w = 2.9 \times 10^3 \text{ m}^{-1}$ and $n_x/L = 100 \text{ m}^{-1}$ for $n_x = 3$, thus fulfilling Eq. (12.11).

In Figs. 12.2 and 12.3 the trajectory of a RBC is plotted in different potentials together with the trajectory for a similar RBC affected by $\frac{1}{2}\langle F_{y,k_x=0} \rangle$. Furthermore the trajectory of a particle experiencing the one-dimensional pressure force is calculated for comparison. We notice the great agreement between the actual trajectory and the $(1/2)\langle F_{y,k_x=0} \rangle$ trajectory as predicted by our theory.

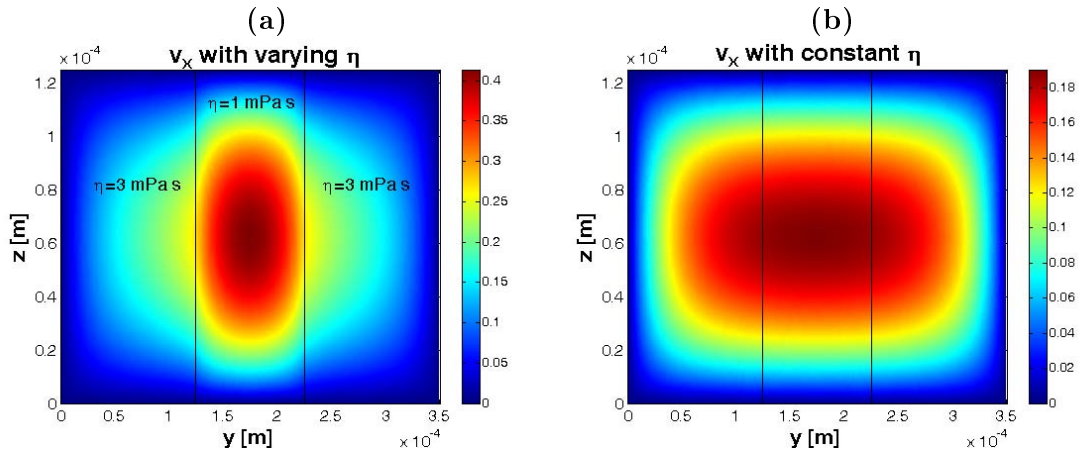


Figure 12.4: (a) A cross-section of the Pouseille-flow in a BWB-channel with different viscosities, respectively blood and water. The velocities are given in m s^{-1} . (b) A cross-section of the Pouseille-flow in a BWB-channel with constant viscosity. Notice that v_x is measured in m s^{-1} .

In Fig. 12.3b we have furthermore shown the proposed dependency on the flow velocity Eq. (12.9), when plotting the trajectories of RBCs in a $n_x = 3$ potential for different flow velocities in the x -direction. We find that the case with the highest flow velocity has the best agreement between the actual particle trajectory and the particle affected by $(1/2)\langle F_{y,k_x=0} \rangle$, showing that the averaging approximation is best when operating with large flow velocities, which confirms Eq. (12.9).

We conclude that if the flow velocities compared to the nodes per length in the two directions fulfill Eq. (12.9), and we furthermore have the dimensions of the channel fulfilling Eq. (12.11), the particle trajectory in the actual potential can very well be approximated by the trajectory of a particle affected by $(1/2)\langle F_{y,k_x=0} \rangle$.

12.2 The Influence of the Viscosity on the Pouseille-flow

An effect we have neglected in our analysis of the separation of RBCs from lipids or WBCs is that the viscosity of the buffer medium is not necessarily the same as that of the transport medium. For blood we have used that $\eta = 0.0027 \text{ Pa s}$. However the viscosity of water, which is a reasonable approximation for what could be used as buffer medium, at 20°C is 0.0010 Pa s [5]. The differential equation for the Pouseille flow in each medium can be derived from the Navier–Stokes equation, since η only varies at the boundaries between two flows so it can be assumed constant in each medium. We notice that a steady-state flow in a channel which is translational invariant in the x -direction, cannot depend the x position. Furthermore the flow velocity can only have an x -component. Hence the velocity in each medium must have the form $\mathbf{v}(y, z) = v_x(y, z)\mathbf{e}_x$. With a steady-state velocity of this form we see from the Navier–Stokes equation that the velocity must fulfill the differential equation, [5],

$$-\eta [\partial_y^2 + \partial_z^2] v_x(y, z) = \frac{\Delta p}{L}. \quad (12.12)$$

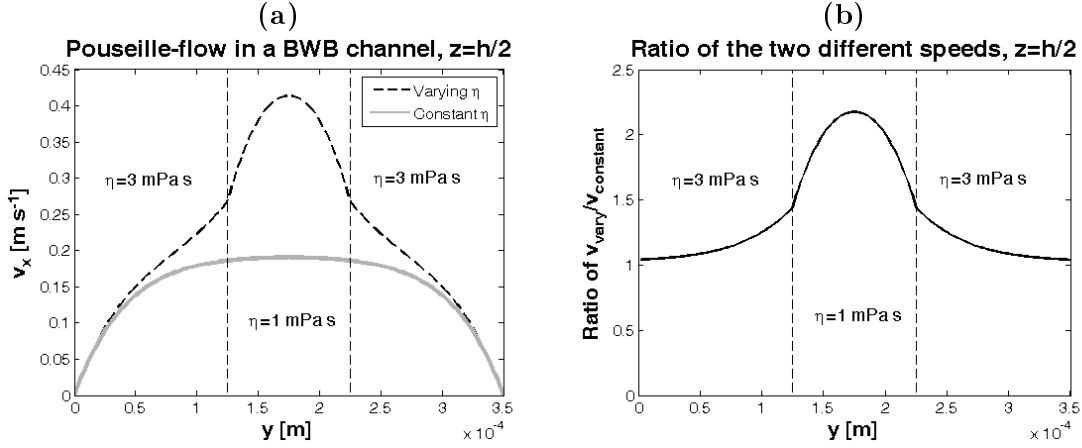


Figure 12.5: (a) A comparison of the flow-speeds in the middle of the channel for the two different models using the viscosity of water and blood respectively. The two vertical lines show the splitting of the three inlets. (b) The ratio of v_x found using the model with different viscosities to the v_x found using constant viscosity.

The boundary condition at the edges of the channel is that v_x goes to zero. At the interface between the two flows we have that the shear stress is constant, and since the shear stress is given as $\sigma = \eta \nabla \mathbf{v}$, we get

$$\eta_1 \nabla v_{x,1} = \eta_2 \nabla v_{x,2}. \quad (12.13)$$

where the indices refer to the different media. We have implemented Eqs. (12.12) and (12.13) in COMSOL with the three-channel BWB-system described in Section 8.4 where we are assuming that the interfaces between the media are flat. In the optimal separation setup we had blood in the interval $[0 \mu\text{m}; 125 \mu\text{m}]$ and $[225 \mu\text{m}; 350 \mu\text{m}]$ and buffer in-between.

A cross-section of the velocity-field with different viscosities in the channel can be seen in Fig. 12.4a. We have also simulated the flow with constant $\eta = 0.0027 \text{ Pa s}$ which can be seen in Fig. 12.4b. Notice that there is a clear difference in the flow-type. The speed changes a lot in the middle of the channel when having different viscosities.

We have plotted a cross-sectional view of v_x at $z = h/2$ to compare the results for the two models in Fig. 12.5a. We see that the biggest difference between the two models appears in the middle of the channel.

Furthermore we have plotted the ratio between the two flow-speeds, see Fig. 12.5b. From this figure we deduce that the conclusion from the RBC–lipid section not will be changed dramatically, since it was the lipids that were the limiting factor, and they will not move into the middle subdomain where v_x is much larger. However we still see that the innermost lipids in the blood inlet (and RBCs for that sake) move almost 50 % faster in the center when using the more sophisticated model than assuming the same viscosity in the buffer- and transport-medium.

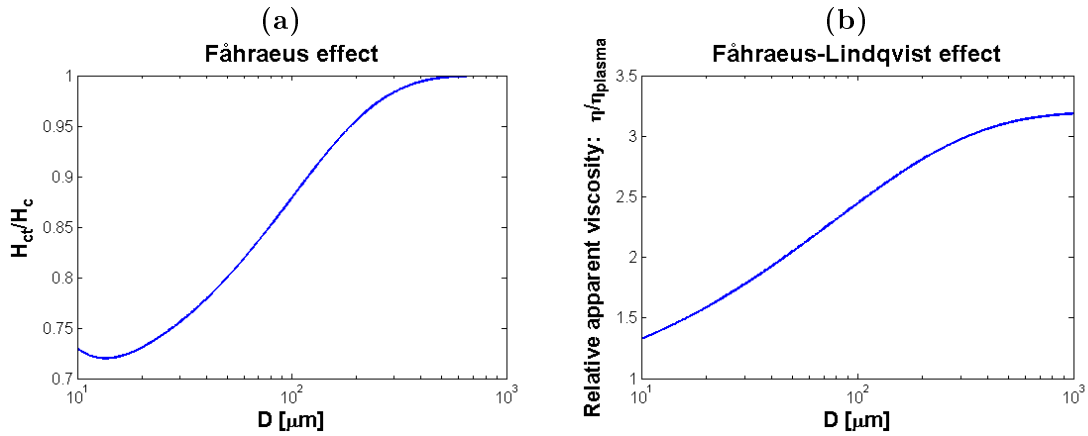


Figure 12.6: (a) The Fåhræus effect. Plot of the relative haematocrit H_{ct}/H_c vs. the tube diameter D . (b) The Fåhræus–Lindqvist effect. Plot of the apparent viscosity in the tube, η_{app} , against the tube diameter D . More advanced models of the non-Newtonian behavior is given in [18] and gives small deviations (up to 0.15 in η_{app}) from the simple model, but the tendency is still the same.

12.3 The Fåhræus effect and Fåhræus–Lindqvist effect

Two of the most relevant non-linear effects which are observed in blood flowing in small tubes are according to [18] the Fåhræus effect and the Fåhræus–Lindqvist effect. Without going into details with the models behind these two effects we will just state the consequences. Note that the models are for straight, circular channels with diameter D where we in our work use rectangular cross-sections, but we assume that the same effects are present in rectangular channels.

The standard haematocrit is denoted H_c when the blood is in a large reservoir. The Fåhræus-effect predicts a decrease in the concentration of RBCs, described by the dynamic haematocrit H_{ct} , *i.e.* the apparent haematocrit value in the tube, when the diameter of the tube is reduced. The altered haematocrit values is due to the formation of a depleted plasma layer at the channel edges. The layer is formed because of migration of cells from the channel walls (where the migration has a higher flow velocity than the axial flow velocity). Thus the Fåhræus effect can be reduced by increasing the flow velocity, v_x .

An empirical parametric description of the Fåhræus effect is given in [23], and this is plotted in Fig. 12.6a. The parameters used for the plot are unspecified, but it gives a qualitative but not quantitative description of the Fåhræus effect.

The Fåhræus–Lindqvist effect states a decrease in the apparent viscosity in the tube, η_{app} , when the tube diameter is reduced. Due to stress-induced cell migration from the Fåhræus effect a slippage layer of plasma-rich, cell-depleted fluid appears near the tube walls in small tubes, $D = 5 \mu\text{m} - 0.3 \text{ mm}$ [18]. The thickness of the layer depends of the flow rate and the tube diameter, but is experimentally shown more or less to remain in the range $2 - 4 \mu\text{m}$ for all tube diameters [7]. Thus the relative volume of the plasma layer (with low viscosity due to the Fåhræus effect) to the tube volume is increased with decreasing tube diameter. This effect is describe as the Fåhræus–Lindqvist effect. A simple model is given in [25] and plotted in Fig. 12.6b to give a qualitative impression of

the Fåhræus–Lindqvist effect. We see that the effect can change the viscosity significantly when having flow in small channels. But as noted in Section 6.2 the value of the viscosity does not affect the particle trajectories in the channel, $x(y)$, but only the time profiles, $y(t)$ and $x(t)$. Hence we conclude that this effect is not that important to our determination of the channel length.

The Fåhræus–Lindqvist effect as described above is valid for a haematocrit value up to 95 % [10]. When the haematocrit is higher, we will have a high dense packing of the RBCs which contributes to the non-Newtonian behavior of the fluid. Further discussions on the non-Newtonian behavior of blood and the effect of having a blood flow in channels (such as *cell screening* and *plasma skimming*) are described in detail in [18].

12.4 Temperature Dependence

Many of our parameters used in the simulations depend on the temperature. In this section we will look closer at what this means for our results.

First we will look at the viscosity. According to [8] the viscosity of blood decreases with temperature, for values see Appendix F. Generally the viscosity of blood increases with approximately 2 % with a one degree decrease in temperature, see [8]. However as discussed in Section 6.2 this will not change the required travel lengths but only the time to get there, and since we assume that we are in steady-state, this dependence can be neglected. However if we were to use a buffer medium at 20°C and blood at 37°C, the cooling and heating of the two fluids would change the relative viscosity between them thus leading to a different Pouseille-flow as discussed in Section 12.2, and this would be very difficult to model.

We also know that the density and speed of sound in fluids change with temperature. From [17] we found values for the speed of sound versus temperature in water in 10°C increments given in Appendix F. Regarding the density we found the following expression¹

$$\rho = \frac{\rho_{\text{at } \tau_0}}{1 + a_0 (\tau - \tau_0)}, \quad \text{where } a_{0, \text{water}} = 0.88 \times 10^{-4} \text{ } ^\circ\text{C}^{-1}, \quad (12.14)$$

where τ is the temperature and τ_0 is a reference temperature. Using that the density of water at $\tau_0 = 4 \text{ } ^\circ\text{C}$ is $\rho_0 = 1000 \text{ kg m}^{-3}$, we can find the Φ -factors as a function of temperature, where we neglect the change in density and temperature of the particles in our fluid.

Using the above results for water Fig. 12.7a shows the change in Φ -factors versus temperature using water as our buffer medium. Notice that the values are scaled to the Φ -factor at 20 °C. In the simulations made in part II we used blood and milk as transport mediums, but we were not able to find the temperature dependence of the density and speed of sound for those two parameters. To see if running the system at different temperatures would make it easier to separate our particles, we plot the ratio of the Φ -factor of RBCs to lipid and to WBCs in Fig. 12.7b, taking the absolute value of the RBC to lipid ratio for clarity. We see that the ratio for RBCs–WBCs is almost independent of temperature, however it seems like we could improve our results for RBC to lipid separation. We stress

¹http://www.engineeringtoolbox.com/fluid-density-temperature-pressure-d_309.html

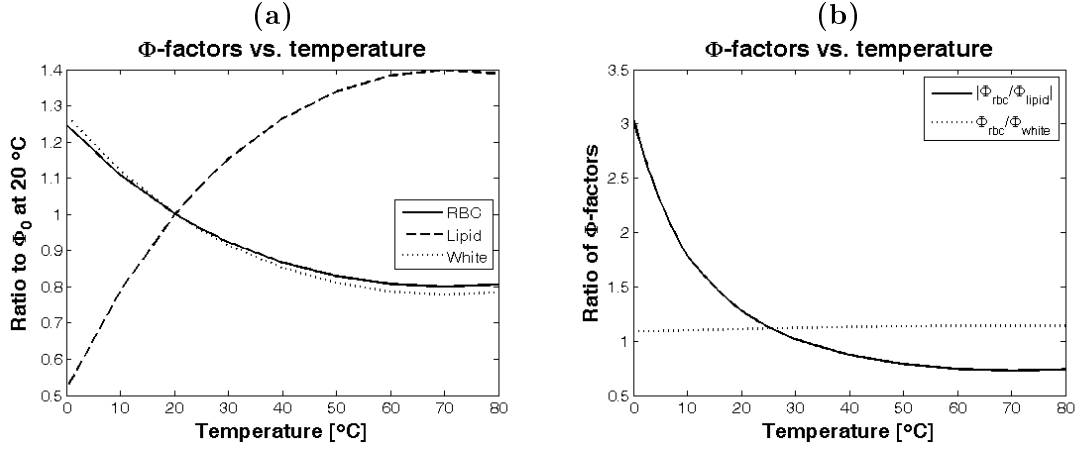


Figure 12.7: (a) The ratio of the Φ -factors to Φ at 20 °C as a function of temperature. Notice that these ϕ -factors are found with water as medium compared to the blood and milk we used in our simulations (b) The ratio of the Φ -factors as a function of temperature. Notice that we have taken the absolute value of the RBC/lipid ratio for clarity.

that the temperature dependence of density and speed of sound for the particles is not included in the prior discussions. Furthermore as seen in Fig. 12.7a the Φ -factor for lipid particles decreases with decreasing temperature which would mean that it would require a longer channel to separate the particles, as we discussed in Chapter 8. Still the temperature dependence is something that could be looked deeper into, since it could possibly make the separation easier.

12.5 Effects of Concentration

In the previous discussion we only considered single point-like particles. This is not the case in reality where RBCs, WBCs, and lipids have a finite extension. Furthermore we have multiple particles. This means that there is a maximum of the concentration in our channels. To simplify the analysis we will assume non-compressible spherical particles and cylinders.

To derive an expression for the concentration in our outlets as a function of the inlet concentration we consider $N/\Delta t$ particles flowing in a channel per time. Thus $N_{in}/\Delta t$ and $N_{out}/\Delta t$ particles are entering and leaving the channel respectively. We define Γ as the percentage of particles from the inlet leaving in a desired outlet. The width of the stream is w . Since we assume that we have reached steady-state, we have for a time step Δt

$$\frac{N_{out}}{\Delta t} = \frac{\Gamma N_{in}}{\Delta t}. \quad (12.15)$$

Using that $N = cV$ we get

$$\frac{c_{out} V_{out}}{\Delta t} = \frac{\Gamma c_{in} V_{in}}{\Delta t} \Leftrightarrow \frac{c_{out} w_{out} \Delta L_{out} \cdot h}{\Delta t} = \frac{\Gamma w_{in} \Delta L_{in} \cdot h}{\Delta t}, \quad (12.16)$$

where we have used that the volume entering the channel during the time step Δt can be expressed as $w_{in} h \Delta L_{in}$ and similarly the volume leaving the channel as $w_{out} h \Delta L_{out}$, where

h is the height of the channel. ΔL_{in} and ΔL_{out} are the length of the volume element and can be expressed by the velocity of the fluid in the channel as $\Delta L = v_x \Delta t$. By assuming a time-independent flow profile in the channel, we get

$$c_{\text{out}} = c_{\text{in}} \frac{w_{\text{in}}}{w_{\text{out}}} \Gamma \frac{v_{\text{out}}}{v_{\text{in}}} = \Gamma \cdot c_{\text{in}} \cdot \frac{w_{\text{in}}}{w_{\text{out}}} \quad (12.17)$$

This equation allows us to find the smallest possible proportion of the width of the outlet channel compared to the inlet because there are a physical maximum value for c_{out} . According to the Kepler conjecture, the highest average density in a regular lattice arrangement of spheres is approximately $c_{\text{max}} = 74 \text{ Vol\%}$. This can be achieved with hexagonal close-packed or face centered cubic structure.

However since the red blood cells are not spherical but rather toroidal shaped one could imagine a stacking of cylinders instead of spheres. In this case the closest packing would be parallel cylinders placed in a hexagonal grid. Thus the maximum concentration becomes $c_{\text{max}} \approx 91 \text{ \%}$, which is significantly higher than for stacking of spheres.

Assuming that we are examining male blood with a haematocrit value of 46 Vol\% [20], we are now able to find the smallest possible outlet channel assuming all the RBCs have moved into the outlet channel, *i.e.* $\Gamma = 1$. Using Eq. (12.17) we arrive at

$$c_{\text{out}} \leq c_{\text{max}} = 1 \cdot c_{\text{in}} \cdot \frac{w_{\text{in}}}{w_{\text{out}}} \Leftrightarrow \frac{w_{\text{out}}}{w_{\text{in}}} = \frac{c_{\text{in}}}{c_{\text{out}}} \geq \frac{c_{\text{in}}}{c_{\text{max}}} = \frac{0.46}{0.74} = 0.62, \quad (12.18)$$

using spherical stackings. Thus the outlet channel has to be at least 62 \% of the inlet channel if we want to have all the RBCs contained in it. However this value is a conservative estimate since we have neglected compressibility, and the fact that the RBCs are not spherical. If we use the results for stacking of cylinders, we get that the outlet channel should be at least 50 \% of the inlet channel, still neglecting the compressibility of the RBCs.

This shows that we have to be careful not to choose too small an outlet channel for the RBCs if we want the calculations from the single-particle approach to be valid. We have not considered the lipids since the concentration is considerable smaller [2], but the same argument applies for them as well.

12.6 Diffusion

In this section we consider the many-particle effect connected with the diffusion of particles when there is a gradient in the concentration present. According to [5] the diffusion force in a weak solution (low concentration) is given by

$$\mathbf{F}_{\text{diff}} = -\nabla \mu, \quad \mu(T, \rho) = \mu_0 + k_B T \ln(\rho/\rho_0), \quad (12.19)$$

where $\mu(T, \rho)$ is the chemical potential, and where the subscript 0 refers to some constant standard concentration. This leads to an expression for the size of the diffusion force in the y -direction given as

$$F_{\text{diff}} = k_B T \frac{\partial_y \rho}{\rho} = k_B T \frac{\partial_y c}{c}. \quad (12.20)$$

In Section 5.5 we have shown, that the acoustical force drives the RBCs towards the middle of the channel. According to Eq. (12.20) this leads to a diffusion force counteracting the acoustical force Eq. (5.91c). In steady-state when the particles do not move, the size of the two forces must be equal,

$$k_B T \frac{\partial_y c}{c} = 4\pi k_y R^3 \langle E_{ac} \Phi \rangle \sin\left(2\pi n_y \frac{y}{w}\right), \quad (12.21)$$

where $k_y = \pi n_y/w$. Solving this differential equation for the first mode, $n_y = 1$, gives

$$c(y) = c_0 \exp\left[-\frac{2\pi \langle E_{ac} \rangle R^3 \Phi}{k_B T} \left(1 + \cos\left(2\pi \frac{y}{w}\right)\right)\right], \quad (12.22)$$

where $c_0 = c(w/2)$ is the concentration in the middle of the channel. Using our choice of parameters for RBCs at $T = 293$ K, the constant in the exponential takes the value

$$\frac{2\pi \langle E_{ac} \rangle R^3 \Phi}{k_B T} = 4.16 \times 10^6. \quad (12.23)$$

The exponential of this constant is huge, and thus we can say that according to this, the beam should only be only as wide as the particle diameter. Therefore the diffusion cannot be responsible for the finite size of the beam, as we observe in practice in Fig. 1.2, as long as we can assume the expression of the diffusion force Eq. (12.19), which requires low concentrations of particles in the transport medium.

To examine if the solution in the center of the channel actually is low, as it was assumed for this derivation, we determine the maximum possible concentration of RBCs assuming that these are spherical in shape. In stacking of spheres in a fcc structure we can achieve the maximum concentration of

$$c_{\max} = \frac{\sqrt{2}}{R^3} \approx \frac{\sqrt{2}}{(5 \times 10^{-6} \text{ } \mu\text{m})^3} = 1.1 \times 10^{16} \text{ m}^{-3}, \quad (12.24)$$

using a particle radius $R = 5 \text{ } \mu\text{m}$. We must remember that this estimate requires the particles to be very tightly stacked. For that reason we also want to make an estimate on the size of the diffusion force when we assume a finite beam width with the concentration c_{\max} and the width $L_0 \approx 30 \text{ } \mu\text{m}$. We estimate the derivative of the concentration by $\partial_y c \approx c_{\max}/L_0$, and the diffusion force Eq. (12.20) can thus be estimated as

$$F_{\text{diff}} \approx \frac{k_B T}{c_{\max}} \frac{c_{\max}}{L_0} = \frac{k_B T}{L_0} \approx \frac{4.14 \times 10^{-21} \text{ J}}{30 \text{ } \mu\text{m}} = 1.4 \times 10^{-16} \text{ N} \quad (12.25)$$

From Eq. (12.25) we find that the diffusion force is small compared to the typical value of the pressure force on particles of size $R = 5 \text{ } \mu\text{m}$, where the force is of the order $\langle F_{\text{Pressure}} \rangle \approx 10^{-9} \text{ N}$.

12.7 Many Particle Forces — Secondary Bjerknes Force

The force between two adjacent particles has been neglected throughout the analysis in the previous parts of the thesis. In this section we estimate the size of the force between two particles in a fluid in an acoustic field and compare it to the pressure force that has been discussed in the previous chapters.

In [9] the force between two particles is presented as a secondary effect in the scattered field caused by the sound fields emitted by the other particles, hence the customary name *secondary Bjerknes force*. We will use this theory for the interaction between two particles even though it was first developed to describe the forces between two gas bubbles in a liquid. We follow a derivation made by [39] modified according to our own approach in deriving the pressure force. The final expression of the secondary Bjerknes force is given by numerous authors [9], [39], [34].

Derivation of Expression for the Secondary Bjerknes Force

This derivation considers stationary particles/bubbles, and we will for simplicity adopt this limitation in the derivation.

Consider two spherical particles, A and B, in a stationary fluid in a stationary acoustic field. We assume that the inter-particle distance, d , fulfills $\lambda \gg d$. According to Eq. (3.45) this assumption leads to the conclusion that in the vicinity of the particles, the fluid between the particles can be regarded as incompressible. Furthermore we have to assume that the particles remain spherical with radii $R_A(t)$ and $R_B(t)$ at all times.

We want to derive an expression for the force experienced by particle B caused by the pressure gradient from the scattered sound field at A. We start by considering the velocity of the wave scattered by A at a position r .

From Section 5.2.1 we have that in the region close to the particles $r \ll \lambda$ the velocity potential to first-order is given as

$$\phi_{\text{sc},A} = \frac{a(t)}{r} - \frac{\mathbf{A}(t) \cdot \mathbf{e}_r}{r^2} + \dots \quad (12.26)$$

We are only interested in the scattered velocity potential created by particle A at the place of particle B, and we have assumed that the distance d between the two of them fulfills $\lambda \gg d$. This is indicating the correctness of only considering the limit $\lambda \gg r$, when we want to study the effect of the scattered wave on particle B. We limit ourselves to the lowest order in r , hence considering the scattered velocity potential as $\phi_{\text{sc},A} = a(t)/r$.

Because we are considering an incompressible fluid with the density ρ_0 , we see that the mass flux ejected from the surface of the particle A can be expressed as

$$\rho_0 \dot{V}_{\text{sc},A} = \rho_0 \int_{\partial V_A} \mathbf{v}_{\text{sc},A}(t) \cdot \mathbf{e}_r \, dS = \rho_0 \int_{\partial V_A} (\nabla \phi_{\text{sc},A}) \cdot \mathbf{e}_r \, dS. \quad (12.27)$$

In analogy to the calculations made in Section 5.2.1 leading to Eq. (5.15) the right-hand side of Eq. (12.27) gives $-4\pi a(t)$, and the left-hand side yields $\rho_0 \dot{V}_{\text{sc},A} = \rho_0 4\pi R_A^2 \dot{R}_A$. Finally we conclude that to the lowest order in r the scattered velocity potential from

particle A in the region $\lambda \gg r$ is given as

$$\phi_{\text{sc},A} = -\frac{R_A^2 \dot{R}_A}{r}. \quad (12.28)$$

From the relation between velocity potential and the velocity in first-order perturbation $\mathbf{v}_{\text{sc},A} = \nabla \phi_{\text{sc},A}$, we get

$$\mathbf{v}_{\text{sc},A} = \frac{R_A^2 \dot{R}_A}{r^2} \mathbf{e}_r. \quad (12.29)$$

This also outlines the difference with the calculations made in Section 5.2.1. In Section 5.2.1 we considered the field present in the region $\lambda \ll r$ where we could not assume incompressibility of the fluid. In this section it suffices to consider the velocity field in the region $\lambda \gg r$ because of the assumption $\lambda \gg d$. Furthermore in Section 5.2.1 we expanded the model to moving particles, where this section only focuses on stationary spheres in stationary sound fields.

To calculate the pressure fields from the velocity field Eq. (12.29), we consider the first-order inviscid Navier–Stokes equation which is seen from Eq. (2.8a) and Eq. (2.8c) to be

$$\rho_0 \partial_t \mathbf{v}_1 = -\nabla p_1. \quad (12.30)$$

Because this equation is linear, the scattered velocity from particle A, which in resemblance with Section 5.2.1 is first-order, gives the pressure gradient

$$\rho_0 \partial_t \mathbf{v}_{\text{sc},A} = -\nabla p_A \Leftrightarrow \nabla p_A = -\frac{\rho_0}{r^2} \partial_t \left(R_A^2 \dot{R}_A \right) \mathbf{e}_r. \quad (12.31)$$

The particle B (with volume V_B) experiences the pressure gradient ∇p_A , hence it is subject to the force from the scattered field from A, given as

$$\mathbf{F}_{A,B} = -V_B \nabla p_A. \quad (12.32)$$

Substituting Eq. (12.31) into Eq. (12.32) we obtain the force exerted from the particle A on particle B which is at a distance d ,

$$\mathbf{F}_{A,B} = V_B \nabla p_A \Big|_{r=d} = V_B \left[\frac{\rho_0}{r^2} \partial_t \left(R_A^2 \dot{R}_A \right) \right] \Big|_{r=d} \mathbf{e}_r = V_B \frac{\rho_0}{d^2} \partial_t \left(R_A^2 \dot{R}_A \right) \mathbf{e}_r. \quad (12.33)$$

Because the time derivative of the volume of a sphere is given as $\dot{V} = 4\pi R^2 \dot{R}$, we can rewrite Eq. (12.33) as

$$\mathbf{F}_{A,B} = \frac{\rho_0}{4\pi d^2} V_B \partial_t^2 V_A \mathbf{e}_r. \quad (12.34)$$

Due to the rapid oscillating fields we are not interested in the momentary force but rather in the time-averaged force experienced by particle B. Integrating over a full period of oscillation T and using integration by parts, assuming that V_A and V_B have the same

harmonic variation in time, we obtain

$$\langle \mathbf{F}_{A,B} \rangle = \frac{\rho_0}{4\pi d^2} \langle V_B \partial_t^2 V_A \rangle \mathbf{e}_r \quad (12.35a)$$

$$= \frac{\rho_0}{4\pi d^2} \frac{1}{T} \int_0^T V_B \partial_t^2 V_A dt \mathbf{e}_r \quad (12.35b)$$

$$= \frac{\rho_0}{4\pi d^2} \frac{1}{T} \left([V_B \partial_t V_A]_0^T - \int_0^T \partial_t V_B \partial_t V_A dt \right) \mathbf{e}_r \quad (12.35c)$$

$$= -\frac{\rho_0}{4\pi d^2} \frac{1}{T} \left(\int_0^T \partial_t V_B \partial_t V_A dt \right) \mathbf{e}_r = -\frac{\rho_0}{4\pi d^2} \langle \dot{V}_A \dot{V}_B \rangle \mathbf{e}_r, \quad (12.35d)$$

which is the result obtained in [9] and [39]. We observe that this force can be both attractive or repulsive depending on the phase between the oscillation of the particles.

As the volume change is very difficult to estimate, we want to rewrite Eq. (12.35d) with the aim of expressing the volume changes by the compressibilities of the spheres and fluid. We first notice the definition of compressibility as stated in Chapter 7, which we can use to express the time-change in volume by

$$\beta = -\frac{1}{V} \partial_p V, \quad (12.36a)$$

$$-\beta V = \frac{\partial t}{\partial p} \frac{\partial V}{\partial t}, \quad (12.36b)$$

$$\dot{V} = \beta V \omega p_1. \quad (12.36c)$$

where we have used that to first-order we can assume a harmonic time-dependence. Notice that we assume that both the fluid and the sphere are compressible and thus get that $\beta = \beta_{\text{fluid}} - \beta_{\text{particle}}$.

Inserting Eq. (12.36c) in Eq. (12.35d) assuming that particle A and B are of the same type, we obtain

$$\langle \mathbf{F}_{A,B} \rangle = -\frac{\rho_0}{4\pi d^2} \langle (\beta V \omega p_1)^2 \rangle \mathbf{e}_r = -\frac{\rho_0}{8\pi d^2} \beta^2 V^2 \omega^2 p_1^2 \mathbf{e}_r = -\frac{2\pi \rho_0}{9d^2} \beta^2 R^6 \omega^2 p_1^2 \mathbf{e}_r, \quad (12.37)$$

where a factor of 1/2 appears due to time-averaging. To estimate the magnitude of this expression we rewrite the amplitude of the first-order perturbation in pressure via the potential formulation of the first-order pressure $p_1 = -\rho_0 \partial_t \phi_1$, see Eq. (3.7). Still assuming harmonic first-order terms and noticing that the magnitude of the velocity potential is u_0/k , where u_0 is the magnitude of the first-order velocity, and k is the wavenumber of the standing wave, we get

$$p_1 = -\rho_0 \partial_t \phi_1 = \rho_0 \omega \phi_1, \quad (12.38)$$

$$|p_1| = \rho_0 \omega \frac{u_0}{k} = \rho_0 \omega u_0 \frac{c_a}{\omega} = \rho_0 u_0 c_a. \quad (12.39)$$

If we use that the relation between the average acoustical energy density and the first-order velocity amplitude, derived in Eq. (5.90c), $\langle E_{ac} \rangle = (1/4) \rho_0 u_0^2$, we can express the magnitude of the first-order pressure as $|p_1| = c_a \sqrt{4\rho_0 \langle E_{ac} \rangle}$. With this we can estimate the magnitude of the secondary Bjerknes force as

$$\left| \langle \mathbf{F}_{A,B} \rangle \right| = \frac{8\pi \rho_0^2}{9d^2} \beta^2 R^6 \omega^2 c_a^2 \langle E_{ac} \rangle. \quad (12.40)$$

Estimate of the Magnitude of the Force

As the final step in the analysis we want to estimate the size of the secondary Bjerknes force expressed in Eq. (12.40). In the estimate we use the typical parameters shown in Tables 7.2 and 7.3 assuming an interparticle distance of $d = 20 \mu\text{m}$ with a particle radius of $R = 5 \mu\text{m}$,

$$\begin{aligned} \left| \langle F_{A,B} \rangle \right| &\approx \frac{8\pi \times (10^3 \text{ kg m}^{-3})^2}{9 \times (20 \mu\text{m})^2} \times \left[5.88 \times 10^{-10} \text{ Pa}^{-1} - 3.48 \times 10^{-10} \text{ Pa}^{-1} \right]^2 \\ &\quad \times (5 \mu\text{m})^6 \times (2\pi \times 2 \times 10^6 \text{ s}^{-1})^2 \times (1483 \text{ m s}^{-1})^2 \times 10^3 \text{ Jm}^{-3} \\ &\approx 2.2 \times 10^{-12} \text{ N} \end{aligned} \quad (12.41)$$

The pressure force on similar RBCs are of the order $2 \times 10^{-9} \text{ N}$. So we conclude that we are making an error of about 10^{-3} when neglecting this kind of particle interaction. We notice a very important fact from the estimate made above, that the secondary Bjerknes-force scales notably with the particle size. Reducing the particle radius to half the size, $R \approx 2.5 \mu\text{m}$, we reduce the time-average of the secondary Bjerknes-force to $3.4 \times 10^{-14} \text{ N}$ for an interparticle distance $d = 20 \mu\text{m}$.

Another important point to be made is the scaling with the interparticle distance. At low concentrations this ensures that it is reasonable to neglect the secondary Bjerknes force altogether. But we notice that we can anticipate a larger interparticle interaction at high concentrations. For example the secondary Bjerknes force is of the order of magnitude $8.7 \times 10^{-12} \text{ N}$ for particles with $R = 5 \mu\text{m}$ touching each other.

For particles touching each other we need particles of the size $R \approx 20 \mu\text{m}$ for the secondary Bjerknes force to be of the order 10^{-9} N and hence of the same order of magnitude as the pressure force.

The secondary Bjerknes force derived here is independent of direction compared to the acoustic wave. If this was included, we would get an extra angular dependent term in the secondary Bjerknes force as stated in [42].

12.8 Acoustic Streaming

Acoustic streaming is in general a viscosity effect leading to time independent second-order velocity terms. In this section we will treat boundary effects at a solid wall as a reason to acoustic streaming. In this approach the acoustic streaming is caused by the viscosity of the fluid near the boundary and leads to a time-independent flow near the boundary. This flow is shown to be independent of the viscosity even though it originates from the viscosity.

Derivation of the Acoustic Streaming Velocity

We will follow the ideas of [16] where we consider a boundary between a potential flow strictly in the x -direction and a solid wall placed in the xz -plane, making the problem invariant in the z -direction. When applying a no-slip boundary condition we get a change in velocity from the full flow far away from the boundary to zero velocity at the boundary as sketched in Fig. 12.8. This change occurs in a boundary layer of the thickness δ . To

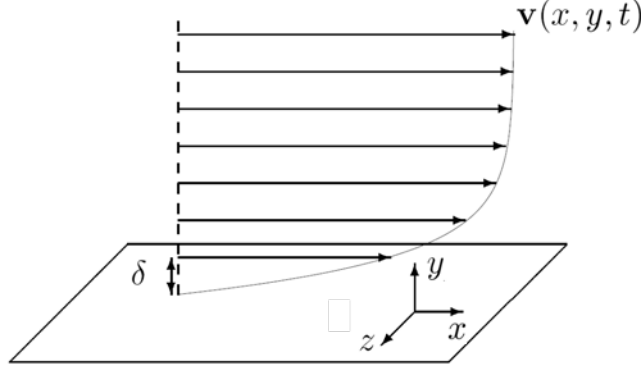


Figure 12.8: Shows a sketch of the standing wave problem with a boundary layer to a solid wall. From [22].

ensures that we are considering a thin boundary layer compared to the other length scales, we assume that the characteristic length of the problem, L_0 , is much larger than δ . In Appendix E it is shown that the thickness of the boundary layer is given as the length scale over which the first-order velocity field is approaching the flow far from the boundary. It is found to be

$$\delta = \sqrt{\frac{2\eta}{\rho_0\omega}} = \sqrt{\frac{2 \times 0.89 \times 10^{-3} \text{ Pa s}}{10^3 \text{ kg m}^{-3} \times 2\pi \times 10^6 \text{ s}^{-1}}} = 0.53 \text{ } \mu\text{m} \quad (12.42)$$

Furthermore we notice that the boundary layer is much smaller than the wavelength of the typical used acoustic wave, $\lambda \gg \delta$. Thus enabling us to consider the fluid as incompressible in the boundary layer, hence denoting the constant density $\rho = \rho_0$, leading to the continuity condition $\nabla \cdot \mathbf{v} = 0$, *cf.* Eq. (2.2). All in all we are assuming that we are considering a problem where

$$\lambda \gg L_0 \gg \delta. \quad (12.43)$$

We start the analysis by considering the incompressible flow in the boundary layer with the aim of deriving the equation of motion for the fluid in the boundary layer. Close to the solid wall it is not possible to neglect the viscosity, when we notice that the velocity decreases towards zero at the interface. First we make the perturbation to first-order in the pressure ($p = p_0 + p_1 + p_2$) and velocity ($\mathbf{v} = \mathbf{v}_0 + \mathbf{v}_1 + \mathbf{v}_2 = \mathbf{v}_1 + \mathbf{v}_2$) of the viscid Navier–Stokes equation, Eq. (2.1). Hence the equation of motion to first-order becomes,

$$\partial_t \mathbf{v}_1 = -\frac{1}{\rho_0} \nabla p_1 + \frac{\eta}{\rho_0} \nabla^2 \mathbf{v}_1. \quad (12.44)$$

We notice that the Navier–Stokes equation has been reduced using the incompressibility condition, $\nabla \cdot \mathbf{v} = 0$, before we made the perturbation.

To second-order the equation of motion is obtained in the same way as Eq. (12.44),

$$\partial_t \mathbf{v}_2 + (\mathbf{v}_1 \cdot \nabla) \mathbf{v}_1 = -\frac{1}{\rho_0} \nabla p_2 + \frac{\eta}{\rho_0} \nabla^2 \mathbf{v}_1. \quad (12.45)$$

Following the notation of [16] we introduce the constant $\nu = \eta/\rho_0$ to simplify the notation.

These equations can be reduced by the assumption in Eq. (12.43). As $L_0 \gg \delta$ we conclude that the boundary layer is thin and that we must have the majority of the flow in the boundary layer to be in the x -direction, hence $v_x \gg v_y$.

Using the no-slip condition between the boundary and the solid wall. This means that the fluid is at rest at the wall, but outside the boundary layer we have flow in the x -direction (a potential flow). Over the length scale of δ the velocity therefore changes from the flow velocity far from the boundary to zero. Implying a large derivative of the velocity in the y -direction compared to the derivative in the x -direction, where the velocity changes over a length scale of L_0 , hence $\partial_y \gg \partial_x$.

Exploiting these assumptions we conclude that the first-order equation Eq. (12.44) in the x -direction becomes

$$\partial_t v_{1,x} = -\frac{1}{\rho_0} \partial_x p_1 + \nu \partial_y^2 v_{1,x}, \quad (12.46)$$

and the corresponding second-order equation Eq. (12.45) in the x -direction becomes,

$$\partial_t v_{2,x} + (v_{1,x} \partial_x + v_{1,y} \partial_y) v_{1,x} = -\frac{1}{\rho_0} \partial_x p_2 + \nu \partial_y^2 v_{2,x}. \quad (12.47)$$

The pressure can now be related to the velocity in the main stream, *i.e.* the potential flow outside the boundary layer. Because the flow in the y -direction is small compared with the flow in the x -direction as stated above, we conclude that the pressure gradient is small in the y -direction compared to the pressure gradient in the x -direction, $\partial_x p \gg \partial_y p$. Neglecting $\partial_y p$ implies that $\partial_x p$ must be the same in the boundary layer and the main stream, *i.e.* the potential flow outside the boundary layer. Using Bernoulli equation, Eq. (A.3), we express $\partial_x p$ by the flow outside the boundary layer,

$$f(t) = \partial_t \phi + \frac{1}{2} |\nabla \phi|^2 + \frac{1}{\rho_0} p \quad (12.48)$$

$$0 = \partial_x \partial_t \phi + \frac{1}{2} \partial_x |\nabla \phi|^2 + \frac{1}{\rho_0} \partial_x p \quad (12.49)$$

$$\frac{1}{\rho_0} \partial_x p = -\partial_t U_1(x) - U_1(x) \partial_x U_1(x). \quad (12.50)$$

Denoting the first-order velocity field outside the boundary layer $U_1(x)$ remembering that the velocity is zero in the y -direction outside the boundary layer. To first- and second-order we get from Eq. (12.50),

$$\frac{1}{\rho_0} \partial_x p_1 = -\partial_t U_1(x), \quad (12.51)$$

$$\frac{1}{\rho_0} \partial_x p_2 = -U_1(x) \partial_x U_1(x). \quad (12.52)$$

Inserting this into Eqs. (12.46) and (12.47), we get

$$\partial_t v_{1,x} - \nu \partial_y^2 v_{1,x} = \partial_t U_1(x), \quad (12.53a)$$

$$\partial_t v_{2,x} + (v_{1,x} \partial_x + v_{1,y} \partial_y) v_{1,x} - \nu \partial_y^2 v_{2,x} = U_1(x) \partial_x U_1(x). \quad (12.53b)$$

To simplify the second-order equation of motion we confine ourselves to consider only the time-averaged values. Due to the high driving frequencies, it is only possible experimentally to observe the time-averaged values of the fields. From Eq. (3.47) we conclude that the time average of a periodic varying derivative must vanish. Notice that we do not assume that the second-order terms vary with the same period as in the region outside the boundary layer, but merely states that they must vary periodically. Hence the time average of Eq. (12.53b) becomes

$$\nu \langle \partial_y^2 v_{2,x} \rangle = \langle v_{1,x} \partial_x v_{1,x} \rangle + \langle v_{1,y} \partial_y v_{1,x} \rangle - \langle U_1(x) \partial_x U_1(x) \rangle. \quad (12.54)$$

In order to solve for the second-order time-averaged velocity in Eq. (12.54), it is necessary to first solve Eq. (12.53a) for the first-order velocity. We consider the potential flow in the x -direction outside the boundary layer as being a standing wave with amplitude U_0 and wavenumber k , which to first-order is given as,

$$U_1(x) = U_0 \cos(kx) e^{-i\omega t} \quad (12.55)$$

Furthermore we are employing the no-slip condition at the solid wall and the fact that the velocity must remain finite in all space as the boundary conditions for the problem,

$$|v_x| < \infty \quad \text{for } y \rightarrow \infty, \quad (12.56a)$$

$$v_x = v_y = 0 \quad \text{for } y = 0. \quad (12.56b)$$

In Appendix E we have solved in details the equations of motion Eqs. (12.53a) and (12.54) subject to the boundary conditions Eq. (12.56) with the flow in the main stream given as Eq. (12.55). Solving for the the second-order time-averaged velocity far from the boundary at the solid wall, at $y \rightarrow \infty$, we get

$$\langle v_{2,x} \rangle = \frac{1}{8} \frac{U_0^2}{c_a} \sin(2kx), \quad (12.57)$$

where c_a is the velocity of sound in the fluid. We notice that the acoustic streaming gives rise to a velocity which oscillates at twice the frequency of the generating standing wave. Furthermore we notice that the acoustic streaming velocity is independent of the viscosity even though it was an effect created by the viscosity at the boundary.

Estimate of the Acoustic Streaming „Drag Force”

We first estimate the velocity associated with the acoustic streaming and then express this velocity as though it was a drag force trying to move the particles as to compare it with the other neglected effects and the pressure force.

To estimate the magnitude of the velocity due to acoustic streaming, we notice that we defined $\langle E_{ac} \rangle = (1/4)\rho_0 U_0^2$ in Eq. (5.90c). Using this and the typical parameter values mentioned in Chapter 7, we estimate the magnitude of the velocity

$$\left| \langle v_{2,x} \rangle \right| = \frac{1}{2} \frac{\langle E_{ac} \rangle}{\rho_0 c_a} \approx \frac{1}{2} \frac{10^3 \text{ J m}^{-3}}{10^3 \text{ kg m}^{-3} \times 1483 \text{ m s}^{-1}} = 3.4 \times 10^{-4} \text{ m s}^{-1} \quad (12.58)$$

Compared to the flow velocity in the x -direction (≈ 0.1 m/s) we observe that $|\langle v_{2,x} \rangle|$ is very small.

To compare the effect of the acoustic streaming compared to the pressure force we rewrite Eq. (12.58) the drag force the velocity gives rise to according to Eq. (6.2), $\mathbf{F}_{\text{drag}} = 6\pi\eta R\mathbf{v}$. The acoustic streaming velocity for RBCs can be compared to a „drag force” of the magnitude

$$\left| \mathbf{F}_{\text{drag}} \right| = 3\pi \frac{\eta R \langle E_{\text{ac}} \rangle}{\rho_0 c_a} \approx 3\pi \frac{0.0027 \text{ Pa s} \times 5 \text{ } \mu\text{m} \times 10^3 \text{ J m}^{-3}}{10^3 \text{ kg m}^{-3} \times 1483 \text{ m s}^{-1}} = 8.6 \times 10^{-11} \text{ N}. \quad (12.59)$$

The pressure force on similar RBCs is $2 \times 10^{-9} \text{ N}$, and we conclude that the force due to acoustic streaming is 10^2 times smaller than the pressure force. Notice however, that the acoustic streaming as treated above is an effect in the boundary layer, $\delta \approx 0.5 \text{ } \mu\text{m}$, and thus not of the same magnitude in the whole channel.

12.9 Summary of Neglected Effects

In this part we have focused on the effects not covered in the analysis in part II, and a short overview of the effects is given in Table 12.1. We started by considering the effects influencing on particles in the x -direction. Longitudinal modes introduced a varying force field in the x -direction instead of the previously considered translation-invariant field. We showed that the particle trajectory in this force field can be well approximated in the considered setups by the trajectory of a particle in a force field without longitudinal modes but with half the acoustic energy density.

The flow in the x -direction is furthermore affected if we have different viscosities in the transport- and the buffer-medium respectively. This leads to a change in the flow-profile in the channel in the x -direction where we no longer can assume a constant flow profile in the center of the channel.

Secondly we are considering effects affecting the properties of the fluid. This includes the Fåhræus effect and temperature dependence. The Fåhræus effect leads to a lower concentration of RCBs in the outlets than expected because a depleted plasma layer is created at the channel edges. The thickness of the layer is experimentally shown to remain fairly constant when reducing the channel width. This relative volume change of the plasma layer together with the Fåhræus effect leads to a decrease in viscosity and this tendency is described by the Fåhræus–Lindqvist effect.

The pressure force changes with the acoustical properties of the fluid, and some of these are temperature dependent. We found that the pressure force can be changed by a factor of 0.5 – 1.5 for RBCs and by approximately 0.4 for WBCs and lipid particles.

We have discussed a couple of extensions to the single-particle approach used in part II. The simple effect of the finite size of the particles leading to a maximum concentration is discussed and extended with a discussion of diffusion effects. The diffusion force is estimated to be

$$F_{\text{diff}} = k_B T \frac{\partial_y c}{c} \approx \frac{k_B T}{L_0}, \quad (12.60)$$

where L_0 is a characteristic length over which the concentration changes notably. This force is estimated to have a magnitude of the order 10^{-16} N . We notice that this force scales inversely with the distance between the particles, d , as we can interpret L_0 as

Table 12.1: Effects affecting particles in a standing wave. Magnitude refers to the force relative to the pressure force on a $R = 5 \mu\text{m}$ particle in blood plasma ($F_{\text{effect}}/F_{\text{pressure}}$).

Effect	Affecting	Magnitude Scaling	
Pressure force	Force on suspended particles	1	$\propto R^3$
Temperature	Changing the acoustical properties of fluid/particles	0.5-1.5	- -
Diffusion	Force counteracting high concentration	10^{-7}	$\propto d^{-1}$
Secondary Bjerknes	Attractive/repulsive inter-particle force	10^{-3}	$\propto R^6, d^{-2}$
Acoustical streaming	Second-order fluid velocity change affecting the particles	10^{-2}	$\propto R$
Longitudinal modes	Potential field	- -	-
Viscosity differences	Change of the flow profile in the x -direction	- -	- -
Fåhræus-Lindqvist	Creating depleted boundary layer affecting viscosity of the fluid	- -	- -

being proportional to the distance between the particles. Another effect scaling with the interparticle distance is the secondary Bjerknes force which describes the force exerted by one particle on another,

$$\langle F_{\text{Bjerknes}} \rangle = \frac{8\pi\rho_0}{9d^2} \beta^2 R^6 \omega^2 c_a^2 \rho_0 \langle E_{\text{ac}} \rangle. \quad (12.61)$$

The Bjerknes force scales as $\sim d^{-2}$, hence faster than the diffusion force when d decreases. Furthermore we observe that this force scales significantly with the particle size as R^6 , a lot more than the pressure force which scales with the volume, $\sim R^3$, see Eq. (5.91c). For particles of size $R = 5 \mu\text{m}$ and an interparticle distance of $d = 20 \mu\text{m}$ the secondary Bjerknes force has a magnitude of the order 10^{-12} N of. The secondary Bjerknes force becomes an important effect for high concentrations which indicates low interparticle distance and also for large particles of the size $R \approx 20 \mu\text{m}$.

The last effect considered is the acoustic streaming which gives a force,

$$\langle F_{\text{A. streaming}} \rangle = 3\pi\eta R \frac{\langle E_{\text{ac}} \rangle}{\rho_0 c_a}, \quad (12.62)$$

which has a magnitude of 10^{-12} N with a particle size of $R = 5 \mu\text{m}$. We observe that this force scales linearly with radius, thus making this force more important than both the pressure ($\sim R^3$) and the secondary Bjerknes force ($\sim R^6$) when we consider smaller particles.

Chapter 13

Conclusion

In this thesis we have described the governing equations for microfluidics and the perturbations that arise due to an applied acoustic field. We have in details derived an expression for the time-independent pressure force on a particle immersed in a fluid affected by an acoustic field, as sketched by Gor'kov in 1962 [14].

We have by numerical and analytical considerations shown that this pressure force is applicable for separation of particles in a microchannel where we considered three applications in the single-particle approach. In the first case we looked at separation of lipid cells from red blood cells and used the fact that the red blood cells move towards the nodes in the standing pressure wave and the lipid particles towards the anti-nodes, thus driving them in opposite directions. By applying the force over a sufficient amount of time, the two types of particles were separated in each part of the channel and could easily be taken out in two different flow outlets. We presented a way to optimize the channel setup by describing how short the channels could be, compared to the throughput.

The second case dealt with separation of red and white blood cells in blood. The direction of the pressure force on these particles is the same, but for separation we use the fact that the properties as size and compressibility of the cells are different, thus leading to a smaller pressure force on the red blood cells. In contrast to the first case, where the channel just had to be long enough or have a sufficiently small flow rate to make sure that the particles were separated, we determined the limitations of the channel length. We found that the separation is possible in a certain interval of channel lengths, thus making separation impossible if we make the channel too long. There exists channel lengths in this interval where red blood cells of all the considered sizes are able to be fully separated from the white blood cells.

In the third case we presented a channel solution where large lipid particles in milk could be separated away such that other large particles like cells with a pressure force with an opposite sign could be further analyzed in the milk. This was done using a $3\lambda/2$ -system. We generalize this to size-sorting of particles with the same acoustical properties but various sizes. We showed that by only operating in the central $1/3$ -part of a channel we could assume a constant flow profile which led to a simple analytic solution to find the required channel length for a given separation. With this setup we also proposed a method for determining the time-averaged acoustical energy density in the channel.

We proposed a way to optimize the separation setups by using the pressure force to

focus the particles in a channel before they are led into the separation channel. The focusing could be done in a $2\lambda/2$ -channel, and afterward the separation of particles with positive acoustophoretic sign could be done in a $\lambda/2$ -channel and for negative sign in a $3\lambda/2$ -channel. This system had two significant advantages compared to the systems without focusing. The concentrations in the inlet beam were higher than *e.g.* using a blood–buffer–blood-inlet channel system. Furthermore no buffer medium appears in the region in which we consider the analytical solution for separation length, and thus the flow profile is almost constant as assumed for the solution to be valid.

In the last part of the thesis we discussed different neglected effects related to the flow profile, the fluid, particle properties, and many-particle effect. We showed that longitudinal modes in the channel introduced a periodicity in the pressure force lengthwise in the channel. With our choice of parameters, a good approximation to the particle trajectory in the two dimensional force field is the trajectory of a particle affected by half the transverse force field when not considering longitudinal modes.

When considering forces affecting the particle separation, we found that the acoustic streaming gave rise to the greatest extra contribution. The acoustic streaming scaled as the radius of the considered particles, $\propto R$, as opposed to the pressure force which is a volume effect, $\propto R^3$. We found that if the considered particles get an order of magnitude smaller than the ones considered in the thesis ($1 - 5 \mu\text{m}$) the acoustical streaming becomes a more important effect than the pressure force.

13.1 Outlook

Although we have looked at many things in this thesis, there is still plenty of work to be done. First of all a deeper understanding of the standing acoustical waves in the fluid and the silicon is needed. It would be interesting to implement the results of Rune Barnkob [4], which considers how the standing waves in the channels actually look taking into account the whole chip design and materials.

For our calculations we assume that the time-averaged acoustical energy density in the channel is well-known. Our design for determination of the energy density could be tested in practice, and one could look into other ways to determine the energy density in a microchannel.

Lab-on-a-chip systems have been produced for separation of red blood cells and lipid particles in blood [28], [29]. But this system together with the other systems for separation and sorting could be expanded to include our design with focusing in a channel with another $\lambda/2$ -width before the separation. This setup should be tested in practice before the model is expanded further as we for example are not sure about the effects in the transition between the two channel parts.

Finally the simulations could be made more advanced by including more effects. Here we should focus on determining the acoustic streaming effect, especially if we want to miniaturize the system farther. For larger particles the interparticle forces such as the secondary Bjerknes force should be included in the analyses. Furthermore temperature effects both for the particles and the fluid could be considered.

Part IV
Appendices

Appendix A

Bernoulli's Equation for Incompressible Inviscid Fluids

As described in Section 3.3 it is under certain circumstances possible to describe the fluid as incompressible and thus simplifying the governing equations considerably. In this section we will be deriving a relationship between the velocity and the density (pressure) called the Bernoulli's equation.

In the main part of this thesis we will be considering circumstances where the flow can be considered as a potential flow, and we may write $\mathbf{v} = \nabla\phi$. This leads to the equality $(\mathbf{v}\cdot\nabla)\mathbf{v} = (1/2)\nabla v^2$ [5]. The time-dependent inviscid Navier-Stokes equation reduces from Eq. (2.1) to

$$\rho_0 [\partial_t \mathbf{v} + (\mathbf{v}\cdot\nabla)\mathbf{v}] = -\nabla p \Leftrightarrow \partial_t \mathbf{v} + \frac{1}{2}\nabla v^2 = -\frac{1}{\rho_0}\nabla p, \quad (\text{A.1})$$

where we have set the non-changing density to be ρ_0 and used the incompressibility condition $\nabla\cdot\mathbf{v} = 0$ expressed by the continuity equation Eq. (2.2) when $\rho = \rho_0$ is a constant.

Introducing the velocity potential it is easily shown that we get an invariant quantity taking the same value everywhere in the fluid,

$$0 = \partial_t \nabla\phi + \frac{1}{2}\nabla|\nabla\phi|^2 + \frac{1}{\rho_0}\nabla p \quad (\text{A.2})$$

$$f(t) = \partial_t \phi + \frac{1}{2}|\nabla\phi|^2 + \frac{1}{\rho_0}p, \quad (\text{A.3})$$

where we have used that time and spatial derivatives commute and $f(t)$ is an arbitrary function of time.

Eq. (A.3) is one formulation of the time-dependent Bernoulli's equation and holds for incompressible, inviscid potential flows.

Appendix B

Multipole Solution to the Spherical Wave Equation

As we discussed in Section 5.2.1 we want to show that the multipole expansion of the potential is a solution to the wave equation. We are considering a potential of the form

$$\phi = \frac{a(t - r/c)}{r} + \nabla \cdot \left(\frac{\mathbf{A}(t - r/c)}{r} \right) + \dots, \quad (\text{B.1})$$

which also contains higher order derivatives. We are looking at the first two terms and want to show that they are satisfying the wave equation,

$$\nabla^2 \phi - \frac{1}{c^2} \partial_t^2 \phi = 0. \quad (\text{B.2})$$

Here r is the distance from the chosen origin and c is the speed of sound in the fluid. Furthermore a is an arbitrary constant and \mathbf{A} is an arbitrary vector, both retarded functions depending only on time and the radial distance.

First we consider some convenient differential formulas to use during the following derivations. We use the index notation where summation over dummy indices is implied, and the 'dot' notation indicates differentiation with respect to the argument. First we consider the simple formula for taking the gradient of the power functions r^n where n is an integer

$$\nabla(r^n) = \partial_j(r^n) = nr^{n-1} \partial_j r = nr^{n-1} \frac{2r_j}{2\sqrt{x^2 + y^2 + z^2}} = nr^{n-1} e_j, \quad (\text{B.3})$$

where e_j indicates the j 'th component of the unit vector \mathbf{e} , making the expression independent of the choice of coordinates.

Based on Eq. (B.3) we derive both the divergence and the gradient (here a tensor) of the arbitrary vector $\mathbf{A}(t - r/c)$ depending only on time and the radial distance r

$$\nabla \cdot \mathbf{A}(t - r/c) = \partial_j A_j = \dot{A}_j \partial_j [t - r/c] = -\frac{1}{c} \dot{A}_j \partial_j r = -\frac{1}{c} \dot{A}_j e_j, \quad (\text{B.4a})$$

$$\nabla \mathbf{A}(t - r/c) = \partial_i A_j = \dot{A}_j \partial_i (t - r/c) = -\frac{1}{c} \dot{A}_j \partial_i r = -\frac{1}{c} \dot{A}_j e_i. \quad (\text{B.4b})$$

Next we consider the divergence of the position vector \mathbf{r}

$$\nabla \cdot \mathbf{r} = \partial_j r_j = \partial_x x + \partial_y y + \partial_z z = 3. \quad (\text{B.5})$$

We can now find both the gradient and the divergence of the unit vector

$$\nabla \mathbf{e}_r = \partial_i e_j = \partial_i \frac{r_j}{r} = (\partial_i r_j) \frac{1}{r} + r_j \partial_i \frac{1}{r} = \frac{\delta_{ij}}{r} - \frac{e_i r_j}{r^2} = \frac{\delta_{ij} - e_i e_j}{r}, \quad (\text{B.6a})$$

$$\nabla \cdot \mathbf{e}_r = \partial_j e_j = \partial_j \frac{r_j}{r} = (\partial_j r_j) \frac{1}{r} + r_j \partial_j \frac{1}{r} = \frac{3}{r} - \frac{e_j r_j}{r^2} = \frac{2}{r}. \quad (\text{B.6b})$$

Finally we consider the following expression

$$\frac{\nabla \cdot \mathbf{e}_r}{r^2} = \partial_j \frac{e_j}{r^2} = 4\pi \delta^3(\mathbf{r}), \quad (\text{B.7})$$

where we have introduced the three dimensional Dirac-distribution. Note also that Eq. (B.7) implies that

$$\nabla \cdot \nabla \left(\frac{1}{r} \right) = \partial_j^2 \left(\frac{1}{r} \right) = -4\pi \delta^3(\mathbf{r}). \quad (\text{B.8})$$

We are now ready to show that Eq. (B.1) is a solution to the wave equation, Eq. (B.2). Because Eq. (B.2) is a linear ordinary differential equation, we conclude that each of the terms in Eq. (B.1) must satisfy the wave equation. We therefore start by considering the first term in Eq. (B.1).

Taking the Laplacian of the first term gives

$$\begin{aligned} \nabla^2 \left(\frac{a(t-r/c)}{r} \right) &= \partial_i^2 \left(\frac{a(t-r/c)}{r} \right) = \partial_i \left[\left(\partial_i a(t-r/c) \right) \frac{1}{r} + a(t-r/c) \partial_i \left(\frac{1}{r} \right) \right] \\ &= \left[\partial_i^2 a(t-r/c) \right] \frac{1}{r} + 2 \left[\partial_i a(t-r/c) \right] \partial_i \left(\frac{1}{r} \right) + a(t-r/c) \partial_i^2 \left(\frac{1}{r} \right). \end{aligned} \quad (\text{B.9})$$

$$(\text{B.10})$$

We calculate Eq. (B.10) term-by-term exploiting that a only depend on time and r in the indicated manner and use Eq. (B.6b) and $e_i e_i = 1$,

$$\left[\partial_i^2 a(t-r/c) \right] \frac{1}{r} = -\frac{1}{cr} \partial_i (\dot{a} e_i) = -\frac{1}{cr} \left(-\frac{1}{c} \ddot{a} e_i e_i + \dot{a} \frac{2}{r} \right) = \frac{1}{rc^2} \ddot{a} - \dot{a} \frac{2}{cr^2}. \quad (\text{B.11a})$$

The second term gives, using the relations Eq. (B.3) and Eq. (B.6b),

$$2 \left[\partial_i a(t-r/c) \right] \partial_i \left(\frac{1}{r} \right) = 2 \left(-\frac{1}{c} \dot{a} e_i \right) \left(-\frac{e_i}{r^2} \right) = \frac{2}{cr^2} \dot{a}. \quad (\text{B.11b})$$

The third term is directly given by Eq. (B.8),

$$a(t-r/c) \partial_i^2 \left(\frac{1}{r} \right) = -4\pi a \delta^3(\mathbf{r}). \quad (\text{B.11c})$$

From Eq. (B.10) and Eq. (B.11) we can now calculate the left-hand side of the wave equation Eq. (B.2) for the first term of the considered solution Eq. (B.1)

$$\left[\nabla^2 - \frac{1}{c^2} \partial_t^2 \right] \left(\frac{a(t-r/c)}{r} \right) = \left[\frac{1}{rc^2} \ddot{a} - \dot{a} \frac{2}{cr^2} + \dot{a} \frac{2}{cr^2} - 4\pi a \delta^3(\mathbf{r}) \right] - \frac{1}{rc^2} \dot{a} \quad (\text{B.12})$$

$$= -4\pi a \delta^3(\mathbf{r}). \quad (\text{B.13})$$

We conclude that the first term of Eq. (B.1) is in fact a solution to the wave equation, except for the expected divergence in polar coordinates when we let r go to zero — represented with the Dirac-distribution.

Next we consider whether the second term of Eq. (B.1) is a solution to the scalar wave equation. Taking the Laplacian of this term yields

$$\nabla^2 \left[\nabla \cdot \left(\frac{\mathbf{A}(t-r/c)}{r} \right) \right] = \partial_i^2 \left[(\partial_j A_j) \frac{1}{r} + A_j \partial_j \left(\frac{1}{r} \right) \right] \quad (\text{B.14a})$$

$$= \partial_i \left[(\partial_i \partial_j A_j) \frac{1}{r} + (\partial_j A_j) \partial_i \left(\frac{1}{r} \right) + (\partial_i A_j) \partial_j \left(\frac{1}{r} \right) + A_j \partial_i \partial_j \left(\frac{1}{r} \right) \right] \quad (\text{B.14b})$$

$$= (\partial_i \partial_i \partial_j A_j) \frac{1}{r} + (\partial_i \partial_j A_j) \partial_i \left(\frac{1}{r} \right) + (\partial_i \partial_j A_j) \partial_i \left(\frac{1}{r} \right) + (\partial_j A_j) \partial_i \partial_i \left(\frac{1}{r} \right) \quad (\text{B.14c})$$

$$+ (\partial_i \partial_i A_j) \partial_j \left(\frac{1}{r} \right) + (\partial_i A_j) \partial_i \partial_j \left(\frac{1}{r} \right) + (\partial_i A_j) \partial_i \partial_j \left(\frac{1}{r} \right) + A_j \partial_i \partial_i \partial_j \left(\frac{1}{r} \right)$$

$$= (\partial_i \partial_i \partial_j A_j) \frac{1}{r} + 2(\partial_i \partial_j A_j) \partial_i \left(\frac{1}{r} \right) + (\partial_j A_j) \partial_i \partial_i \left(\frac{1}{r} \right) \quad (\text{B.14d})$$

$$+ (\partial_i \partial_i A_j) \partial_j \left(\frac{1}{r} \right) + 2(\partial_i A_j) \partial_i \partial_j \left(\frac{1}{r} \right) + A_j \partial_i \partial_i \partial_j \left(\frac{1}{r} \right).$$

For simplicity we have omitted the arguments of the vector \mathbf{A} .

To keep track of the following calculations we calculate each term in Eq. (B.14d) separately using the relations Eq. (B.3) to Eq. (B.8). The first term gives

$$\left(\partial_i \partial_i \partial_j A_j \right) \frac{1}{r} = -\frac{1}{rc} \partial_i \partial_i \left(\dot{A}_j e_j \right) = \frac{1}{rc} \partial_i \left(\frac{1}{c} \ddot{A}_j e_i e_j - \dot{A}_j \frac{\delta_{ij} - e_i e_j}{r} \right) \quad (\text{B.15a})$$

$$= \frac{1}{c^2 r} (\partial_i \ddot{A}_j) e_i e_j + \frac{1}{c^2 r} \ddot{A}_j (\partial_i e_i) e_j + \frac{1}{c^2 r} \ddot{A}_j e_i (\partial_i e_j) \quad (\text{B.15b})$$

$$- (\partial_i \dot{A}_j) \frac{\delta_{ij} - e_i e_j}{cr^2} - \dot{A}_j \frac{\partial_i \delta_{ij} - (\partial_i e_i) e_j - e_i (\partial_i e_j)}{cr^2}$$

$$= -\frac{1}{c^3 r} \ddot{A}_j e_i e_i e_j + \frac{1}{c^2 r} \ddot{A}_j \frac{2}{r} e_j + \frac{1}{c^2 r} \ddot{A}_j e_i \frac{\delta_{ij} - e_i e_j}{r} \quad (\text{B.15c})$$

$$+ \ddot{A}_j e_i \frac{\delta_{ij} - e_i e_j}{c^2 r^2} - \dot{A}_j \frac{-\frac{2}{r} e_j - e_i \frac{\delta_{ij} - e_i e_j}{r}}{cr^2}.$$

We notice that $e_i \delta_{ij} = e_j$ and $e_i e_i = 1$ which reduces Eq. (B.15c) to

$$-\frac{1}{c^3 r} \ddot{A}_j e_j + \frac{2}{c^2 r^2} \ddot{A}_j e_j + \frac{2}{cr^3} \dot{A}_j e_j. \quad (\text{B.16})$$

Continuing with the calculation of the second term in Eq. (B.14d) exploiting that we have calculated $\partial_i \partial_j A_j$ in Eq. (B.15a) gives

$$2\left(\partial_i \partial_j A_j\right) \partial_i \left(\frac{1}{r}\right) = 2\left(\frac{1}{c^2} \ddot{A}_j e_i e_j - \dot{A}_j \frac{\delta_{ij} - e_i e_j}{cr}\right) \left(-\frac{e_i}{r^2}\right) = -\frac{2}{c^2 r^2} \ddot{A}_j e_j. \quad (\text{B.17})$$

Considering the third and sixth term together using Eq. (B.8) we write

$$\left(\partial_j A_j\right) \partial_i \partial_i \left(\frac{1}{r}\right) + A_j \partial_i \partial_i \partial_j \left(\frac{1}{r}\right) = -4\pi(\partial_j A_j) \delta^3(\mathbf{r}) - 4\pi A_j \left[\partial_j \delta^3(\mathbf{r})\right] \quad (\text{B.18a})$$

$$= -4\pi \partial_j \left[A_j \delta^3(\mathbf{r})\right]. \quad (\text{B.18b})$$

Next we consider the fourth term

$$\left(\partial_i \partial_i A_j\right) \partial_j \left(\frac{1}{r}\right) = \partial_i \left(-\frac{1}{c} \dot{A}_j e_i\right) \left(-\frac{e_j}{r^2}\right) \quad (\text{B.19a})$$

$$\left(\frac{1}{c^2} \ddot{A}_j e_i e_i - \frac{1}{c} \dot{A}_j \frac{2}{r}\right) \left(-\frac{e_j}{r^2}\right) = -\frac{1}{c^2 r^2} \ddot{A}_j e_j + \frac{2}{c r^3} \dot{A}_j e_j, \quad (\text{B.19b})$$

and the fifth term gives

$$2\left(\partial_i A_j\right) \partial_i \partial_j \left(\frac{1}{r}\right) = 2\left(-\frac{1}{c} \dot{A}_j e_j\right) \partial_i \left[-\frac{e_j}{r^2}\right] \quad (\text{B.20a})$$

$$= 2\left(\frac{1}{c} \dot{A}_j e_j\right) \left[\left(\partial_i e_j\right) \frac{1}{r^2} + e_j \partial_i \left(\frac{1}{r^2}\right)\right] \quad (\text{B.20b})$$

$$= 2\left(\frac{1}{c} \dot{A}_j e_j\right) \left[\left(\frac{\delta_{ij} - e_i e_j}{r}\right) \frac{1}{r^2} + e_j \left(-2\frac{1}{r^3}\right)\right] \quad (\text{B.20c})$$

$$= -\frac{4}{c r^3} \dot{A}_j e_j. \quad (\text{B.20d})$$

Inserting the obtained results into the original expression for the Laplacian of

$$\nabla \cdot (\mathbf{A}(t - r/c)/r), \quad (\text{B.21})$$

we get

$$\nabla^2 \left[\nabla \cdot \left(\frac{\mathbf{A}(t - r/c)}{r}\right) \right] = -\frac{1}{c^3 r} \ddot{\ddot{A}}_j e_j + \frac{2}{c^2 r^2} \ddot{A}_j e_j + \frac{2}{c r^3} \dot{A}_j e_j - \frac{2}{c^2 r^2} \ddot{A}_j e_j \quad (\text{B.22a})$$

$$- 4\pi \partial_j \left[A_j \delta^3(\mathbf{r})\right] - \frac{1}{c^2 r^2} \ddot{A}_j e_j + \frac{2}{c r^3} \dot{A}_j e_j - \frac{4}{c r^3} \dot{A}_j e_j \\ = -\frac{1}{c^3 r} \ddot{\ddot{A}}_j e_j - \frac{1}{c^2 r^2} \ddot{A}_j e_j - 4\pi \partial_j \left[A_j \delta^3(\mathbf{r})\right]. \quad (\text{B.22b})$$

Next step in confirming that the term $\nabla \cdot (\mathbf{A}(t - r/c)/r)$ is indeed a solution to the wave equation is calculating the double time-derivative,

$$\partial_t^2 \left[\nabla \cdot \left(\frac{\mathbf{A}(t - r/c)}{r}\right) \right] = \partial_t^2 \left[\left(\partial_j A_j\right) \frac{1}{r} + A_j \partial_j \left(\frac{1}{r}\right) \right] \quad (\text{B.23a})$$

$$= \partial_t^2 \left[-\frac{1}{rc} \dot{A}_j e_j - \frac{1}{r^2} A_j e_j \right] = -\frac{1}{rc} \ddot{\ddot{A}}_j e_j - \frac{1}{r^2} \ddot{A}_j e_j. \quad (\text{B.23b})$$

Inserting the calculated terms Eq. (B.22b) and Eq. (B.23b) into the wave equation, Eq. (B.2), we get

$$\begin{aligned} & -\frac{1}{c^3 r} \ddot{A}_j e_j - \frac{1}{c^2 r^2} \ddot{A}_j e_j - 4\pi \partial_j [A_j \delta^3(\mathbf{r})] - \frac{1}{c^2} \left(-\frac{1}{rc} \ddot{A}_j e_j - \frac{1}{r^2} \ddot{A}_j e_j \right) \\ & = -4\pi \partial_j [A_j \delta^3(\mathbf{r})] = -4\pi \nabla \cdot [\mathbf{A} \delta^3(\mathbf{r})]. \end{aligned} \quad (\text{B.24})$$

Thus we have shown that the second term of Eq. (B.1) also fulfills the wave equation except at the origin, where we have the expected divergence due to the choice of polar coordinates.

Because the wave equation is linear, we can now from Eq. (B.13) and Eq. (B.24) conclude that Eq. (B.1) is a solution to the wave equation everywhere except at the origin where the divergence is taken care of by the delta-functions.

Appendix C

Scattered Wave From Incoming Traveling Plane Wave

In this appendix we find an expression for the scattered wave from an incoming plane wave, as we describe in Section 5.3. We consider the incoming traveling plane wave described by the velocity potential

$$\phi_{\text{in}}(x, t) = -\frac{u_0}{k} \cos(kx - \omega t). \quad (\text{C.1})$$

This gives the incoming velocity field as the gradient of Eq. (C.1)

$$\mathbf{v}_{\text{in}} = (\partial_x \phi_{\text{in}}) \mathbf{e}_x = u_0 \sin(kx - \omega t) \mathbf{e}_x = v_{\text{in},0} \mathbf{e}_x, \quad (\text{C.2})$$

where we have defined $v_{\text{in},0}$ as the amplitude of the incoming field in the x -direction. Importantly we notice that the time derivative of the velocity potential can be written in terms of this component in the following way:

$$\partial_t \phi_{\text{in}} = -\frac{u_0 \omega}{k} \sin(kx - \omega t) = -c_a v_{\text{in},0}. \quad (\text{C.3})$$

We can from the incoming velocity potential determine the scattered potential of Eq. (5.36) using that from Eq. (C.3) we have

$$\rho_{\text{in}} = -\frac{\rho_0}{c_a^2} \partial_t \phi_{\text{in}} = \frac{\rho_0}{c_a} v_{\text{in},0}. \quad (\text{C.4})$$

This gives us

$$\phi_{\text{sc}}(t - r/c_a) = -\frac{R^3}{3c_a r} f_1 \dot{v}_{\text{in},0}(t - r/c_a) - \frac{R^3}{2} f_2 \nabla \cdot \left(\frac{\mathbf{v}_{\text{in}}(t - r/c_a)}{r} \right). \quad (\text{C.5})$$

We neglect terms of higher orders in r , because we are not considering r values close to the origin (inside the sphere). Noting that the dot notation implies differentiation with respect to the argument, we get

$$\phi_{\text{sc}}(t - r/c_a) = -\frac{R^3}{3c_a r} f_1 \dot{v}_{\text{in},0}(t - r/c_a) + \frac{R^3}{2c_a r} f_2 \dot{\mathbf{v}}_{\text{in}}(t - r/c_a) \cdot \mathbf{e}_r + \mathcal{O}(r^{-2}). \quad (\text{C.6})$$

The velocity is then given as the gradient of Eq. (C.6)

$$\mathbf{v}_{\text{sc}}(t - r/c_a) = \nabla \phi_{\text{sc}}(t - r/c_a) \quad (\text{C.7})$$

$$= \left(\frac{R^3}{3c_a^2 r} f_1 \ddot{v}_{\text{in},0}(t - r/c_a) - \frac{R^3}{2c_a^2 r} f_2 \ddot{\mathbf{v}}_{\text{in}}(t - r/c_a) \cdot \mathbf{e}_r \right) \mathbf{e}_r + \mathcal{O}(r^{-2}) \quad (\text{C.8})$$

$$= v_{\text{sc},0} \mathbf{e}_r + \mathcal{O}(r^{-2}), \quad (\text{C.9})$$

where we have defined $v_{\text{sc},0}$ as the radial component of the scattered velocity.

Using the incoming velocity

$$\mathbf{v}_{\text{in}}(t - r/c_a) = -u_0 \sin \left[\omega(t - r/c_a) \right] \mathbf{e}_x, \quad (\text{C.10})$$

and taking the double-derivative we get

$$\ddot{\mathbf{v}}_{\text{in}}(t - r/c_a) = u_0 \omega^2 \sin \left[\omega(t - r/c_a) \right] \mathbf{e}_x = \ddot{v}_{\text{in},0} \mathbf{e}_x, \quad (\text{C.11})$$

the scattered velocity field is found by inserting into Eq. (C.8),

$$\begin{aligned} \mathbf{v}_{\text{sc}}(t - r/c_a) &= \left(\frac{R^3}{3c_a^2 r} f_1 u_0 \omega^2 \sin \left[\omega(t - r/c_a) \right] - \frac{R^3}{2c_a^2 r} f_2 u_0 \omega^2 \sin \left[\omega(t - r/c_a) \right] \mathbf{e}_x \cdot \mathbf{e}_r \right) \mathbf{e}_r \\ &= \frac{R^3 u_0 \omega^2}{c_a^2 r} \sin \left[\omega(t - r/c_a) \right] \left(\frac{1}{3} f_1 - \frac{1}{2} f_2 \cos \theta \right) \mathbf{e}_r. \end{aligned} \quad (\text{C.12})$$

As was the case for the time derivative of the incoming velocity potential, the scattered velocity potential can be expressed by the component of the scattered velocity field

$$\partial_t \phi_{\text{sc}}(t - r/c_a) = -\frac{R^3}{3c_a r} f_1 \ddot{v}_{\text{in},0}(t - r/c_a) + \frac{R^3}{2c_a r} f_2 \ddot{\mathbf{v}}_{\text{in},0}(t - r/c_a) \cdot \mathbf{e}_r = -c_a v_{\text{sc},0} \quad (\text{C.13})$$

Appendix D

RBC-lipid Separation — Five-inlet Channel

An optimization of the BWB-systems, described in Section 8.4, could be to make a WBWBW-system instead. This is done to avoid having RBCs at the channel edged, *i.e.* near anti-nodes where the pressure is small, and the RBCs thus must use a long channel to reach the central outlet. The optimization are done in two steps: First optimizing the separation of RBCs and lipids by varying the channel position with a constant width of the channel afterwards by keeping the position constant but varying the position.

D.1 Varying the Position of the Blood Inlets

We keep the width of the inlet channel at $w_{\text{inlet}} = 30 \mu\text{m}$ and vary the position of the center. Fig. D.1 shows a sketch of the system. The required channel length before 95% of the incoming particles are in the correct outlet, is seen in Fig. D.2a. The farther we move the inlet channel towards the center of the channel, the faster the RBCs are separated, and faster separation of the lipid particles is achieved by moving the inlet towards the channel edge as the situation comparable to the considered BWB-system. The optimal length of the channel at the intersection between the two curves in Fig. D.2b, where 95 % of the RBCs are in the center outlet channel, and 95 % of the lipids are in the outer outlet. This almost correspond to the position, where the inner edge of the blood inlets is where the outer edge of the center outlet is. The best separation is achieved when the blood is injected outside the center outlet because the lipid moves about 10^2 slower in the y -direction than the RBCs.

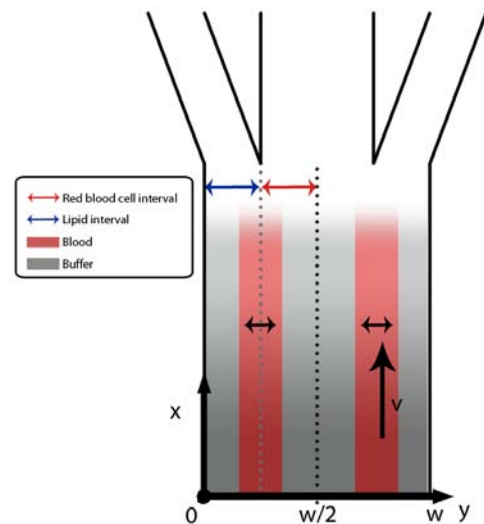


Figure D.1: The five-channel WBWBW-system where we vary the center of the blood inlets.

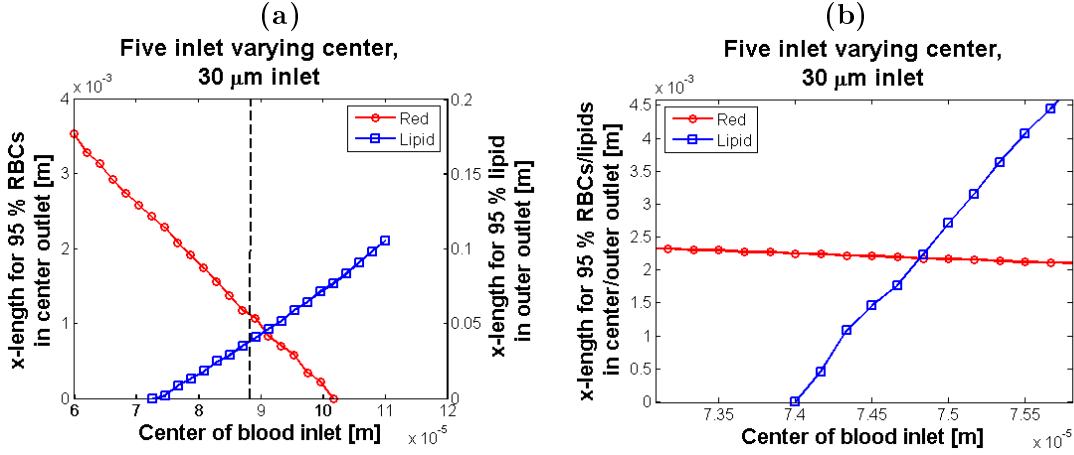


Figure D.2: (a) A five-inlet system with $w_{\text{inlet}} = 30 \mu\text{m}$ where we vary the center of the blood inlet. The dashed line indicates the split between the inner and outer outlet channel. (b) Zoom of (a) to see the intersection between the two curves and thus the optimal separation length.

D.2 Varying the Width of the Blood Inlets

To see if we can optimize the separation by using smaller blood inlet channel, we consider a fixed center of the blood inlet at $y_{\text{center}} = 87.5 \mu\text{m}$ (corresponding to the maximum of the pressure force) and vary the width of the blood inlet channel; a sketch of the system is shown in Fig. D.3a, and the results can be seen in Fig. D.3b. We see that the required length of the channel grows as we make the inlets larger. This is due to the fact that we inject particles farther and farther away from the outlet splitting point and where the pressure force is smaller the wider we make the inlet. If we again compare with the BWB-system, we conclude that the required length of the channel is not noticeably shorter. If we for instance picked a design with an inlet $60 \mu\text{m}$ wide, *i.e.* $y_{\text{inlet}} \in [57.5 \mu\text{m}; 117.5 \mu\text{m}]$, we would get approximately the same channel length as for the BWB-system. However this would lead to a flow rate, $Q_{\text{blood}} = 1.91 \times 10^{-9} \text{ m}^3/\text{s} = 0.12 \text{ mL}/\text{min}$, or only 60 % of the BWB-design or approximately 40 % of the one-inlet design. Thus we conclude that this five-inlet system is not the optimal choice if we want a high throughput since a big part of the inlets are filled with buffer.

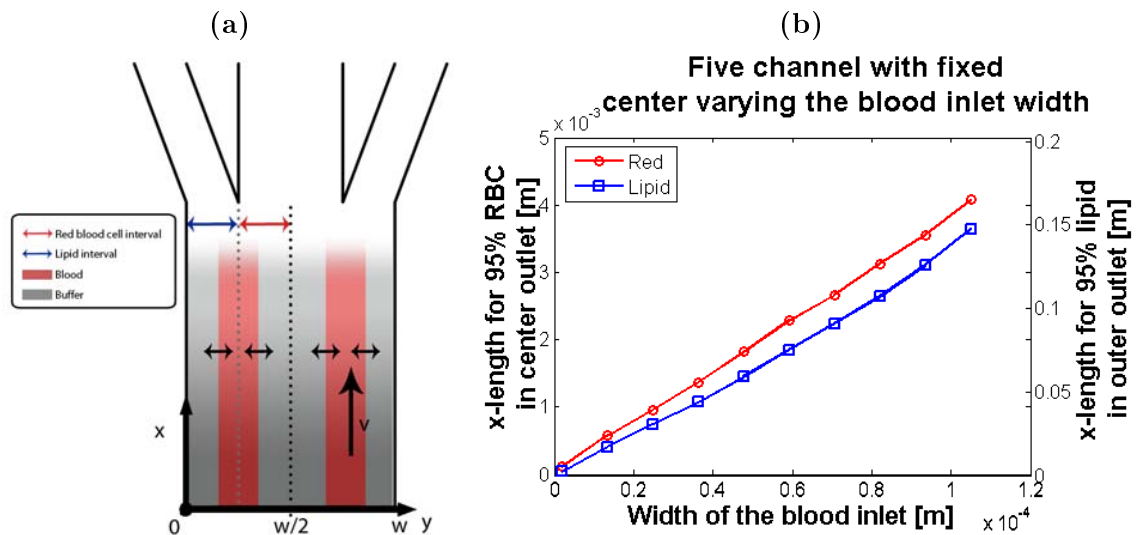


Figure D.3: (a) The five-channel inlet system where the widths of the inlets are varied. The dashed line indicates the split between the inner and outer outlet channel. (b) A five-channel system with a fixed center at $y_{\text{center}} = 87.5 \mu\text{m}$ and varying width of the blood inlet.

Appendix E

Derivation of the Acoustic Streaming Term

In Section 12.8 we found that the governing equations of the boundary layer problem outline in the section was given as

$$\partial_t v_{1,x} - \nu \partial_y^2 v_{1,x} = \partial_t U_1(x), \quad (\text{E.1a})$$

$$\nu \partial_y^2 \langle v_{2,x} \rangle = \langle v_{1,x} \partial_x v_{1,x} \rangle + \langle v_{1,y} \partial_y v_{1,x} \rangle - \langle U_1(x) \partial_x U_1(x) \rangle. \quad (\text{E.1b})$$

To solve those for the single solid-boundary problem considered in Section 12.8 we start by solving the first-order problem, as this enters into the second-order equation Eq. (E.1b).

We assume a first-order stationary standing wave in the region outside the boundary region,

$$U_1(x) = U_0 \cos(kx) e^{-i\omega t}, \quad (\text{E.2})$$

where we have used complex notation for convenience, remembering to take the real part at the end.

This implies that the first-order equation for the velocity Eq. (E.1a) becomes a second-order inhomogeneous partial differential equation in time and y ,

$$\partial_t v_{1,x} - \nu \partial_y^2 v_{1,x} = -i\omega U_0 \cos(kx) e^{-i\omega t}. \quad (\text{E.3})$$

The boundary condition for this partial differential equation is that the velocity must remain finite as y approach infinity *i.e.* $|v_{1,x}| < \infty$ for $y \rightarrow \infty$. At the other boundary $y = 0$ we employ the usual no-slip condition at the solid wall (which we for convenience have placed at $y = 0$), such that $v_{1,x} = 0$ for $y = 0$.

We assume for the time dependence that the first-order perturbation in velocity oscillates in phase with the oscillations in the main stream, *i.e.* that the first-order velocity perturbation has a harmonic time dependence. Given this condition we search for a solution to Eq. (E.3) of the form,

$$v_{1,x} = F(y) U_0 \cos(kx) e^{-i\omega t}, \quad (\text{E.4})$$

where $F(y)$ is an arbitrary function that only depends on y . Inserting Eq. (E.4) into Eq. (E.3) we get an ordinary differential equation for $F(y)$,

$$-i\omega F(y)U_0 \cos(kx) e^{-i\omega t} - \nu F''(y)U_0 \cos(kx) e^{-i\omega t} = -i\omega U_0 \cos(kx) e^{-i\omega t} \quad (\text{E.5})$$

$$\frac{\nu}{i\omega} F''(y) + F(y) = 1, \quad (\text{E.6})$$

where the prime notation indicates differentiation with respect to the argument. Solving the corresponding homogeneous equation gives us

$$F(y) = A \exp\left(\sqrt{\frac{-i\omega}{\nu}} y\right) + B \exp\left(-\sqrt{\frac{-i\omega}{\nu}} y\right), \quad (\text{E.7})$$

where A and B are arbitrary integration constants. From the boundary condition $|v_{1,x}| < \infty$ for $y \rightarrow \infty$ we conclude that $A = 0$ and the solution to the corresponding homogeneous equation of Eq. (E.6) is,

$$F(y) = B \exp\left(-\sqrt{-i}\sqrt{\frac{\omega}{\nu}} y\right) = B \exp\left(-\left[\frac{1}{\sqrt{2}} - \frac{i}{\sqrt{2}}\right] \sqrt{\frac{\omega}{\nu}} y\right) \quad (\text{E.8})$$

$$= B \exp\left(-[1-i]\frac{y}{\delta}\right), \quad (\text{E.9})$$

where we have introduced $\delta = \sqrt{2\nu/\omega}$, and we will show below that this is in fact an estimate for the thickness of the boundary layer.

As a guess for a solution to the inhomogeneous equation, Eq. (E.6), we choose a constant $F(y) = F_0$ which we by substituting into the equation finds to be $F_0 = 1$. Thus we obtain the solution to Eq. (E.3) of the form Eq. (E.4), and by use of the other boundary condition, $v_{1,x} = 0$ for $y = 0$, we conclude that $B = -1$. Hence we finally get, remembering to take the real part,

$$v_{1,x} = \text{Re}\left\{U_0 \cos(kx) e^{-i\omega t} \left(1 - e^{-[1-i]y/\delta}\right)\right\}. \quad (\text{E.10})$$

We notice that we can estimate the thickness of the boundary layer from Eq. (E.10). The solution grows exponentially towards the stationary standing wave in the main stream Eq. (E.2) with the characteristic length δ .

In Section 12.8 we concluded that the flow is invariant in the z -direction, *i.e.* $\partial_z v_z = 0$, leading to another formulation of the continuity condition $\nabla \cdot \mathbf{v} = 0$,

$$\partial_x v_x + \partial_y v_y = 0. \quad (\text{E.11})$$

To ensure that this is automatically fulfilled, we introduce the so called stream function $\psi(x, y, t)$ which is defined as

$$v_x \equiv \partial_y \psi \quad \wedge \quad v_y \equiv -\partial_x \psi. \quad (\text{E.12})$$

The definition Eq. (E.12) is seen to fulfill the two-dimensional continuity condition Eq. (E.11)

$$\partial_x(\partial_y \psi) + \partial_y(-\partial_x \psi) = 0, \quad (\text{E.13})$$

as long as the velocity and stream function are connected via Eq. (E.12). The first-order stream function ψ_1 corresponding to Eq. (E.10) is given from Eq. (E.12) via integration, where we take $\psi_1 = 0$ for $y = 0$ equivalent to the earlier mentioned condition $v_{1,x} = 0$ for $y = 0$,

$$\psi_1(x, y, t) = \text{Re} \left\{ U_0 \cos(kx) e^{-i\omega t} \left(y + \frac{e^{-\kappa y}}{\kappa} \right) \right\} = \text{Re} \left\{ U_0 \cos(kx) e^{-i\omega t} C_1(y) \right\}, \quad (\text{E.14})$$

where we for notation simplicity have introduced $\kappa = [1 - i]/\delta$ and $C_1(y) = (y + e^{-\kappa y}/\kappa)$. From this stream function the first-order velocity component in the y -direction can be derived from Eq. (E.12),

$$v_{1,y} = \text{Re} \left\{ U_0 k \sin(kx) e^{-i\omega t} C_1(y) \right\}. \quad (\text{E.15})$$

We have now derived the first-order perturbations to the velocity, and from Eq. (E.1b) we can now find the second-order perturbation. We turn our attention to the right-hand side of Eq. (E.1b) and first focus on the time-dependence. We notice that the terms have the form considered in Section 3.5, such that the time average of the product of $A(t) = \text{Re} \{ A_0 e^{i\omega t} \}$ and $B(t) = \text{Re} \{ B_0 e^{i\omega t} \}$ is given as, Eq. (3.55),

$$\langle A(t)B(t) \rangle = \frac{1}{2} \text{Re} [A_0 B_0^*], \quad (\text{E.16})$$

where the prime denotes complex conjugation.

Carrying out the spatial differentiation of the expressions given in Eqs. (E.2), (E.10), and (E.15) respectively, we get

$$\begin{aligned} \nu \partial_y^2 \langle v_{2,x} \rangle &= -\frac{1}{2} U_0^2 k \cos(kx) \sin(kx) \text{Re} \{ C_1'(y) C_1'^*(y) \} \\ &\quad + \frac{1}{2} U_0^2 k \cos(kx) \sin(kx) \text{Re} \{ C_1(y) C_1''^*(y) \} \\ &\quad + \frac{1}{2} U_0^2 k \cos(kx) \sin(kx). \end{aligned} \quad (\text{E.17})$$

Using that $\cos(\alpha) \sin(\alpha) = 1/2 \sin(2\alpha)$ we reduce Eq. (E.17) to,

$$\nu \partial_y^2 \langle v_{2,x} \rangle = \frac{1}{4} U_0^2 k \sin(2kx) \left[1 + \text{Re} \{ C_1(y) C_1''^*(y) \} - |C_1'^*|^2 \right]. \quad (\text{E.18})$$

We notice from earlier that $C_1(y) = (y + e^{-\kappa y}/\kappa)$ and $\kappa = [1 - i]/\delta$ so that the right-hand side of Eq. (E.18) is known, and we by two-fold integration in y get

$$\begin{aligned} \nu \langle v_{2,x} \rangle &= \frac{1}{4} U_0^2 k \sin(2kx) \left[\frac{1}{2} \delta y e^{-y/\delta} \cos(y/\delta) - 2\delta^2 e^{-y/\delta} \sin(y/\delta) \right. \\ &\quad \left. - \frac{1}{2} \delta y e^{-y/\delta} \sin(y/\delta) - \frac{1}{4} e^{-2y/\delta} \delta^2 + Ay + B \right], \end{aligned} \quad (\text{E.19})$$

where A and B are arbitrary integration constants with respect to y .

It is clear that the second-order time-averaged velocity must stay finite at all times indicating the boundary condition $|v_{2,x}| < \infty$ for $y \rightarrow \infty$. Exploiting this boundary condition, we get $A = 0$ in Eq. (E.19). Furthermore we still apply the no-slip condition at the boundary of the solid wall, implying that also $v_{2,x} = 0$ for $y = 0$. Using this in Eq. (E.19) we conclude that $B = \delta^2/4$.

Far from the boundary layer we therefore have the velocity field due to the viscid effects at the boundary,

$$\nu \langle v_{2,x} \rangle \Big|_{\infty} = \frac{1}{16} U_0^2 k \sin(2kx) \delta^2 \quad \Leftrightarrow \quad \langle v_{2,x} \rangle \Big|_{\infty} = \frac{1}{8} \frac{U_0^2}{c_a} \sin(2kx), \quad (\text{E.20})$$

where we in the last equality have used that the wavenumber in the acoustic wave outside the boundary layer is $k = \omega/c_a$, and that we have already concluded that the characteristic length of the boundary layer could be expressed as $\delta = \sqrt{2\nu/\omega}$.

Appendix F

Temperature Dependence of Viscosity and Speed of Sound

In Section 12.4 we determine the temperature dependence of η and of the Φ -factor. The value of η for different temperatures is found in [8] and given in Table F.1. The temperature dependence is taken from [17] and is also shown in Table F.1.

Table F.1: Viscosity of blood and speed of sound in water as a function of temperature.

τ [°C]	η [mPa s]	c_a [m s ⁻¹]
0	-	1401.0
10	-	1447.8
20	-	1483.2
22	3.4	-
25	-	1497.4
30	-	1509.5
37	2.7	-
40	2.4	1528.4
50	-	1541.4
60	-	1549.5
70	-	1553.2
80	-	1552.8

Appendix G

Gor'kov's Article

Here follows the original Gor'kov article from 1962, [14]. It should be noted that this is a scanned document, since we have not been able to find it electronically.

ON THE FORCES ACTING ON A SMALL PARTICLE
IN AN ACOUSTICAL FIELD IN AN IDEAL FLUID

L. P. Gor'kov

S. I. Vavilov Institute of Physical Problems, Academy of Sciences, USSR
(Presented by Academician L. D. Landau, April 28, 1961)
Translated from Doklady Akademii Nauk SSSR, Vol. 140, No. 1,
pp. 88-91, September, 1961
Original article submitted April 22, 1961

When a particle is suspended in the field of a sound wave, the fluid exerts hydrodynamical forces on it. In the linear approximation, these forces are proportional to the velocity of the fluid [1] and, on the average, do not lead to a displacement of the particle. In problems of acoustical coagulation, an important part is played by average forces acting on the particle which arise as the result of second order effects. These forces are of a nature related to that of the radiation-pressure forces in a sound wave [2, 3]. The magnitude of the forces has been found only for particles which are in an ideal fluid, in a paper by King [2]. The method of [2] was to solve exactly the problem of the flow around a small sphere in the field of a sound wave. So far as is known to us, no account was taken of effects associated with viscosity and thermal conductivity.

We present here a simple method which allows us to determine the magnitude of the average forces that act on the particle in an arbitrary acoustical field when the size of the particle is much smaller than the wavelength of the sound. In this paper we shall treat the case of an ideal fluid.

The magnitude of the force is equal to the average flux of momentum through any closed surface in the fluid which encloses the particle:

$$F_i = - \oint \bar{\Pi}_{ik} df_k.$$

Here Π_{ik} is the momentum flux density tensor in the ideal fluid: $\Pi_{ik} = p \delta_{ik} + \rho v_i v_k$. We shall take as the surface a sphere with a radius much larger than λ , the wavelength of the sound. In the linear approximation the velocity potential φ is the sum of waves incident on the particle and scattered by it:

$$\varphi(r, t) = \varphi_{in}(r, t) + \varphi_{sc}(r, t). \tag{1}$$

At the same time, we have from Euler's equations

$$(p = p_0 + p') \quad p' = -\rho \frac{\partial \varphi}{\partial t} - \rho \frac{v^2}{2} + \frac{\rho}{2c^2} \left(\frac{\partial \varphi}{\partial t} \right)^2$$

Since $\overline{(\partial \varphi / \partial t)} = 0$, we get for the average force

$$F_i = - \oint \left\{ \left[-\rho \frac{v^2}{2} + \frac{\rho}{2c^2} \left(\frac{\partial \varphi}{\partial t} \right)^2 \right] \delta_{ik} + \rho \overline{v_i v_k} \right\} df_k.$$

Thus, for the calculation of the average force correct up to terms of the second order in the velocity, it is sufficient to find the solution of the linear scattering problem.

In the wave zone the potential of the scattered wave can be expanded in terms of multipoles:

$$\varphi_P = \frac{a(t - r/c)}{r} + \frac{A(t - r/c, n)}{rc} + \dots \tag{4}$$

For particles of size $R \ll \lambda$, the coefficients in Eq. (4) are in turn determined from the solution of the problems of the flow of an incompressible fluid around the body (cf. [1]). In fact, for $r \ll \lambda$ the wave equation goes over into the equation of an incompressible liquid, $\Delta \varphi_{sc} = 0$, and the decreasing solutions of this equation are:

$$\varphi_{sc} = \frac{a(t)}{r} - \frac{A(t, n)}{r^2} + \dots \tag{4'}$$

For the potential flow of an ideal fluid around a stationary sphere the second term is of the form:

$$- (\mathbf{v}_{in}(t), \mathbf{n}) \frac{R^3}{2r^2}. \tag{5}$$

where $\mathbf{v}_{in}(t)$ is the velocity in the incident wave at the place where the sphere is located. The first term corresponds to the "ejection" of mass owing to the compression of the gas in the incident wave, and is given by

$$a(t) = - \frac{R^3}{3\rho} \rho_{in}(t). \tag{6}$$

The expressions (5) and (6) relate only to a stationary rigid sphere. In the general case, the sphere is partially entrained by the fluid and acquires a velocity $\mathbf{u}(t)$:

$$\mathbf{u}(t) = \frac{3\rho}{\rho + 2\rho_0} \mathbf{v}_{in}(t),$$

where ρ_0 is the density of the sphere. Therefore, if ρ_0 is comparable with the density of the fluid we must insert in Eq. (5) the relative velocity $\mathbf{v}_{in} - \mathbf{u}$.

If one takes into account compressibility of the sphere itself, one gets instead of Eq. (6),

$$a(t) = -\frac{R^3}{3\rho} \dot{p}_{in}(t) \left(1 - \frac{c^2 \rho}{c_0^2 \rho_0}\right)$$

Collecting the results, we find for the potential (4) of the waves scattered by the sphere the expression

$$\varphi_p = -\frac{R^3}{3\rho r} \dot{p}_{in} f_1 - \frac{R^3}{2} f_2 \operatorname{div}(\mathbf{v}_{in} \frac{1}{r}) \quad (7)$$

where

$$f_1 = 1 - c^2 \rho / c_0^2 \rho_0, \quad f_2 = 2(\rho_0 - \rho) / (2\rho_0 + \rho).$$

As was shown in [2], the magnitude of the average force in a standing wave is larger than in a plane running wave. In the former case, in the quadratic expression (3) for the force there are also important contributions from the interference terms between the incident and scattered waves, whereas for a running wave the magnitude of the momentum imparted to the particle by the waves is determined only by the momentum carried away by the scattered wave. In fact, by using the relations between the quantities in a plane running wave, we can rewrite Eq. (3) in the following form:

$$F_x = -\rho \oint [v_{in} v_{in} (1 + \cos \theta) + v_{sc}^2 \cos \theta] df \quad (8)$$

(the x axis is taken in the direction of propagation of the incident wave, and v_{sc} is the projection of the velocity of the scattered waves in the direction of the radius of the sphere). On the other hand, in the absence of dissipation, the average flux of energy through the closed surface is zero. Expanding the expression for the energy flux $Q = \rho \mathbf{v} (v^2/2 + w)$ [1] to terms of second order, we find

$$\oint Q df = \rho c \oint [v_{in} v_{in} (1 + \cos \theta) + v_{sc}^2] df \equiv 0. \quad (9)$$

From this we have

$$F_x = \rho \oint v_{sc}^2 (1 - \cos \theta) df. \quad (8')$$

From a monochromatic wave we get

$$F = \frac{4\pi I}{9c} R^2 (kR)^4 \left[f_1^2 + f_1 f_2 + \frac{3}{4} f_2^2 \right], \quad (10)$$

where $I = \rho c u_0^2 / 2$ is the average energy flux density in the incident waves.

The formula (8') is valid only in a plane running wave. In an arbitrary acoustical field the main contribution to the expression (3) for the force comes from interference terms between the incident and scattered radiation, which lead to forces much larger than that given by Eq. (10). Confining ourselves to these terms in Eq. (3), we find

$$F_i = -\oint \left\{ \left[-\rho (\overline{v_{sc} v_{in}}) + \frac{c^2}{\rho} \overline{\rho'_{in} \rho'_{sc}} \right] \delta_{ik} + \rho (\overline{v_{is} v_{k in}} + \overline{v_{in} v_{k sc}}) \right\} df_k.$$

Changing to a volume integral, and using the Euler equations and the fact that the flow is a potential flow, we get

$$F = -\int_V \mathbf{v}_{in} \left(\rho \operatorname{div} \mathbf{v}_{sc} + \frac{\partial \rho_{sc}}{\partial t} \right) dV \\ = -\rho \int_V \mathbf{v}_{in} \left(\Delta \varphi_{sc} - \frac{1}{c^2} \frac{\partial^2 \varphi_{sc}}{\partial t^2} \right) dV; \quad (11)$$

but, according to Eq. (7):

$$\Delta \varphi_{sc} - \frac{1}{c^2} \frac{\partial^2 \varphi_p}{\partial t^2} = \frac{4\pi}{3\rho} f_1 R^3 \rho_{in} \delta(\mathbf{r}) \\ + 2\pi f_2 R^3 \operatorname{div}(\mathbf{v}_{in} \delta(\mathbf{r})).$$

Substituting this in Eq. (11) and introducing the quantity $U(\mathbf{r})$, the potential of the forces $\mathbf{F} = -\nabla U$ we get

$$U = 2\pi R^3 \rho \left\{ \frac{\overline{p_{in}^2}}{3\rho c^2} f_1 - \frac{\overline{v_{in}^2}}{2} f_2 \right\} \quad (12)$$

($\overline{p_{in}^2}$ and $\overline{v_{in}^2}$ are the mean square fluctuations of the pressure and velocity in the wave at the point where the particle is located). The force in a standing wave $\varphi_{in} = - (u_0/k) \cos \omega t \cos kx$:

$$F = 4\pi \bar{E} R^2 (kR) \sin 2kx \left\{ \frac{\rho_0 + 2/3(\rho_0 - \rho)}{2\rho_0 + \rho} - \frac{1}{3} \frac{c^2 \rho}{c_0^2 \rho_0} \right\} \quad (13)$$

(\bar{E} is the average density of the acoustical energy). The formulas (10) and (11) agree with the results of [2, 3].

In the field $U(\mathbf{r})$, particles collect near the minimum of the potential energy (12). The equilibrium density distribution of the suspended particles $n(\mathbf{r})$ follows the Boltzmann formula

$$n(\mathbf{r}) \propto \exp \{-U(\mathbf{r})/kT\}. \quad (14)$$

At the places where the density is greatest the further coagulation of the particles is facilitated. At ordinary sound intensities $I \sim 0.1$ w/cm² and $\omega \sim 10^4$ sec⁻¹ the accumulation of particles at the nodes or antinodes of the wave plays an important role. For example, the width Δ of the region in which the particles are concentrated in a standing wave, Eq. (13), is given in order of magnitude by*

*For very small distances between the particles, or near a wall, forces of interaction between the particles and between the particles and the wall become important.

$$(k\Delta)^2 = \frac{3kT}{10\pi R^3 E}.$$

(For $E \approx 4 \cdot 10^{10}$ erg/cm³, $\nu \approx 1$ kc, $\Delta \approx 1.5 \cdot 10^{-6} R^{-3/2}$)
The time after which the distribution (4) is established is $\tau \sim \eta (kR)^{-2} (E)^{-1}$, where η is the viscosity of the medium.

We emphasize that Eq. (12) holds for an arbitrary field, with the exception of fields closely similar to that of a plane running wave. In particular, in a spherically converging or diverging wave

$$U(r) = \frac{\bar{Q}R^3}{2c} \left\{ \frac{f_1}{3r^2} - \frac{f_2}{2} \left(\frac{1}{r^2} + \frac{1}{k^2 r^4} \right) \right\} \quad (15)$$

(Q is the power of the source).

When $f_2 > 0$, $f_1 > 3/2 f_2$, the particles either collect at the center or move out to infinity, depending on the distance from the center; for $f_2 > 0$, $f_1 < 3/2 f_2$ there is a collapse to the center; if $f_1 < 3/2 f_2$, $f_2 < 0$ Eq. (15) has a minimum at distances of the order of a wavelength; finally, if $f_1 > 3/2 f_2 > 0$, the particles are pushed out to infinity. Of course, at very large distances from the center the quantity (15) becomes small, the spherical wave goes over into a plane wave, and the main part is played by the forces (10):

$$U(r) = \pm \frac{\bar{Q}R^2}{3cr} (kR)^4 \left\{ f_1^2 + f_1 f_2 + \frac{3}{4} f_2^2 \right\} \quad (16)$$

(the plus sign is for a diverging wave and the minus sign for a converging wave).

The values of (16) and (15) are comparable for $r \sim R (kR)^{-4}$. For the results given here to be valid it is necessary for the condition $\sqrt{\eta/\rho\omega} \ll R$ to hold.

In conclusion the author expresses his gratitude to Academician L. D. Landau for a discussion of this work and for valuable advice.

LITERATURE CITED

1. L. D. Landau and E. M. Lifshits, *Mechanics of Continuous Media* [in Russian] (1954).
2. L. V. King, *Proc. Roy. Soc.*, **A147**, 212 (1954).
3. R. Yosioka and G. Kawasima, *Acoustica*, **5**, 167 (1955).

All abbreviations of periodicals in the above bibliography are letter-by-letter transliterations of the abbreviations as given in the original Russian journal. Some or all of this periodical literature may well be available in English translation. A complete list of the cover-to-cover English translations appears at the back of this issue.

Appendix H

Matlab Source Code

In this appendix we print some of the MATLAB code we used in the thesis. Due to space restrictions we have only included the code for the most important parts, since a lot of the code is just off-the-shelf plotting code *etc.* The rest of the code can, however, be obtained by contacting the authors.

H.1 Least-square Fit

Here follows the source code for the least-square fit we used in Section 6.3.

H.1.1 Source Code for yOFt.m

The first source code is the file yOFt.m an auxiliary function for the main program.

```
1 % This function is called from Fit_E_ky.m and contains the analytic
2 % expression for y(t)
3
4 function F = yOFt(x,t)
5 % x(1) corresponds to E, and x(2) corresponds to k_y
6 global const;
7 global y0;
8 constants;
9 coefFit=2/3/const.eta*const.R_PS^2*const.const_phi_PS % alpha-
   coefficient - but without E and k_y
10 F = 1/x(2)*atan(exp(2*x(2)^2*coefFit*x(1)*t/1000)*tan(x(2)*y0))*1000000
```

H.1.2 Source Code for Fit_E_ky.m

This is the source code for the main function in our least-square fit analysis.

```

1  %%% Script Fit_E_ky.m %%%
2  % Makes a two-parameter fit of E and k_y from particle trajectory y(t)
   from
3  % a particle affected by pressure force
4
5  clear all;
6  close all;
7  % All lengths are in um and times in ms
8  global const
9  global y0
10
11 % Loading of the data
12 constants;
13 load PartA_1V_bred % Data must be from left side of channel, otherwise
   uncomment the following line
14 %part(:,2)=377-part(:,2);
15 y0=part(1,2)*1e-6;
16
17 % Sets the options for the curve fit
18 options = optimset('tolx',1e-18,'tolfun',1e-18);
19 lb = [0 0];
20 ub = [1000 200000];
21 [x,resnorm] = lsqcurvefit('yOft',[20 8000],part(:,1),part(:,2),lb,ub,
   options);
22
23 % Fit of the data
24 ttfit=linspace(part(1),part(length(part(:,1))),1000);
25 yyfit=1./x(2)*atan(exp(2*x(2)*const.coef_PS.*x(1).*ttfit/1000).*tan(x
   (2)*y0))*1000000;
26
27 % Plot of the data
28 figure(1);
29 plot(part(:,1),part(:,2),'ok',ttfit,yyfit,'-b');
30 legend('Exp. result', 'MATLAB fit',4);
31 xlabel('t [ms]');
32 ylabel('y [\mu{m}]');
33
34 E=x(1)
35 ky=x(2)
36 lambda=2*pi/x(2)
37
38 title(['Fit of trajectory in channel with width w=' num2str(const.w*1e6
   ) ' \mu{m} where E=' num2str(E) ' J/m^3 and \lambda/2=' num2str(
   lambda*1e6/2) ' \mu{m}'])

```

H.2 Simulation of Single-particle in Rectangular Channel

This is the basic code for the simulations of the single-particles in our rectangular channel including the source file we used for all the constants.

H.2.1 Source Code for constants.m

This is the source code for all the constants we used in our simulation

```

1  %%%% constants.m %%%%
2  % A common file containing the constants we use in the simulations
3
4  global const
5
6  % Diameter of RBC is 6-8 um, thickness is 2 um, so volumes are
7  % approximately 50 - 100 um^3
8  V_red=75e-18; % m
9  % Converting to a radius when assuming spherical RBCs
10 const.R_red=(V_red*3/4/pi)^(1/3); % m
11 const.R_lipid=1.5e-6; % m
12 % WBCs are approximately spherical in shape, range from about 5 to 20
    um in
13 % diameter. 10 um is a good average diameter
14 const.R_whi=5e-6; % m
15 % Radius of polystyrene
16 const.R_PS=2.58e-6; % m
17
18 % Here we use the viscosity of blood
19 const.eta=0.0027; % Pa s
20 % Density of blood
21 const.rho_0=1052.2; % kg m^(-3)
22 % Speed of sound in water
23 const.c=1483; % m s^(-1)
24 % Densities of the particles
25 const.rho_s_red=1096; %kg m^(-3);
26 const.rho_s_lipid=920; %kg m^(-3);
27 const.rho_s_whi=1060; %kg m^(-3);
28
29 % Compressibilities
30 const.beta_0=5.88e-10 % Pa^(-1)
31 const.beta_red=3.48e-10; % Pa^(-1)
32 const.beta_lipid=5.34e-10; % % Pa^(-1)
33 % We assume that beta_whi=beta_red
34 const.beta_whi=const.beta_red; % % Pa^(-1)
35
36 % Calculating the Phi-factors
37 const.const_phi_red=((const.rho_s_red+2/3*(const.rho_s_red-const.rho_0)
    )/(2*const.rho_s_red+const.rho_0)-1/3*const.beta_red/const.beta_0);
38 const.const_phi_lipid=((const.rho_s_lipid+2/3*(const.rho_s_lipid-const.
    rho_0))/(2*const.rho_s_lipid+const.rho_0)-1/3*const.beta_lipid/
    const.beta_0);

```

```

39 const.const_phi_whi=((const.rho_s_whi+2/3*(const.rho_s_whi-const.rho_0)
    )/(2*const.rho_s_whi+const.rho_0)-1/3*const.beta_whi/const.beta_0);
40 const.const_phi_PS=0.226;
41
42 % Channel parameters
43 % Height
44 const.h=125e-6; % m
45 % Width
46 const.w=350e-6; % m
47 % The wavenumber, assuming that we have half a wavelength
48 const.k=pi/const.w; % m(-1)
49
50 % We assume that the incoming wave is given as
51 % phi=-u_0/k*cos(omega*t)*cos(k*x)
52 % Amplitude of the potential
53 const.u_0=100; % m s(-1)
54 const.E=1000; % J m(-3)
55
56 % The change in pressure per unit length
57 const.del_p_L=3e5; % Pa m(-1)
58
59 % The flow-rate using the first term
60 Q=const.h3*const.w*const.deltaP_flow_over_L/12/const.eta*(1-192/pi5*
    const.h/const.w*tanh(pi*const.w/(2*const.h))) % m3/s
61 mLprMin=Q*60*1e6 % mL min(-1)
62 % The average velocity in the x-direction
63 v_x=Q/const.h/const.w % m s(-1)
64
65 % How many terms to include in the pousielle flow
66 const.orderPouseille=4;

```

H.2.2 Source Code for Pos_Equation.m

This file calculates the derivatives we use in our ode45-function. It is an auxially function for CalcPosition.m.

```

1 %%%% Script Pos_Equation.m %%%%
2 % Set-up of the differential-equations in our problem
3 % They will later be used in the ode45 method
4
5 function dpos=Pos_Equation(t, pos)
6
7 %Loads constants
8 global const
9 global part_nr
10
11 %Define the velocity-vector, dpos(2) is the y-component and dpos(1) the
12 %x-component
13 dpos=zeros(2,1);
14

```

```

15 % Get the right differential-equations in the y-direction from the
    particle
16 % number
17 if part_nr==1 %RBC
18     const.coef_red=2/3/const.eta*const.E*const.k*const.R_red^2*const.
        const_phi_red;
19     dpos(2)=const.coef_red*sin(2*const.k*pos(2));
20 elseif part_nr==2 %Lipid
21     const.coef_lipid=2/3/const.eta*const.E*const.k*const.R_lipid^2*
        const.const_phi_lipid;
22     dpos(2)=const.coef_lipid*sin(2*const.k*pos(2));
23 elseif part_nr ==3 %WBC
24     const.coef_whi=2/3/const.eta*const.E*const.k*const.R_whi^2*const.
        const_phi_whi;
25     dpos(2)=const.coef_whi*sin(2*const.k*pos(2));
26 else
27     disp(['Choose a valid particle!'])
28 end
29
30 %Pouseille flow at z=h/2
31 for ii=1:const.orderPouseille
32     nn=ii*2-1;
33     dpos(1)=dpos(1)+1/(nn)^3*(1-cosh(nn*(pi*(pos(2)-const.w/2)))/const.h
        )/cosh(nn*pi*const.w/(2*const.h)))*(-1)^((nn-1)/2);
34 end
35 dpos(1)=dpos(1)*4*const.h^2*const.del_p_L/(pi^3*const.eta);

```

H.2.3 Source Code for CalcPosition.m

In this file we find the required x -length and time for a particle to go from y_{start} to y_{end} . It requires the scripts Pos_Equation.m and constants.m.

```

1  %%% Script CalcPosition.m %%%
2  % Calculates the particle trajectories using the ode45 function and our
3  % function Pos_Equation.m
4
5  % Returns the positions and times given a y_start, y_end, and a
   particle
6  % number
7  function [Tslut, Xslut] = CalcPosition(y_start, y_end, particle)
8
9  % Loads our constants file
10 global const
11 global part_nr
12
13 % 1 is RBC, 2 is Lipid, and 3 is WBC
14 part_nr=particle;
15
16 % Options for the ode45 function including tolerances
17 options = odeset('RelTol',1e-12,'AbsTol',[1e-12 1e-12]);
18 % The time-interval we are looking at
19 TimeLength=100;
20
21 % Solving the differential equations using our Pos_Equation.m
22 [T,y]=ode45(@Pos_Equation,[0 TimeLength], [0 y_start],options);
23
24 Tslut=0;
25 Xslut=0;
26
27 % Finding the required lengths before particles are at y_end
28 if particle==1 | particle ==3 % For RBC and WBC
29     indexslut=min(find(y(:,2)>y_end));
30     ttemp=T(indexslut);
31     xtemp=y(indexslut,1);
32
33     % If the particles reaches y_end return time and x-position
34     if isnan(ttemp) == 0
35         Tslut=ttemp;
36     end
37
38     if isnan(xtemp) == 0
39         Xslut=xtemp;
40     end
41 elseif particle==2 % For lipids
42     indexslut=min(find(y(:,2)<y_end));
43     ttemp=T(indexslut);
44     xtemp=y(indexslut,1);
45

```

```
46     % If the particles reaches y_end return time and x-position
47     if isnan(ttemp) == 0
48         Tslut=ttemp;
49     end
50
51     if isnan(xtemp) == 0
52         Xslut=xtemp;
53     end
54 end
```


Bibliography

- [1] Private conversation with Jacob Riis Folkenberg at the company FOSS.
- [2] Private communication with the Thomas Laurell group at Lund University, Sweden.
- [3] Private conversation with the group of H. T. Soh at University Center Santa Barbara.
- [4] Rune Barnkob. Acoustofluidics in Microsystems. Master's thesis, DTU (Technical University of Denmark), 2009.
- [5] Henrik Bruus. Theoretical Microfluidics. Oxford University Press, Oxford, 2008.
- [6] Henrik Bruus, Jonathan Adams, and H. T. Soh. Continuous separation of red and white blood cells by acoustic radiation forces from transverse, standing ultrasound waves in a microfluidic channel. Unpublished note., 2008.
- [7] C. G. Caro, T. J. Pedley, R. C. Schroter, and W. A. Seed. The Mechanics of the Circulation. Oxford University Press, 1978.
- [8] Yildirim Çinar *et al.* Blood viscosity and blood pressure: Role of temperature and hyperglycemia. American Journal of Hypertension, 14(5):433–438, 2001.
- [9] Lawrence A. Crum. Bjerkness forces on bubbles in a stationary sound field. The Acoustical Society of America, 57(6):Part 1, 1975.
- [10] Leopold Dintenfass. Blood viscosity, hyperviscosity, and hyperviscosaemia. Springer, 1985.
- [11] R. L. Earle. Unit operations in food processing. <http://www.nzifst.org.nz/unitoperations/flfltheory4.htm>, visited 2nd of June. Main page: www.nzifst.org.nz.
- [12] Glenn Elert. Density of blood. <http://hypertextbook.com/facts/2004/MichaelShmukler.shtml>, visited 1st of June. Main page: <http://www.hypertextbook.com>.
- [13] Martin A. M. Gijs. Magnetic bead handling on-chip: new opportunities for analytical applications. Microfluidics and Nanofluidics, 1:22–40, 2004.
- [14] L.P. Gor'kov. On the forces acting on a small particle in an acoustic field in an ideal fluid. Doklady Akedemii Nauk SSSR, 140(1):88–91, 1961.

-
- [15] Louis V. King. On the acoustic radiation pressure on spheres. Mathematical and Physical Sciences, 147(861):212–240, 1934.
- [16] L.D. Landau and E.M. Lifshitz. Fluid mechanics, Volume 6 of Course of Theoretical Physics. Pergamon Press, New York, 1987.
- [17] David Lide. CRC Handbook of Chemistry and Physics, 89th edition. Taylor and Francis Group, 2009.
- [18] Miguel Moyers-Gonzales, Robert G. Owens, and Jiannong Fang. A non-homogeneous constitutive model for human blood. part 1. model derivation and steady flow. J. Fluid Mech., 617:327–354, 2008.
- [19] Nicole Pamme. Magnetism and microfluidics. Lab on a Chip, 6:24–38, 2005.
- [20] William K. Purves, David Sadava, Gordon H. Orians, and H. Craig Heller. Life: The Science of Biology. Sinauer Associates, Sunderland, 2004.
- [21] H. Roginski, J. W. Fuquay, and P. F. Fox. Encyclopedia of Dairy Sciences. Academic Press, 2003.
- [22] Peder Skafte-Pedersen. Acoustic forces on particles and liquids in microfluidic systems. Master’s thesis, DTU (Technical University of Denmark), 2008.
- [23] A. R. Pries *et al.* Blood flow in microvascular networks. Experiments and simulation. Circ. Res., 67:826–834, 1990.
- [24] Andreas Nilsson *et al.* Acoustic control of suspended particles in micro fluidic chips. Lab Chip, 4:131–135, 2004.
- [25] A.R. Pries *et al.* Blood viscosity in tube flow: dependence on diameter and haematocrit. Am. J. Physiol, 263:H1770–H1778, 1992.
- [26] C. Grenvall *et al.* Harmonic microchip acoustophoresis - a route to on line raw milk sample precondition in protein and lipid content quality control. Submitted for Analytical Chemistry.
- [27] Dwayne A. Johnson *et al.* Methodology for fractionating suspended particles using ultrasonic standing wave and divided flow fields. Separations Technology, 5:251–258, 1995.
- [28] Filip Petersson *et al.* Separation of lipids from blood utilizing ultrasonic standing waves in microfluidic channels. The Analyst, 129(1):938–943, 2004.
- [29] Filip Petersson *et al.* Continuous separation of lipid particles from erythrocytes by means of laminar flow and acoustic standing wave forces. Lab on a Chip, 5:20–22, 2005.
- [30] Filip Petersson *et al.* Free flow acoustophoresis: Microfluidic-based mode of particle and cell separation. Analytical Chemistry, 79(14):5117–5123, 2007.

-
- [31] J. Hultström *et al.* Proliferation and viability of adherent cells manipulated by standing-wave ultrasound in a microfluidic chip. Ultrasound in Medicine and Biology, 33(1):145–151, 2007.
- [32] Jeremy J. Hawkes *et al.* Force field particle filter, combining ultrasound standing wave and laminar flow. Sensors and Actuators B, 75:213–222, 2001.
- [33] J.F. Spengler *et al.* Observation of yeast cell movement and aggregation in a small-scale mhz ultrasonic standing wave field. Bioseparation, 9(6):329–341, 2001.
- [34] Kyuichi Yasui *et al.* Strongly interacting bubbles under an ultrasonic horn. Physical Review, E 77:016609, 2008.
- [35] M.Z. Bazant *et al.* Diffuse-charge dynamics in electrochemical systems. Physical Review, E 70(021506):1–24, 2004.
- [36] M.Z. Bazant *et al.* Induced-charge electrokinetic phenomena: Theory and microfluidic applications. Physical Review, 92(066101):1–4, 2004.
- [37] N.R. Harris *et al.* A silicon ultrasonic microfluidic separator. Sensors and Actuators, B 95:425–434, 2003.
- [38] Per Augustsson *et al.* Buffer medium exchange in continuous cell and particle streams using ultrasonic standing wave focusing. Springer-Verlag, pages 269–277, 2008.
- [39] R. Mettin *et al.* Bjerkness forces between small cavitation bubbles in a strong acoustic field. Physical Review, 56(3):2924–2931, 1997.
- [40] T. S. Simonova *et al.* Low-frequency dielectrophoresis and the polarization interaction of uncharged spherical particles with an induced debye atmosphere of arbitrary thickness. Colloid Journal, 63(1):108–115, 2001.
- [41] Thomas L. Tolt *et al.* Separation of dispersed phases from liquids in acoustically driven chambers. Chemical Engineering Science, 48(3):521–540, 1993.
- [42] Thomas Laurell *et al.* Chip integrated strategies for acoustic separation and manipulation of cells and particles. Chemical Society Reviews, 36:492–506, 2007.
- [43] K. Yosioka and Y. Kawasima. Acoustic radiation pressure on a compressible sphere. Acustica, 5(3):167–173, 1955.